



DISSERTATION

Analysis of retinal cell excitation with visual neuroprostheses

ausgeführt zum Zwecke der Erlangung des akademischen Grades eines
Doktors der technischen Wissenschaften unter der Leitung von

Ao. Univ. Prof. DDr. Frank Rattay
Institut für Analysis und Scientific Computing (E101)

eingereicht an der Technischen Universität Wien
Fakultät für Mathematik und Geoinformation
von

DI SUSANNE RESATZ

Matrikelnummer: 9125092
Novaragasse 24/15, 1020 Wien

Wien, am 23. August 2005

Kurzfassung

Motivation. Retina Implantate sollen blinden Menschen das Sehen ermöglichen, deren Sehverlust auf die Degeneration der Photorezeptoren zurückzuführen ist, und deren Bipolar- und Ganglienzellen noch in der Lage sind die Information zum Gehirn weiterzuleiten. Bei der elektrischen Stimulation des verbliebenen retinalen Netzwerks werden künstliche Signale generiert, mit dem Ziel sinnvolle optische Sinneseindrücke zu erzeugen. Um dieses komplexe Ziel zu verwirklichen muss in einem ersten Schritt erforscht werden, welche neuronalen Elemente das angelegte elektrische Feld erregt, um in einem zweiten Schritt ein Elektrodendesign entwickeln zu können, das diejenigen Strukturen aktiviert von denen man sich reproduzierbare, klar abgegrenzte visuelle Wahrnehmungen erwartet.

Methoden. Die Simulation der Erregungsprozesse der retinalen Zellen erfolgte in zwei Schritten. Zuerst wurde das extrazelluläre Potential für die neuronale Struktur errechnet, entweder mit dem finiten Element Programm FEMLAB unter Berücksichtigung der verschiedenen Strukturen des Auges oder analytisch in einem einfacheren Ansatz unter der Annahme eines unendlichen homogenen Mediums. In einem zweiten Schritt erfolgte die Analyse der Reaktion der Bipolar- und Ganglienzellen durch ein Kompartiment-Modell.

Resultate. Die Simulationen zeigten, dass die beiden untersuchten Zelltypen vollkommen unterschiedlich auf ein elektrisches Feld reagieren. Zum Beispiel ist es möglich, dass die Bipolarzellen die von einem epiretinalen Implantat weiter entfernt liegen als die Ganglienzellen, trotzdem eine höhere Membranspannung erreichen. Die Orientierung der lokalen Zellstruktur relativ zu dem angelegten elektrischen Feld ist dabei der ausschlaggebende Faktor. Basierend auf der Beobachtung, dass lang gestreckte Elektroden ein Feld erzeugen, das die Erregung von parallel verlaufenden Strukturen hemmt, wurde eine Elektroden Konfiguration zur selektiven Stimulation entwickelt. Direkt unter dem Implantat gelegene Zellen werden erregt, aber die problematische Aktivierung von Axonen, die von entfernt gelegenen Teilen der Retina kommend unter der Stimulations-Elektrode vorbei führen wird vermieden.

Folgerung. Die gegenständliche Anwendung zeigt sehr deutlich das enorme Potential aktueller Simulationstechniken für die Entwicklung komplexer Neuropthesen. Auch wenn im Fall des entworfenen Retinaimplantats eine klinische Validierung noch aussteht, konnte klar gezeigt werden, dass die eingebrachten neuartigen Detailanalysemethoden denkbaren experimentellen Herangehensweisen weit überlegen und geeignet sind, den Entwicklungsprozess substantiell zu beschleunigen und zu verbessern.

Abstract

Objectives. A retinal prosthesis has the potential to restore vision to patients with blindness caused by photoreceptor degeneration like retinitis pigmentosa and age related macular degeneration. People suffering from these devastating diseases retain functioning bipolar and ganglion cells, which relay retinal input to the brain. By electrical stimulation of the retina this intact network is used to send artificial signals via optic nerve to the brain with the aim to lead to meaningful visual percepts in blind patients. To perform this complex task the first step is to analyze which neuronal structures are excited by the electric current, and in a second step an electrode design has to be developed to target the elements which are expected to lead to localized, reproducible visual perceptions.

Methods. The excitation process of the electrically stimulated retinal cells is simulated in a two step procedure. In the first step the extracellular potential along the neural structure is calculated either with the finite element software FEMLAB considering the volume conductor inhomogeneities of the eye or analytically in a simpler approach assuming an infinite homogenous medium. In a second step ganglion and bipolar target cells are represented by compartment models and the membrane voltage response is analyzed either with the activating function concept or according to nonlinear membrane kinetics.

Results. The simulations show that the two investigated retinal cell types react completely different to an applied electric field. Although bipolar cells are positioned below the ganglion cells concerning the retinal surface that is more distant to the epiretinal electrode, it is possible that they answer with stronger transmembrane voltage. It turns out that the cell geometry, or more precisely the orientation of the specific neural elements relative to the applied electric field, is the determining factor in electrical stimulation. The obtained insights were used to develop an electrode configuration for selective activation of the underlying target cells that avoids co-stimulation of bypassing fibers from distant regions of the retina. Based on the observation, that long stimulating elements parallel to the main directions of the axonal pathways antagonize their excitation, the main idea of the implant design is that each line of electrodes of an array is in contact with a long slot filled with conducting material. This was done with awareness of the safety charge limits, which are a critical factor in retinal prosthesis technology.

Conclusions. The underlying application clearly demonstrates the enormous potential of contemporary simulation techniques for the development of complex neuroprostheses. Though the clinical validation of the designed retinal implant is still open, it is obvious, that the applied new detail analysis methods are by far superior to all conceivable experimental approaches and speed up and improve the development process substantially.

Acknowledgements

Firstly I want to thank Dr. Toby Velte for providing the data of the traced retinal cells. For financial support, I am indebted to the Austrian Science Foundation (FWF – ‘Fond zur Förderung der wissenschaftlichen Forschung’). Last but not least I am deeply grateful to Professor DDr. Frank Rattay for his competent supervision and the many helpful discussions.

Contents

Abbreviations and Symbols	5
1. Introduction	7
1.1 Retinal prosthesis for the blind	7
1.2 Thesis outline	13
2. The retina	19
2.1 Anatomy of the retina	20
2.2 From optical to neural image	26
2.3 Morphology of the target cells	29
3. Modeling	33
3.1 Electrical network model	33
3.2 Cell membrane models	37
3.3 Volume conductor models	43
3.4 Implementation	47
4. Influence of the cell geometry on the excitation process	54
4.1 Preliminary studies with the activating function	54
4.2 Variation of the soma size	58
4.3 Investigations on the distance between electrode and target structure	64
4.4 Influence of the axonal thin segment on the excitation process	77
4.5 Which neural elements are excited by electrical stimulation?	79
5. Investigations on the stimulus pulse duration	85
5.1 Stimulus strength versus pulse duration	85
5.2 Neural geometry and pulse duration	91
5.3 Safe charge density limit	94
6. Effective electrode configuration for selective stimulation	97
6.1 Dipole distance	97
6.2 Different electrode shapes	101
6.3 A special epiretinal implant	105
7. Concluding discussion	110
References	116
Curriculum vitae	124

Abbreviations and Symbols

The values in parenthesis are used for all simulations of this thesis.

ACSL	Advanced Continuous Simulation Language; simulation program
C	capacity of cell membrane
c	specific membrane capacity ($c = 1 \mu\text{F}/\text{cm}^2$)
Ca_{diss}^{2+}	calcium dissociation constant ($Ca_{diss}^{2+} = 10^{-3} \text{ mMdm}^{-3}$)
$[Ca^{2+}]_i$	intracellular calcium ion concentration
$[Ca^{2+}]_e$	extracellular calcium ion concentration ($[Ca^{2+}]_e = 1.8 \text{ mMdm}^{-3}$)
$[Ca^{2+}]_{res}$	residual level of the intracellular calcium ion concentration ($[Ca^{2+}]_{res} = 10^{-4} \text{ mMdm}^{-3}$)
f	activating function
FCM	Fohlmeister-Coleman-Miller
FEMLAB	finite element software package
g_A	maximum conductance of potassium A type per cm^2 of cell membrane
g_{Ca}	maximum conductance of calcium per cm^2 of cell membrane
g_K	maximum conductance of potassium per cm^2 of cell membrane
$g_{K,Ca}$	maximum conductance of calcium-activated potassium per cm^2 cell membrane
g_L	maximum conductance of leakage per cm^2 of cell membrane
G_m	cell membrane conductance
g_m	specific membrane conductance
g_{Na}	maximum conductance of sodium per cm^2 of cell membrane
HH	Hodgkin-Huxley
I_C	capacitive current
I_{Ca}	calcium current
i_{Ca}	calcium current density
I_{el}	electrode current

I_{ion}	ion current passing through the membrane
i_{ion}	ion current density
I_K	potassium current
i_K	potassium current density
$I_{K,A}$	potassium current (A type)
$i_{K,A}$	potassium current density (A type)
$I_{K,Ca}$	calcium-activated potassium current
$i_{K,Ca}$	calcium-activated potassium current density
I_L	leakage current
i_L	leakage current density
I_{Na}	sodium current
i_{Na}	sodium current density
I_R	ohmic current
I_{stim}	stimulus current
MATLAB	program for technical computing
m, h, c, n, a, h_A	probabilities for ion membrane gating processes
R	resistance
T	simulation temperature
V	reduced cell membrane voltage, i.e. in the resting state is $V = 0$.
V_{Ca}	calcium voltage
V_e	extracellular potential
V_i	intracellular potential
V_K	potassium voltage
V_L	leakage voltage
V_{Na}	sodium voltage
V_{rest}	resting voltage across the membrane
λ	space constant
ρ_e	extracellular resistivity
ρ_i	intracellular resistivity
τ	time constant of calcium removal in the FCM model

1. Introduction

The goal of retinal prosthetic devices is to generate meaningful visual information in blind patients that have lost outer retinal function. This thesis supports the target by analysing the retinal cell excitation with electrical stimulation. The investigations are accomplished by the mean of computer simulations.

1.1 Retinal prosthesis for the blind

Blindness affects millions of people worldwide, and many prevalent and potentially devastating causes of vision loss cannot be effectively treated. For decades, the possibility of restoring sight to blind individuals has been a subject of intense scientific research as well as of science fiction. Recent advances in bioengineering and micro-technology have led to the development of highly sophisticated micro-electronic devices that are designed to stimulate viable neuronal tissue in the hope of regaining some level of functionality. Human clinical trials with visual prosthetic devices are underway and it seems that this popular subject of science fiction is now becoming a tangible scientific reality.

Many attributes characterize a visual scene, including color, motion, depth and form. However, current visual prostheses are designed to address only the most basic of these components: spatial detail. To accomplish this goal, several designs are being pursued.

Visual loss caused by outer retinal degeneration in diseases such as retinitis pigmentosa or age-related macular degeneration can be reversed by electrical stimulation of the retina or the optic nerve (retinal or optic nerve prostheses, respectively). On the other hand, visual loss caused by inner or whole thickness retinal diseases, eye loss, optic nerve diseases (tumors, ischemia, inflammatory processes etc.), or diseases of the central nervous system (not including diseases of the primary and secondary visual cortices) can be reversed by a cortical visual prosthesis. It is generally acknowledged that complete development of the visual system and prior visual experience are necessary for a patient to be able to correctly and meaningfully interpret these visual patterns [Merabet et al. 2005]. Therefore, it remains unclear whether one of these approaches would be appropriate for a patient who was blind from birth or early infancy.

Retinal degenerations such as retinitis pigmentosa initially result in photoreceptor loss. Later in the course of the disease, there is secondary loss of inner retinal neurons. Post-mortem studies demonstrate the presence of inner retinal cells even in eyes severely degenerated by retinitis pigmentosa. Counts of cells in the inner nuclear layer suggest that 40% to 88% are retained, whereas 20% to 48% are retained in the ganglion cell layer, depending on the severity of the degeneration and the retinal area sampled [Stone et al. 1992, Santos et al. 1997, Humayun et al. 1999].

Preservation of the inner retinal neurons in retinitis pigmentosa raises the possibility that appropriate stimulation of these cells may produce vision. The premise of the retinal approach is to stimulate these cells and, in essence, to replace photoreceptor function. This strategy has the advantage of delivering input more proximally along the afferent visual pathway, thereby benefiting from early physiological preprocessing and encoding. In addition, the ganglion cells have a topographic configuration that closely corresponds to the visual field. Driving them with suitable stimulation, electrical signals for example, may mimic their usual signals to the brain. This would suggest that it would be simpler to achieve patterns of stimulation that correspond to objects in the visual field than would be possible with cortical stimulation, where the topographic relationship to the field is much more complex.

Two types of retinal prostheses are currently under development, and differ primarily in their location in the retina. One, the subretinal implant, is placed in the region of degenerated photoreceptors by creating a pocket between the sensory retina and retinal pigment epithelial layer. The other, the epiretinal implant, is attached to the inner surface of the retina, close to the ganglion cell side (Fig. 1.1)

The subretinal design is currently being pursued by two main investigators (artificial silicon array [Chow et al. 2004] and microphotodiode array [Zrenner et al. 1999]). Chow and colleagues have devised an array with approximately 5000 microphotodiodes, each of which contains its own stimulating electrode. When the device is implanted under the retina, photocurrents generated by locally absorbed light stimulate adjacent retinal neurons in a multi-site mode. There is no camera involved in capturing an image and the array is powered solely by incident light. Although this approach is close to the natural situation as the optical qualities of the eye are still used, the implantation is more complicated (Fig. 1.3).

A phase one feasibility trial has been carried out with six patients with profound vision loss from retinitis pigmentosa. Patients were followed from 6 to 18 months after implantation, and reported an improvement in visual function that was evidenced by an increase in visual field size and the ability to name more letters using a standardized visual acuity chart [Chow et al. 2004]. However, these results have been met with controversy. It seems that the purported beneficial outcome might not be the result of direct and patterned electrical stimulation as

initially anticipated, but, instead, an indirect ‘cell rescue’ effect from low-level current generated by the device.

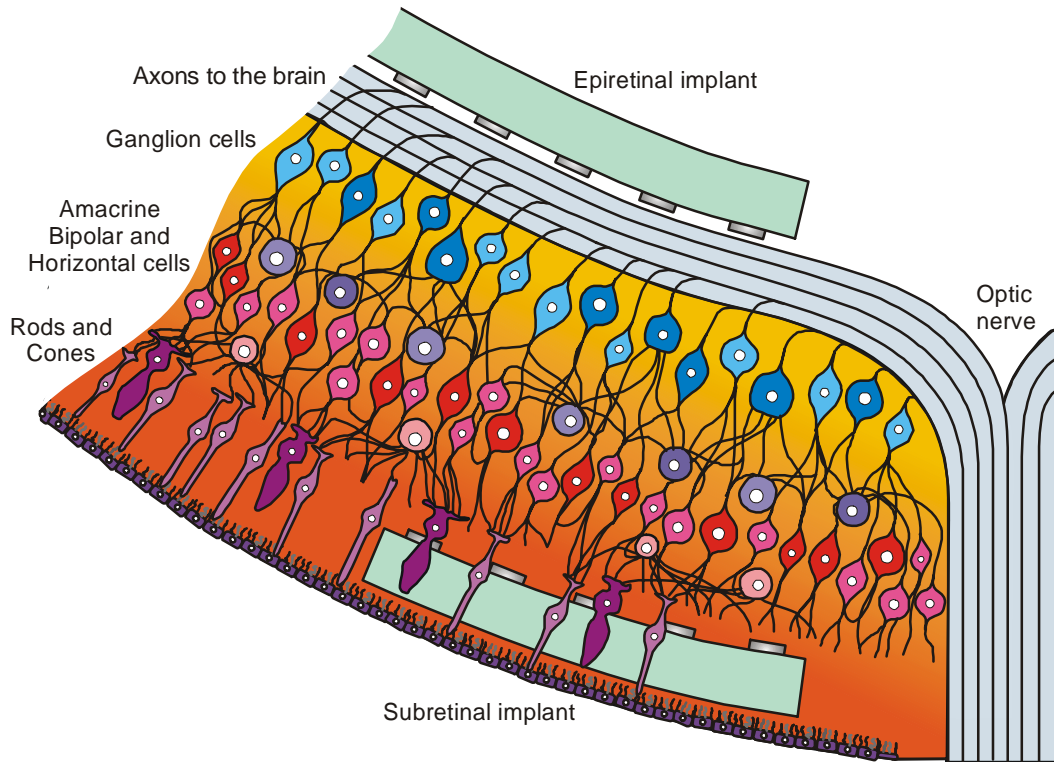


Fig. 1.1 Scheme of retinal cross section with the two available types of inner eye prostheses: epiretinal and subretinal implant. The axons of the ganglion cells are the excitable elements closest to the epiretinal electrodes, whereas in the subretinal approach other neural elements of the retinal network are also directly stimulated. Thus the subretinal implant can use neural preprocessing in a more natural way [Resatz and Rattay 2003b].

The epiretinal approach is intensively pursued by US teams at Johns Hopkins/Mann Foundation in Los Angeles [Humayun et al. 2003] and Harvard/MIT [Rizzo et al. 2003a, 2003b] as well as by Eckmiller in Bonn (Germany) [Eckmiller et al. 1997]. These groups have concentrated on producing an ultra-thin electrode array that can be safely attached to the delicate retinal surface for long periods of time. Like the cortical approach, the design incorporates a digital camera and signal processor mounted on a pair of eyeglasses to capture an image and convert patterns of light into electrical signals (Fig. 1.2 and Fig. 1.3).

By Humayun et al. three subjects were permanently implanted with a retinal prosthesis [Humayun et al. 2004]. The implanted device included an extraocular case to encapsulate the electronic circuit, an intraocular electrode array (platinum disks, 4×4 arrangement) designed to interface with the retina, and a cable to connect the electronics case to the electrode array. The subjects were able to see perceptions of light (spots) on all 16 electrodes of the array. In

addition, the subjects were able to use a camera to detect the presence or absence of ambient light, to detect motion, and to recognize simple shapes.

Rizzo et al. studied five volunteers with severe retinitis pigmentosa and one with normal vision (who underwent enucleation of the eye because of orbital cancer) [Rizzo et al. 2003a, 2003b]. Electrical stimulation of the retina was performed on awake volunteers by placing a single 250 μm diameter handheld needle electrode or a 10 μm thick microfabricated array of iridium oxide electrodes (50 μm , 100 μm , or 400 μm diameter) on the retina. Current sources outside the eye delivered charge to the electrodes. No clinically visible damage to the eye or loss of vision occurred.

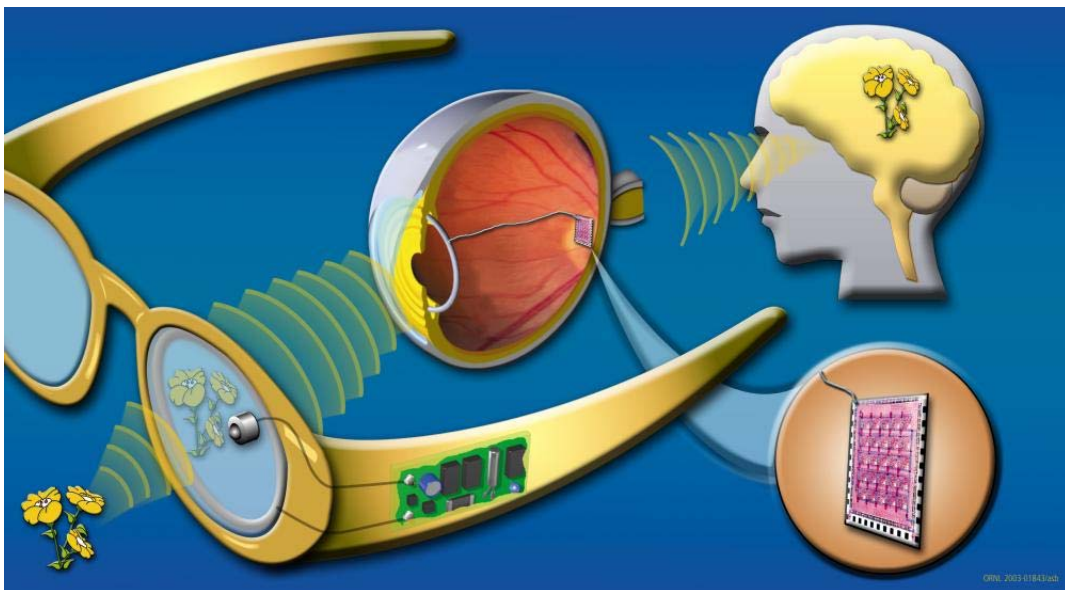


Fig. 1.2 Possible arrangement of an epiretinal prosthesis. The system consists of external and implanted components. Patients wear glasses, like those shown above, with a tiny camera embedded in the lens. The camera records images and transfers them to a micro-controller module (integrated in the temple of the glasses) which extracts control parameters to be transmitted via a wireless link. An antenna along the contours of the lens transmits the signal to a receiving antenna situated in the eye and via a tiny wire to the implanted stimulation unit. The electrode array delivers series of biphasic impulses to stimulate the remaining retinal cells. Finally these cells send visual information along the optic nerve to the visual cortex. [http://www.doemedicalsciences.org/abt/retina/retproth.shtml]

Percepts could not be reliably elicited with 50 μm diameter electrodes using safe charges in one blind patient. With the two larger electrodes, only the normal-sighted patient had thresholds at charge densities below 0.25 and 1.0 mC/cm^2 for 100 μm and 400 μm diameter electrodes, respectively, which is one seemingly reasonable estimate of safety derived from the product of charge per phase and charge density per phase [McCreery et al. 1990]. In blind patients, thresholds always exceeded these levels, although most were close to these limits in patient 6. The range of charge density thresholds with the 400 μm electrode in blind patients was 0.28 mC/cm^2 to 2.8 mC/cm^2 . The normal-sighted patient had a

threshold of 0.08 mC/cm^2 with a $400 \text{ }\mu\text{m}$ electrode, roughly one quarter of the lowest threshold in the blind patients. Strength/duration curves obtained in two blind patients revealed the lowest threshold charge at the 0.25 ms or 1.0 ms stimulus duration [Rizzo et al. 2003a].

On average, volunteers 3, 5, and 6 reported percepts that matched the stimulation pattern 48 % and 32 % of the time for single - and multiple - electrode trials, respectively. Two-point discrimination in the best cases may have been achieved in two blind subjects using (center-to-center) electrode separation of 600 and $1960 \text{ }\mu\text{m}$. Reproducibility was achieved 66% of the time in the blind subjects. By comparison, in the normal sighted subject, perceptual form was reported accurately 57% of the time, with 82% reproducibility, and two-point discrimination may have been achieved in one trial with $620 \text{ }\mu\text{m}$ electrode spacing and in two trials each with $1860 \text{ }\mu\text{m}$ and $2480 \text{ }\mu\text{m}$ electrode spacing. In subjects 5 and 6, perceptual size was inconsistently related to the charge, although relatively large differences in charge (median: $0.55 \text{ }\mu\text{C}$) between two trials produced differently sized percepts. Longer stimuli did not produce rounder percepts [Rizzo et al. 2003b].

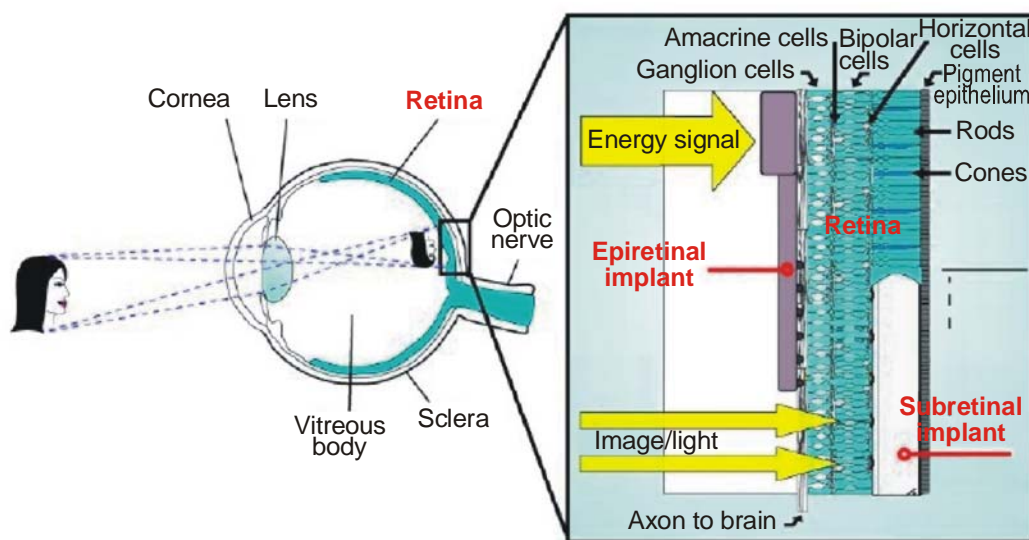


Fig. 1.3 An object (in this case a face) is projected by the cornea and lens onto the retina in an upside-down manner and is transformed into an electrical image by the photoreceptor cells (rods and cones) of the outer retina. With a subretinal implant, the rods and cones are replaced by a silicon plate carrying thousands of light-sensitive microphotodiodes, each equipped with a stimulation electrode. Light from the image directly modulates the microphotodiodes, and the electrodes inject tiny currents around the remaining neural cells (horizontal cells, bipolar cells, amacrine cells, and ganglion cells) of the retinal inner layer. In contrast, the epiretinal implant has no light-sensitive areas but receives electrical signals from a distant camera and processing unit outside of the body. Electrodes in the epiretinal implant (small black knobs) then stimulate the inner-layer ganglion cells [Zrenner 2002].

In summary, volunteers who have been legally blind for many years can see percepts induced by electrical stimulation of the retina. The single percepts were relatively small, which offers hope of generating a montage of such percepts to create useful images. However, the form of percepts, especially with multi-electrode stimulation, often did not match the stimulation pattern. The lack of a better outcome in the normal-sighted patient suggests that retinal degeneration alone does not explain the limited results in blind patients and emphasizes the need to learn effective stimulation methods (Fig. 1.5).

Major issues remain for prosthesis development. Although significant numbers of cells remain in the inner nuclear and ganglion cell layers of the retina in advanced retinitis pigmentosa, we have little information about the types and subtypes of these cells. We do not have a method for noninvasive determination of the viability of these cells. Studies to identify the remaining cells and to noninvasively estimate their function are needed.

The amount of electric current that will be required to stimulate inner retinal cells and produce perception is a critical factor in implant design (Table 1.1). First, the safety of any device will depend on keeping stimulus charge levels in a range that does not damage the retina. Second, the heat created by a device is primarily driven by its power consumption. A large amount of energy is consumed at the electrode-tissue interface because of its electrical resistance. The generated heat must be kept at levels that will not damage any ocular tissues. Third, methods must be developed to deliver sufficient power to a device to allow suprathreshold stimulation at a sufficient number of electrodes to create useful vision. The stimulation threshold is a primary driving factor in determining these parameters.

Table 1.1 Intraocular retinal stimulation thresholds

Electrode location	Species	End Point	Retinal status	Threshold (C/cm ²)
Subretinal	Rabbit	EEP	Normal	3.9×10^{-8} to 7.4×10^{-9}
Epiretinal	Rabbit	EEP	Normal	10^{-5} to 8.9×10^{-6}
Epiretinal	Human	Perception	Normal	4.8×10^{-3} to 8×10^{-5}
Epiretinal	Rabbit	EEP	Loc. deg.	11.9×10^{-6}
Epiretinal	Human	Perception	RP	7×10^{-2} to 1.6×10^{-4}

Abbreviations: EEP: electrically evoked potential, RP: retinitis pigmentosa, Loc. deg.: local degeneration.

[Data obtained from Chow et al. 1997, Humayun et al. 1996, 1994, 1999, Nadig 1999, Rizzo et al. 2000, and Weiland et al. 1999 and converted to charge density in coulombs per centimeter squared.]

The power requirement for a retinal prosthesis depends essentially on the threshold charge needed for perception and the number of electrodes in the stimulating array. Some data are available from measurements of epiretinal

thresholds in subjects with advanced retinitis pigmentosa. These show considerable variability. Most current subretinal device designs consist only of an array of subretinal microphotodiodes. Although the simplicity and similarity to the natural situation are conceptually attractive, experiments show that such devices do not generate sufficient current from ambient light alone to stimulate inner retinal elements in animal eyes [Chow et al. 2001, Zrenner et al. 1999]. Although it seems reasonable to assume that subretinal thresholds will be lower, we do not yet have these numbers [Loewenstein et al. 2004]. Also the number of electrodes needed to achieve form perception, if this indeed can be accomplished, is unknown.

Retinal prostheses are being designed to electrically stimulate cells that survive degeneration to produce artificial vision. Investigators must demonstrate that electrical stimulation excites visual cells in a predictable manner in order for prosthesis to be reliable. Once stimulation parameters give reproducible visual effects, researchers must learn how to adjust these parameters to create useful vision.

Retinal ganglion and bipolar cells are topographically arranged in an orderly distribution across most of the field of vision. This has led to the simple concept that an array of electrodes can be placed against the retina, with rows and columns like lights on a scoreboard, and that activation of electrodes in the array in a given shape might yield perception of a similar shape. Recently however, it was shown experimentally that in several respects, this concept is an oversimplification [Loewenstein et al. 2004].

There are many types of retinal ganglion and bipolar cells, which are small and closely spaced. Electrodes in prostheses will have to be large enough to avoid exceeding safe charge-injection limits. Because of the material dependent minimum size each electrode is likely to stimulate many cell types indiscriminately. These cell outputs would then be very different than the normal physiologic situation in which there is a different orchestration of responses. Even worse is the possibility that focal stimulation might activate ganglion cell axons representing many cells across a broad area of the retina. This is likely to produce diffuse rather than focal perceptions [Loewenstein 2004]. Work in animals and humans as well as computer simulations has therefore been undertaken to investigate the physiologic and perceptual consequences of electrical stimulation.

1.2 Thesis outline

Development of a retinal prosthesis leads to many interesting and difficult challenges in biomedical engineering. Of particular interest for the next generation of devices is the question which neural elements of the retina are primarily affected by the stimulating electrodes, because the quality of visual perception

strongly depends on the local selectivity; i.e. electrode arrays should exclusively excite cells within a local area. Another serious problem is running the implant within safety limits, for example such that the neural tissue will not be damaged by irreversible toxic electrode processes or heating. Up to now all clinical trials where blind patients report perceptions induced by an electrode implant concern the epiretinal situation. Therefore the thesis focuses on this implant type.

Concerning the question which neural elements are excited first, Greenberg and coworkers made the following hypothetical considerations [Greenberg et al. 1999]: At any particular location on the surface of the retina, axons from distant sites overlie the individual ganglion cell bodies. If these superficial passing fibers were preferentially stimulated by a prosthesis, groups of ganglion cells from large areas of the retina would be excited. One might expect the visual perception of such a stimulus to appear as a wedge (patients with selective losses of ganglion cell axons at a focal location experience wedge-shaped visual field defects like the shape shown in Fig. 1.4 I). Since the visual world is mapped onto the surface of the retina such that the area of stimulated retinal ganglion cells corresponds spatially to the visual image perceived, this response seems to be logical.

On the other hand, if the ganglion cells were stimulated near their cell bodies, we would expect the visual perceptions to be focal spots as seen in Fig. 1.4 II (patients with focal ablation of the retina perceive a discrete scotoma or blind spot). Obviously, a prosthesis which produced discrete spots of perceived 'light' would have a higher resolution and produce a better image than one which produced large wedges or streaks of perceived 'light'.

Another hypothesis was that the dendrites are preferentially stimulated (Fig. 1.4 III). Since the dendritic arbor of a single ganglion cell may spread up to 500 μm in diameter and overlap the dendritic field of other ganglion cells [Toris et al. 1995], stimulation of dendrites might lead to larger perceived spots than if the soma would be preferentially stimulated.

The outcome of the clinical trials show that the situation is not as simple as it seems in this thought experiment (Fig. 1.5). There are some encouraging aspects such as patients blind from retinitis pigmentosa report a single, small percept after stimulation through one electrode at or slightly above threshold, but this just holds in 48 % of the trials. The elicited perceptions only matches in 32 % of the testings with the spatial pattern of the multi-electrode stimulation, and in no more than 66 % of the performed investigations, driving the same electrode(s) with the same stimulus parameters at different times will yield the same percept [Rizzo et al. 2003b].

Nevertheless these results advise that the neuronal target of the electrical stimulation is in most of the tests not clearly focused on the retinal cells underlying the active electrode. Till now it is not well understood which neural elements are affected by the stimulus current and how the excitation propagates. This is one of the challenges this thesis focuses on.

Another important problem this thesis deals with is the required energy for effective stimulation of the retina. The power requirement for a retinal prosthesis depends primarily on the number of electrodes in the stimulating array and the threshold charge needed for perception. The number of electrodes needed to achieve accurate form perception is unknown. Certainly the very high spatial resolution of natural photoreceptor cells cannot be achieved because this resolution is based on highly specialized pre- and postsynaptic structures that ensure high gain and high-fidelity transmission to second-order cortical neurons. But surprisingly a grid of 25×25 stimulating points placed over the macula is expected to allow a patient to walk in public spaces and recognize big objects and obstacles without requirement of any other special aid [Cha et al. 1992].

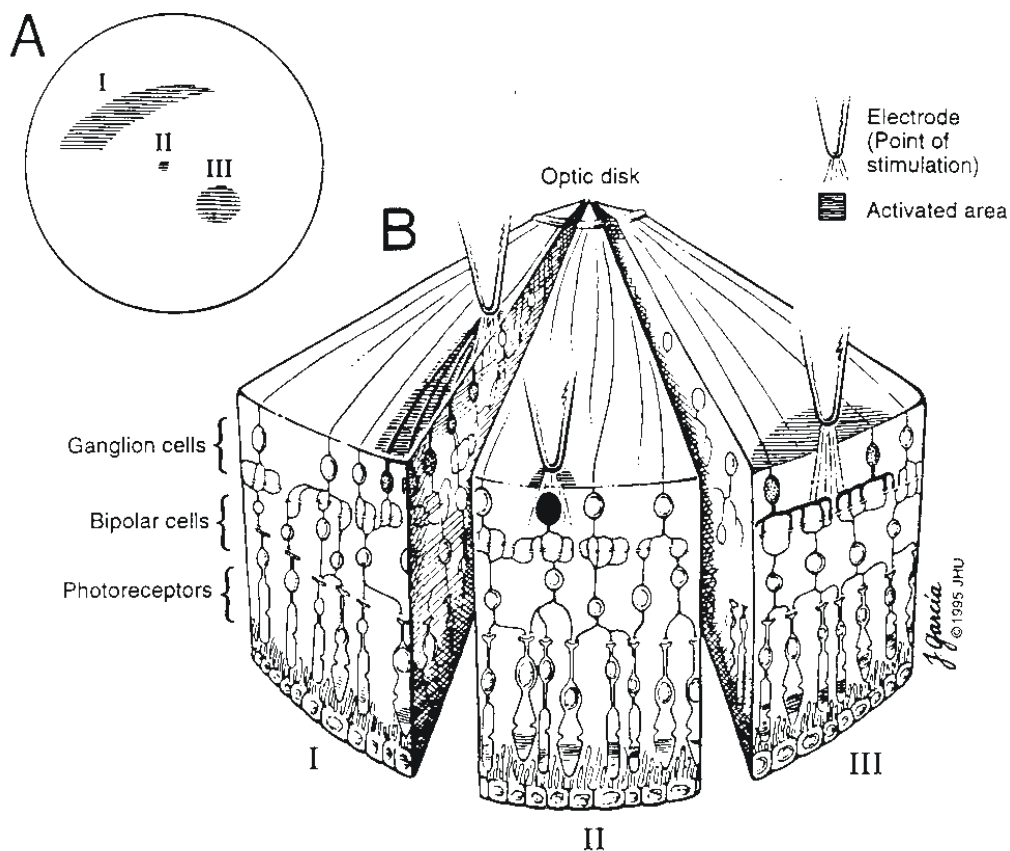


Fig. 1.4 Electrical stimulation of the retinal ganglion cell via its axon (I), soma (II), or dendrites (III): (A) visual fields which would be produced by stimulation of the retinal ganglion cell axon (I), soma (II), or dendrites (III) and (B) cross section of retina showing electrodes and activated ganglion cells. Ganglion cells are shown on the top surface while the bipolar cells and photoreceptors are below. The stimulating electrode is schematically represented above the ganglion cells [Greenberg et al. 1999].

To pack as many electrodes as possible on the implant, respecting the restricted space of the area below or above the retina, very small electrodes would be preferable, with the size of some micrometers. Unfortunately the electrode size

is limited by the safe charge density limit, i.e. the charge per pulse which can be delivered without damaging tissue or electrodes. All existing clinical studies show that the safe charge limits for long term stimulation are difficult to achieve with microelectrodes. Rizzo and coworkers conclude from their clinical trials with 100 μm and 400 μm diameter electrodes that charge densities in blind patients always exceed one seemingly reasonable estimate of safe stimulation [Rizzo et al. 2003a].

Hence it appears that one is forced to use relatively large electrodes, in the order of some hundreds of micrometers, which additionally has the great disadvantage of loosing selectivity. Focused stimulation seems very hard to achieve under this assumption. For clinical application only the electrode surface material with the highest charge safety limits should be used, as oxidized iridium with a limit of about 1-3 mC/cm^2 [Humayun et al. 1996, 1999a, Harpster et al. 2000]. Furthermore a retinal implant with many active electrodes increases the risk of heat damage.

Thus it is evident that beside optimization of the implant fabrication, all possibilities of restricting the required energy have to be considered. This means the goal is to obtain the lowest possible threshold charge required for the stimulation of the neural elements by improvement of electrode design and stimulus pulse properties. This will be a major concern of this thesis pursued with a careful analysis of the excitation process and it will be accomplished by the means of computer simulations.

Chapter 2 discusses anatomical and physiological fundamentals, and the traced target cells with all their special properties are presented. Chapter 3 introduces the models used for the simulations, and drafts their implementation. The excitation process of the electrically stimulated retinal cells is simulated in a two step procedure. In the first step the extracellular potential along the neural structure is calculated either with the finite element software FEMLAB considering the volume conductor inhomogeneities of the eye or analytically in a simpler approach assuming an infinite homogenous medium. In a second step the target cells are represented by compartment models. The membrane kinetics of the diverse retinal cell types are evaluated with three different models.

Chapter 4 is devoted to the question: Which neural elements are excited by electrical stimulation? In the first section the influence of the fundamental retinal cell elements - dendrite, soma, axon - on the excitation process are investigated with the powerful tool of the activating function concept. After that the effect of different soma sizes on the threshold values is examined. This problem arises, because the main morphological difference between the traced mudpuppy ganglion cells and a human ganglion cell is the soma radius, but it turns out that this factor is of minor relevance for the following simulations. The third section deals with the distance between stimulating electrode and target structure. Here a rough estimation is given how many retinal cells can be affected by the stimulating current.

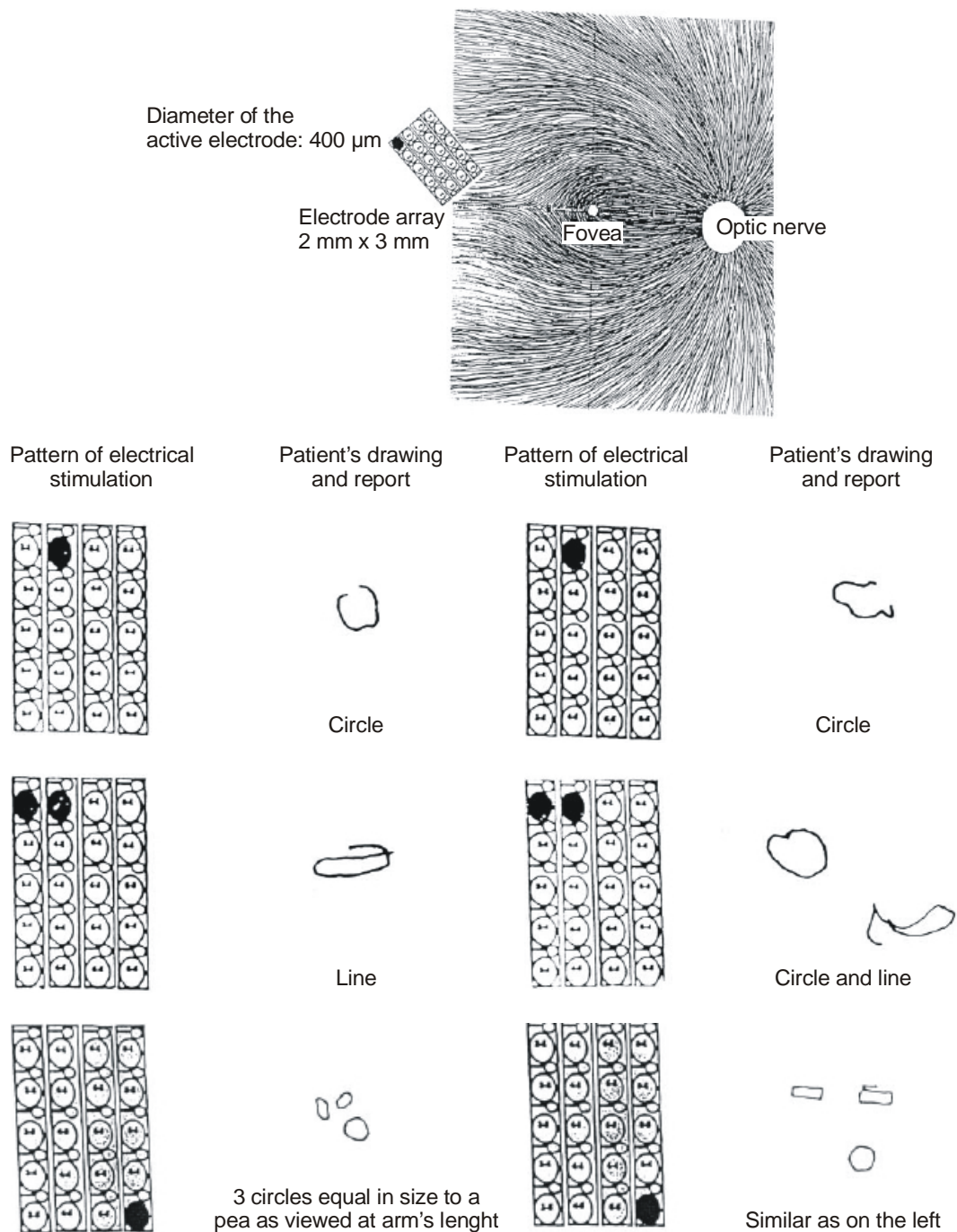


Fig. 1.5 Top: Schematic of the retina of the right eye to show location of the electrode array in relation to the orientation of retinal ganglion cell axons. The array is scaled to size according to the width of the optic nerve head (large, open circular region). Small, open circular region to the left of the optic nerve head represents the fovea. Below: pattern of electrical stimulation, patient's drawing, and record of the elicited percepts. All stimuli were performed by delivering 350 μA per electrode (except bottom line which were 250 μA), 4 ms pulses through a 400 μm electrode (darkened) in bipolar configuration [Rizzo et al. 2003b].

Up to this point it appears that soma and axon are suspected to be the most excitable structure and not the dendrites. But retinal ganglion cells have another special morphological property, a characteristic thinning of the axon, which plays a crucial function in nerve impulse initiation in the natural situation. The fourth section enlightens the role of the axonal thin segment with respect to extracellular electrical stimulation. Finally in the last section the traced retinal bipolar and ganglion cells are included in the model and the initial question is tried to answer. It turns out that the cell geometry, or more precisely the orientation of the specific neural elements relative to the applied electric field, is the determining factor.

Chapter 5 deals with the stimulus duration, which plays an important role in two aspects. First, it is expected that longer pulses support the activation of the bipolar network and in turn lead to small round percepts. Second, with increasing pulse duration the charge density increases, so that the size of the electrode has to be adjusted to the required stimulus length to remain below the safety limit. The strength-duration curves are calculated and show the surprising result that the rheobase (the threshold for a theoretically infinitely long stimulus) has not to be the absolute minimum value. In the second section of Chapter 5 the thresholds for a grid of active electrode positions over a retinal ganglion cell are computed for three different stimulus durations, and once more it reveals the strong influence of the local neuronal geometry. The discussion of the safe charge density limits for spherical electrodes of different size is carried out in the last section. The simulations approve insights concerning the required electrode size resulting from clinical trials.

The aim of Chapter 6 is to develop an effective electrode configuration for selective stimulation with an epiretinal implant. The target is avoiding the co-stimulation of bypassing axons coming from distant regions. The presented results reflect the evolving insights from small disk electrodes, via rectangular electrodes, to a sophisticated implant geometry. In a first step the object of investigation is the optimization of the electrode geometry concerning the dipole distance. It turns out that the threshold curve has a minimum that depends on the distance between electrodes and target structure. This result follows right from the analysis of the activating function. In the second section different electrode designs are investigated. The main results are that disk electrodes need smaller threshold currents than spherical ones, and long electrodes parallel to the axonal pathways at the retinal surface seems to be good candidates for local selective stimulation.

Electrical stimulation with long rectangular electrodes avoids the excitation of bypassing axons, but it has the disadvantage to loose selectivity in the direction of the electrode. Moreover spikes can be generated at the edges of the electrodes, where the curvature of the potential distribution will increase. In the last section a sophisticated epiretinal implant is proposed which minimizes the ‘edge effect’ and improves the ability of focal stimulation.

Discussion and conclusions of the obtained results and a prospect of the challenges in future complete this thesis.

2. The retina

The aim of this chapter is to provide the anatomical and physiological fundamentals for this thesis. The chapter is divided into three sections. In the first section the neural elements of the retina are described. The second section deals with the sophisticated information processing through the retina, and it also goes into which patients are possible candidates for a retinal prosthesis.

In healthy people's eye the signal is transmitted from 130 million photoreceptors to 1 million ganglion cells by serial and parallel pathways by complex mechanisms which are still investigated with great effort. An example of new insights on the visual perception was recently presented by Werblin and coworkers who reported that more than a dozen types of ganglion cells are involved, every of them transporting a different image with individual characteristics [Roska and Werblin 2003]. Although the first generation of retina implants will not be able to take into account the multiple neural images the retina creates, a further generation will have to.

Without going into all details the next two sections review the following literature: Boycott and Wassle 1974, 1991, Kolb 1991, Kolb et al. 1981, 1992, Masland 2001, Polyak 1941, Sterling and Demb 2004, Van Buren 1963, Young and Heath 2000.

The third section is devoted to the retinal cells used for the simulations of this thesis.

Starting with a look into someone's eyes, we can easily see several structures (Fig. 2.1):

- o A black-looking aperture, *the pupil*, which allows light to enter the eye (it appears dark because of the absorbing pigments in the retina).
- o A colored circular muscle, *the iris*. This circular muscle controls the size of the pupil so that more or less light, depending on the brightness, is allowed to enter the eye.
- o A transparent external surface, *the cornea*, which covers both the pupil and the iris. This is the first and most powerful lens of the optical system of the eye and allows, together with *the crystalline lens* the production of a sharp image at the retinal photoreceptor level.
- o The 'white of the eye', *the sclera*, which forms part of the supporting wall of the eyeball. The sclera is continuous with the cornea.

When we remove the eye from the orbit, we can see that the eye is slightly asymmetrical compared to a sphere with an approximate sagittal diameter or

length of 24 to 25 mm, a transverse diameter of 24 mm and a volume of about 6.5 cm³ (Fig. 2.1)

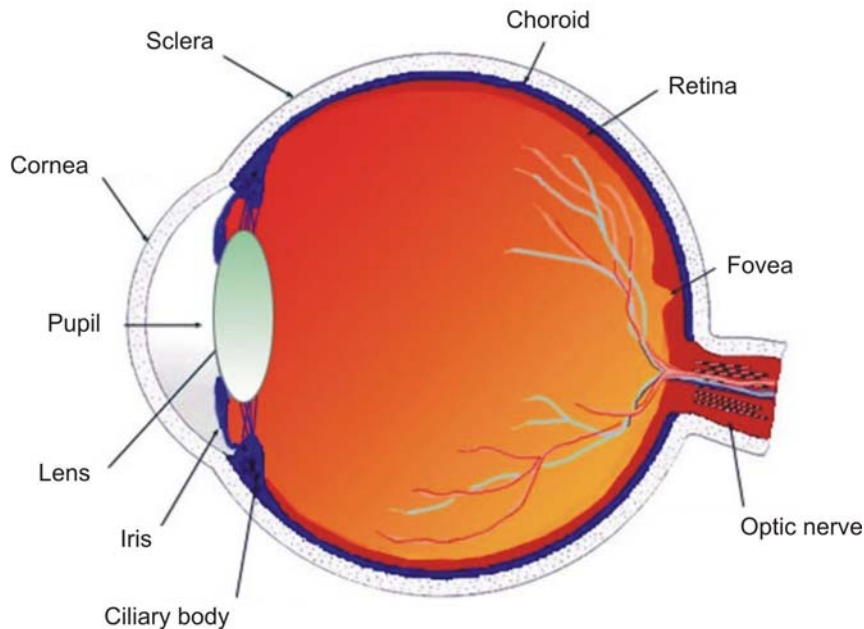


Fig. 2.1 *Sagittal section of the human eye.*
[<http://www.webvision.med.utah.edu/anatomy.html>]

2.1 Anatomy of the retina

The retina is a filmy piece of tissue, barely half a millimeter thick, that lines the inside of the eyeball. The tissue develops from a pouch of the embryonic forebrain, and the retina is therefore considered part of the brain.

The central point for image focus (along the visual axis) in the human retina is the fovea. Here a maximally focused image initiates resolution of the finest detail and direct transmission of that detail to the brain for the higher operations needed for perception. Slightly more nasally than the visual axis is the optic axis projecting closer to the optic nerve head. The optic axis is the longest sagittal distance between the front of the cornea and the furthest posterior part of the eyeball. A circular field of approximately 6 mm around the fovea is considered the central retina while beyond this is peripheral retina stretching to the ora serrata, 21 mm from the center of the optic disc. The total retina is a circular disc of approximately 42 mm diameter (Fig. 2.1).

The retina, like many other central nervous system structures, contains a huge diversity of neuronal types. Mammalian retinas contain many distinct cell types, each with a different function (Fig. 2.2 and Fig. 2.5).

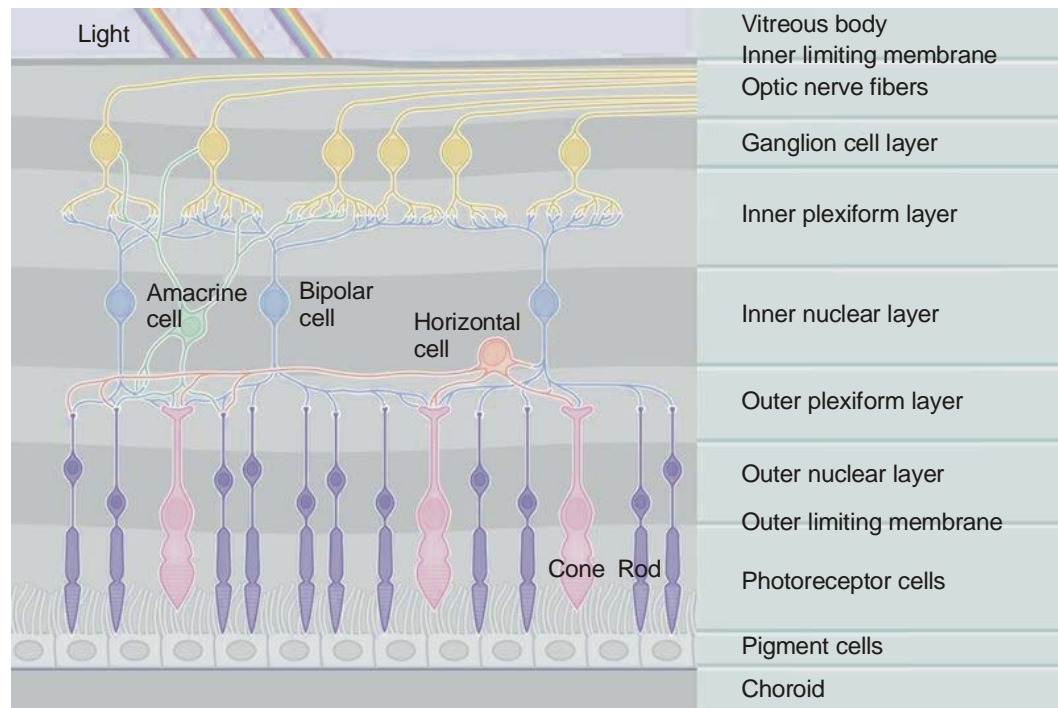


Fig. 2.2 *Schematic section through the retina.*
[Young and Heath 2000]

Input elements: photoreceptors

Intuitively, one might expect that the surface of the retina (the layer exposed to the liquid in the eyeball's vitreous chamber) would contain the sensory cells, the photoreceptors, but actually these cells lie at the very back of the retina; light rays must pass through the entire retina before reaching pigment molecules to excite (Fig. 2.2). This is because the pigment-bearing membranes of the photoreceptors have to be in contact with the eye's pigment epithelial layer, which provides a steady stream of the vital molecule, retinal or vitamin A.

Light intensity in the natural environment varies over a range of about 10^{10} lux, and we can see over this entire range. Two types of receptor divide the range: *rods* and *cones*. Rods are generally used for low-light, night vision and cones for daylight, bright-colored vision.

Cones are robust conical-shaped structures that have their cell bodies situated in a single row right below the outer limiting membrane and their inner and outer segments protruding into the subretinal space towards the pigment epithelium. In the foveal retina, where only cones are concentrated, their cell bodies are layered in oblique columns below the outer limiting membrane. Rods, on the other hand, are slim rod-shaped structures with their inner and outer segments filling the area between the larger cones in the subretinal space and stretching to the pigment epithelium cells. Rod cell bodies make up the remainder of the outer nuclear layer below the cone cell bodies. Apical processes from the pigment epithelium envelope the outer segments of both rods and cones.

Mammals have a single type of rod with a peak sensitivity at about 500 nm. This makes sense because at night photons are too sparse to be worth segregating by wavelength. But in daylight there are plenty of photons, so most mammals gain extra information by using two cone types with different spectral sensitivity. Most cones (at least 90 %) are tuned to middle wavelengths (peak at 550 nm), termed 'M' or green. A few are tuned to short wavelengths (peak at 450 nm), termed 'S' or blue. S cones form a sparse but rectangular mosaic and connect via a selective circuit to a special type of ganglion cell. Old World primates (including humans) are special in being 'trichromatic', meaning that there is an additional cone type tuned to long wavelengths (peak at 570 nm), termed 'L' or red.

Intrinsic elements for forward transmission: bipolar and AII cells

Bipolar cell somas occupy the middle region of the inner nuclear layer. Their dendrites ascend to collect synapses from photoreceptors. One bipolar type collects only from rods, and most other types collect only from cones. However, one bipolar type in rodent retina receives chemical synaptic input directly from both rods and cones. Bipolar axons descend to the inner plexiform layer where they provide ribbon synapses, each directed at a pair of postsynaptic processes (Fig. 2.3).

The rod bipolar soma (about 7 μm diameter) is located high in the outer nuclear layer. The narrow, candelabra-like, dendritic arbor penetrates the stratum of cone terminals to reach the overlying rod terminals where it collects signals from 15-45 rods in human. The rod bipolar axon descends without branching to the deepest stratum of the inner plexiform layer where it contacts not ganglion cells, but a third order intrinsic neuron, termed the AII amacrine cell (Fig. 2.2).

The cone bipolar somas are also small (about 8 μm diameter), and the dendritic fields are narrow (about 15 μm). The dendritic arbor typically collects signals from 5-10 overlying cone terminals without skipping any. An exception is the S cone bipolar cell, which does skip overlying M and L cones to contact S cones exclusively. Cone bipolar axons descend to the inner plexiform layer, where each type selects a particular stratum and contacts both amacrine and ganglion cells. Cone bipolar terminals employ 30-130 ribbon synapses, depending on cell type.

Some bipolar cells are excited (i.e., less polarized) by light onset, whereas others are excited by light offset. The two categories of axons terminate at different levels: OFF axons arborize in the upper half of the inner plexiform layer, and ON axons arborize in the lower half. Within these OFF and ON regions, multiple types segregate in different strata. Note most cell types of the retina do not generate action potentials but operate by changing the transmembrane voltage gradually.

AII cells are small-field amacrine cells that have a seminal role in the rod pathways, and in linking the rod and cone pathways so that the rod signals can

also use the cone bipolar pathways to ganglion cells. The narrow-field bistratified rod amacrine cell, AII, collects purely from rod bipolars and serves a feedforward link in the rod's starlight pathway. AII cells distribute densely and thus constitute about 20 % of the amacrine layer cells.

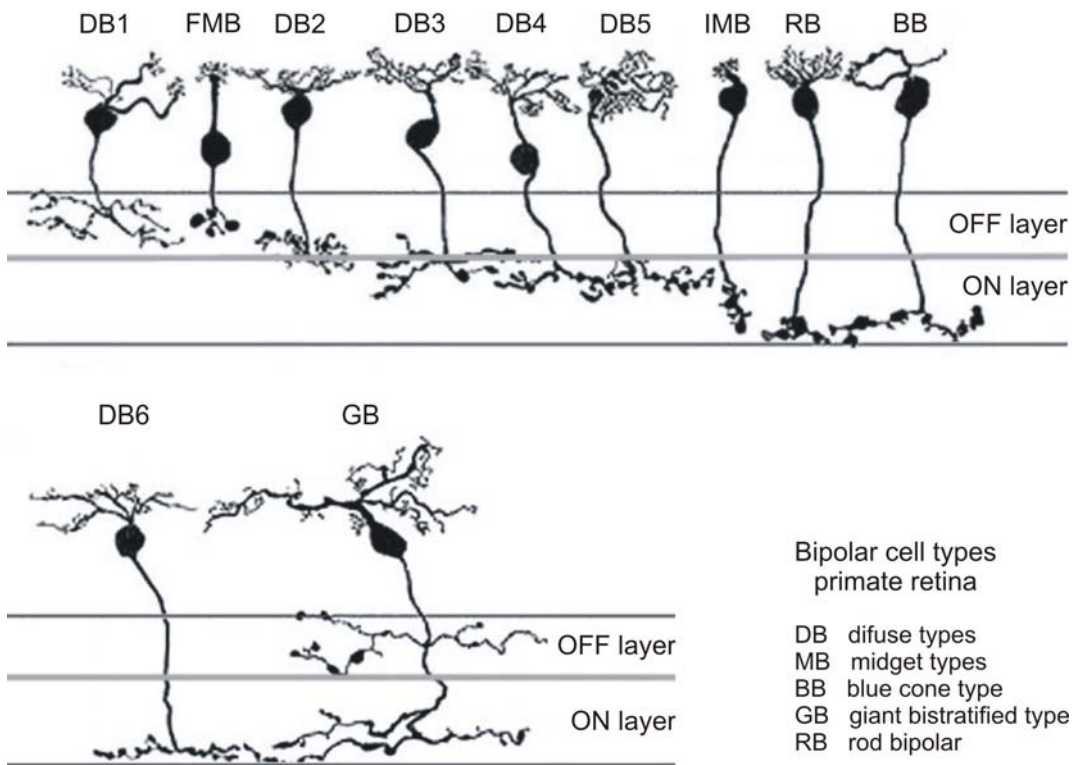


Fig. 2.3 Bipolar cells from Golgi-stained primate retina, seen in a vertical section.

[<http://www.webvision.med.utah.edu/anatomy.html>]

Output elements: ganglion cells

Ganglion cell bodies form the innermost cellular layer of the retina (Fig. 2.2 and Fig. 2.4). Their dendrites penetrate the inner plexiform layer to collect excitatory synapses from bipolar axons and both excitatory and inhibitory synapses from amacrine cells. Ganglion cell axons enter the optic nerve and extend to the brain. The human optic nerve contains about 1.2 million axons.

In respect of their dendritic arbor ganglion cells are remarkably diverse – on the order of 20 types [Sterling and Demb 2004]. Each morphological type has a distinctive physiology. For example, the ganglion cell with a planar, ‘loopy’ dendritic arbor responds selectively to stimuli moving in a particular direction.

Each type of ganglion cell distributes to a particular brain region, which uses the special information carried by that cell. Thus the nucleus of the optic tract, which controls optokinetic eye movements, collects from the directionally selective ganglion cell. And the suprachiasmatic nucleus, which uses light to reset circadian rhythms, collects from another type that branches over extremely wide

areas. This ganglion cell type is unusual, because it expresses its own visual pigment, melanopsin, and thus monitors light levels independently of the rods and cones. Other types of motion-selective ganglion cell project to the superior colliculus – which uses the information to orient the head and eyes. The key region for mammalian visual processing is the striate cortex, which receives its main thalamic input from the dorsal lateral geniculate nucleus. Thus, it is to this nucleus that most ganglion cells project.

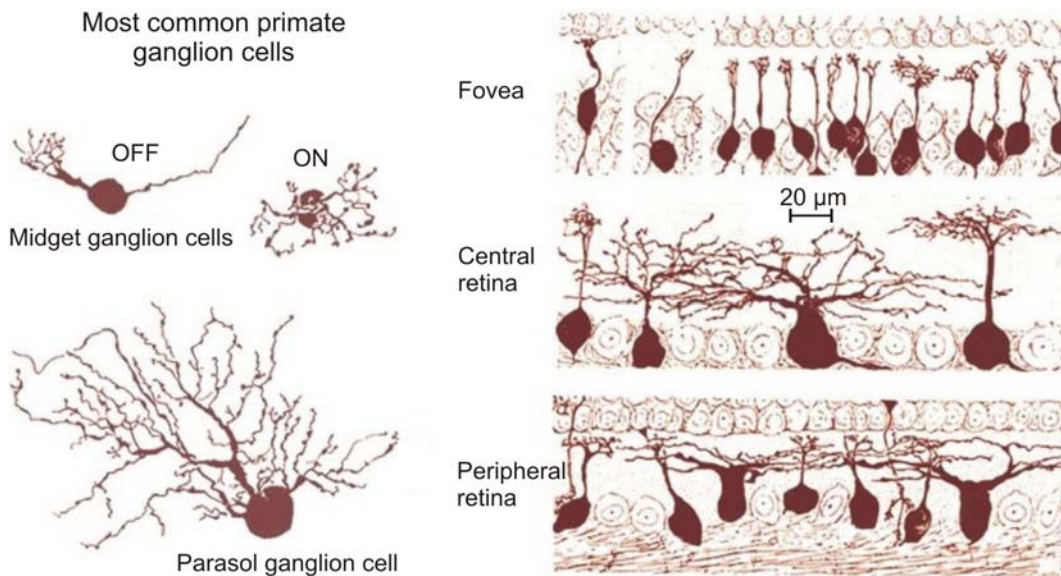


Fig. 2.4 Left: Most common primate ganglion cells are midget ganglion cells (P cells) and parasol ganglion cells (M cells) that occur as ON and OFF pairs.

[From <http://www.webvision.med.utah.edu/anatomy.html>]

Right: View of Golgi stained ganglion cells in vertical section. [From Polyak 1941]

Two basic types of ganglion cells - ON center and OFF center - form the major output of the retina to the visual centers in the brain. ON ganglion cells are activated when a spot of light falls in the center of their receptive field and are inactivated when light falls on the field's periphery. OFF ganglion cells react in the opposite way: Their activity increases when the periphery of their receptive field is lit and decreases when light falls on the center of the field.

The primate retina express a division into ON and OFF versions of narrow-field, tonic cells and wider-field phasic cells (Fig. 2.4). The narrow-field types are termed midget cells because in central retina the dendritic arbor collects from a midget bipolar cell with input from a single cone, but more peripherally the arbor broadens to collect from many midget bipolar cells. Midget cells are also termed 'P' cells because they project to the lateral geniculate's parvocellular layers.

The wider-field cells are morphologically diverse. Some are termed parasol because of their broad, flat dendritic arbors. These are also termed 'M' cells because they project to the geniculate magnocellular layers. However, other

types of wide-field ganglion cell probably also project to the magnocellular layers, so the term M cell probably includes diverse types.

Intrinsic elements for lateral transmission: horizontal and amacrine cells

Horizontal cell somas form the upper tier of the inner nuclear layer, and the processes connect exclusively within the outer plexiform layer. Collecting widely from receptors, their main task is to average the signals and feed negatively back onto receptor terminals and forward onto bipolar dendrites. Horizontal cells couple to each other electrically. The strength of this coupling changes with adaptive state and is modulated by dopamine secreted by certain cells in the amacrine layer.

Two types of horizontal cell in diurnal mammals connect with cones. One has thick dendrites, a wide field and couples strongly to its neighbors; the other has thin dendrites, a narrow field and couples weakly. Generally, each type connects to all the cone terminals in its dendritic field. However, in primate the large-field cell avoids S cones, and the narrow-field cell connects especially strongly to them.

One of the two types of horizontal cell connects with rods. It does so by emitting a fine axon that in cat meanders for several millimeters and then breaks into an elaborate arbor that contacts several thousand rods. This axon also couples to its neighbors and thus pools signals from tens of thousands of rods. This is not the usual sort of axon because it lacks action potentials; further, cone input to the dendrites does not reach the rod axon arbor, so it must be electrically isolated from the soma. On the other hand, the horizontal cell soma does receive strong rod signals, which must therefore come via rod-to-cone gap junctions. Thus, the soma serves metabolically two processes with utterly different connections.

Amacrine cell somas form the lower tier of the inner nuclear layer and are also numerous in the ganglion cell layer, where they are called displaced. Amacrine cells connect exclusively within the inner plexiform layer (plus some synapses in the ganglion cell fiber layer) and are diverse in extreme; there are about 40 types.

Besides the already mentioned AII narrow-field amacrine, which collect purely from rod bipolar, other narrow-field amacrine purely collect from cone bipolar terminals. These types, which exist as both ON and OFF forms, must distribute densely to tile the plane. This pattern of connection may reflect lateral inhibition across a small spatial scale covering tens of microns rather than hundreds as for the horizontal cells.

Certain medium-field amacrine cells collect from cone bipolars and arborize intimately with dendrites of certain ganglion cell types. For example, the starburst amacrine cell associates with other members of its own type to form a loopy pattern that in primate probably associates with the co-planar arbors of parasol ganglion cells. There are separate starburst populations for the ON and the OFF levels of the inner plexiform layer. The starburst cell response phasically to

glutamatergic bipolar input and releases a pulse of acetylcholine onto the ganglion cells. The acetylcholine, binding to the nicotinic receptors, excites ganglion cells. Thus, the starburst circuit probably boosts ganglion cell transient responses, enhancing sensitivity to motion. Several studies suggest that the starburst cell fires action potentials.

Some types of wide-field amacrine connect exclusively to rod bipolar cells, but other wide-field types arborize in strata supplied only by cone bipolar terminals. The dendritic fields reach about 500 to 1000 μm – probably near the bio-electrical resolution limit for fine, passive cables. However, the proximal region of each dendrite sprouts a fine axon that travels centrifugally for at least 3 mm. Such a cell resembles a wagon wheel, with the dendritic field for a hub and the axons as radiating spokes. These axons conduct full action potentials, which appear to travel centrifugally. Long-range amacrine cells mediate the inhibition and excitation of certain ganglion cells evoked by stimuli millimeters beyond the conventional receptive field.

2.2 From optical to neural image

The retina's task is to convert an optical image from the optical system of the eye (cornea, pupil, lens) into a 'neural image' for transmission down the optic nerve to a multitude of centers for further analysis. The task is complex – which is reflected in the synaptic organization. The transformation from optical to neural image involves three stages:

1. transduction of the image by *photoreceptors*;
2. transmission of these signals by excitatory chemical synapses to *bipolar neurons*; and
3. further transmission by excitatory chemical synapses to *ganglion cells*.

Ganglion cell axons collect in the optic nerve and project forward to the brain. At each synaptic stage there are specialized laterally connecting neurons called *horizontal* and *amacrine* cells. These modify (largely by inhibitory chemical synapses) forward transmission across the synaptic layers (Fig. 2.2 and Fig. 2.5).

A closer look at this apparently simple design (three interconnected layers and five broad class of neuron) reveals additional complexity. As described in the last section each neuron class is represented by several or many specific types. Each cell type is distinguished from others in its class by its characteristic morphology, connections, neurochemistry, and function. This diversity is necessary, because it is impossible to encode all the information in an optical image using a single neuronal image. Therefore, the retina uses different cell types to create parallel circuits for simultaneous transmission of multiple neural images to the brain. The retina also creates separate circuits for different light levels –

daylight, twilight, and starlight – but these share certain circuit components and use the same final pathways to the brain.

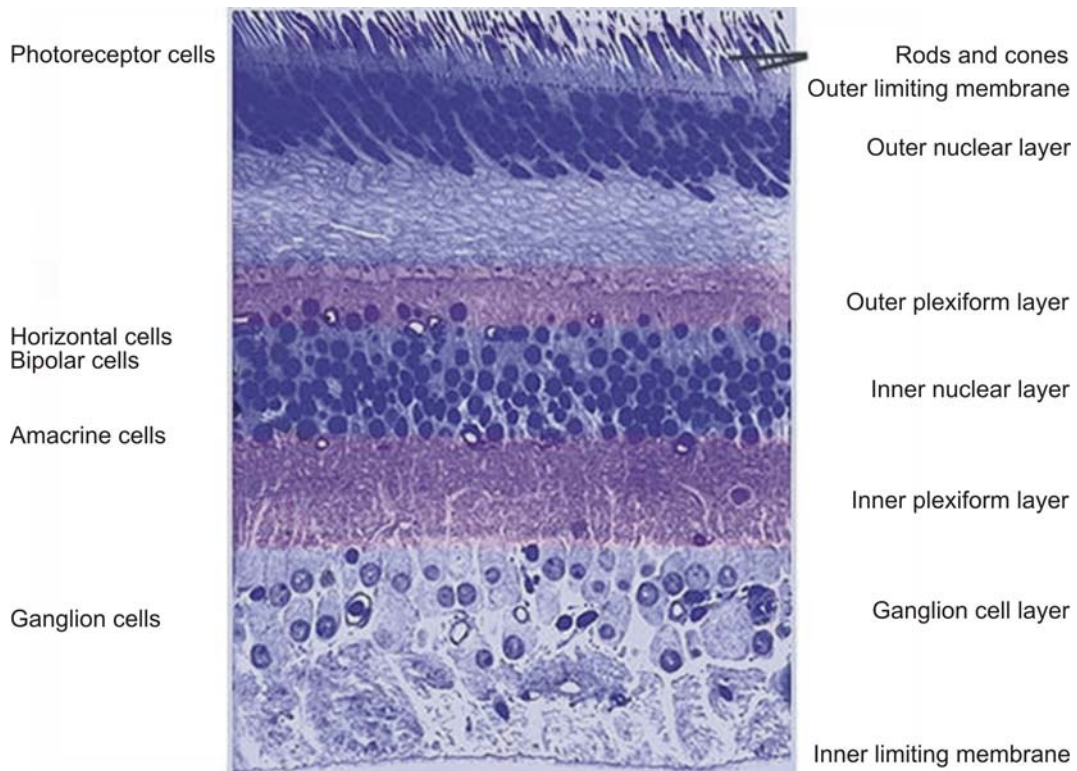


Fig. 2.5 *Light micrograph of a vertical section through central human retina.*
[Young and Heath 2000]

Circuitry for rod signals through the retina

Whereas cones connect in a direct pipeline to bipolar cells to ganglion cells, the bipolar cells that receive input from rods do not synapse with ganglion cells directly. The bipolar cells connected to rods are all of one type, solely transmitting an ON signal, and use the AII and A17 amacrine cells as intermediaries to get signals to ganglion cells. The small-field AII cell collects from about 30 rod-connected bipolar cells and transmits a depolarizing message both to ON (light-detecting) cone bipolar cells and to their ON ganglion cells and to OFF cone bipolar cells and OFF ganglion cells. It is as if the AII cells developed in the rod-dominated parts of the retina as an afterthought to the cone-to-ganglion cell architecture and now takes advantage of the pre-existing cone pathway circuitry.

At the same time, the A17 amacrine cell collects rod messages from thousands of rod-connected bipolar cells. It somehow amplifies and modulates the information from the rod bipolar cells to transmit to the AII cells, but how it does this is not completely understood. In any case, the rod pathway with its series of convergent and then divergent intermediary neurons is clearly well designed to collect and amplify scattered vestiges of light for twilight and night vision.

Circuits for ganglion cell receptive field

The *center* circuit turns out to be fairly simple: the cones co-spatial with the ganglion cell dendritic field modulate glutamate release onto dendrites of cone bipolar cells whose axons contact to the ganglion cell dendritic tree. Brightening these cones depolarizes the ON bipolar cells and delivers glutamate to ON ganglion cell dendrites; dimming these cones depolarizes the OFF bipolar cells and delivers glutamate to OFF ganglion cell dendrites. Thus, the center circuit is purely excitatory.

The number of cones that connect directly to a ganglion cell dendritic arbor depends on species, retinal location, and ganglion cell type. In primates, the receptive field centers are relatively small. For example in the fovea a single cone contacts a pair of ‘midget’ bipolar cells (ON and OFF) that in turn contact, respectively, ON and OFF ‘midget’ ganglion cells. This 1:1 bipolar-to-ganglion cell connection is accomplished with only about 50 synapses. Generally each red or green cone in the central fovea connects to two midget ganglion cells, so at all times each cone can either transmit a dark-on-light (OFF) signal or a light-on-dark (ON) message. The message that goes to the brain carries both spatial and spectral information of the finest resolution.

In the periphery, e.g. 20 degrees, from the axis, about 10 cones overlie the midget ganglion cell. Here, although each cone still contacts its own private midget bipolar cell, several of these converge onto a midget ganglion cell. The wider-field ganglion cells, ‘parasol’ and ‘garland’ cells, collect on the order of 30-50 cones.

The inhibitory *surround* arises first at the cone terminal. Whereas a bright spot hyperpolarizes a central cone, a bright annulus hyperpolarizes surrounding cones. This suppresses their tonic excitation of horizontal cells, reducing GABA released onto the central cone and causing it to depolarize, in antagonism to its light response. Illuminating a small patch of cones, corresponding to the ganglion cell center, hardly affects horizontal cells because the patch constitutes at most a few percent of horizontal cell input. But covering a wide field of cones (50-80 times as many as the center) is effective.

The bipolar cell, by summing center-surround receptive fields of 5-10 converging cones, begins in the outer plexiform layer to establish its own center-surround receptive field. Another contribution to the bipolar cell’s surround comes from horizontal cell release of GABA onto receptors on the bipolar dendrite. Cone glutamate release drives ON and OFF bipolar cells in opposite directions depending on their glutamate receptor. Horizontal cell release also drives ON and OFF bipolar cells in opposite directions, but does so using only one class of receptor. Then the bipolar response pattern carries forward via excitatory synapses onto the ganglion cell.

S-cone pathways

Messages from blue cones are not processed in the same way as from red and green cones for some reason, possibly because the blue system is older in evolutionary terms. Blue cones transmit information through a special blue cone bipolar cell to a different type of ganglion cell, which can carry both a blue ON and a yellow OFF response.

Diseases of the human retina

It is obvious that not in all kinds of blindness a retinal implant can restore vision. To make such a device helpful an essential population of retinal ganglion cells has to have neural connection to the central visual system, which is still able to operate. Therefore primarily patients suffering from the following degenerative diseases, which affect mainly the photoreceptor layer will benefit from a retinal implant:

Retinitis pigmentosa is a general term for a number of diseases that predominately affect the photoreceptor layer of the retina. These diseases are usually hereditary and affect individuals earlier in life. Injury to the photoreceptor cell layer, in particular, reduces the retina's ability to sense an initial light signal. Despite this damage, the remainder of the retinal processing cells in other layers usually continue to function. Although different forms of retinitis pigmentosa may affect different specific areas of the visual field, mostly it affects the mid-peripheral vision first, and – sometimes - progresses to affect the far-periphery and the central areas of vision. The narrowing of the field of vision into 'tunnel vision' can sometimes result in complete blindness.

Age-related macular degeneration refers to a degenerative condition that occurs most frequently in the elderly. This disease progressively decreases the function of specific cellular layers of the retina's macula. The affected areas within the macula are the outer retina and inner retina photoreceptor layer. Patients with macular degeneration experience a loss of their central vision, which affects their ability to read and perform visually demanding tasks. Although macular degeneration is associated with aging, the exact cause is still unknown.

Together, age-related macular degeneration and retinitis pigmentosa affect at least 30 million people in the world. They are the most common causes of untreatable blindness in developed countries and, currently, there is no effective means of restoring vision.

2.3 Morphology of the target cells

For the simulations four retinal cells were used. Three of them are traced retinal cells of a mudpuppy (*Necturus maculosus*). These three cells - two

ganglion cells and one bipolar cell - where stained and traced by Toby Velte, who made them available for this thesis (Fig. 2.6, Fig. 2.7, and Fig. 2.8).

The *Necturus*, an aquatic salamander, is an amphibian that fails to complete its metamorphosis. All the nuclei in its cells begin mitosis and make copies of their chromosomes in preparation for a metamorphosis that never happens. Therefore nuclei contain doubled chromosomes, and hence the cell bodies are relatively large. These large cell bodies are less difficult to impale with microelectrodes, making it possible to record responses from the cells of this salamander retina. Hence also the special membrane model for retinal ganglion cells used in the thesis is derived from voltage clamp studies of this species.

The fourth used retinal cell is a serial reconstruction of a cat rod bipolar cell provided by Barbara McGuire from the University of Pennsylvania Medical Center, Laboratory of Retinal Microcircuitry. A picture of the cell can be found in the Internet under the address http://retina.anatomy.upenn.edu/cells/ret_cells.html (see also Fig. 2.9). In the following these cells will be referred to as Ganglion cell #1, #2, Bipolar cell #1, and #2, respectively. Now a detailed description of them is given.

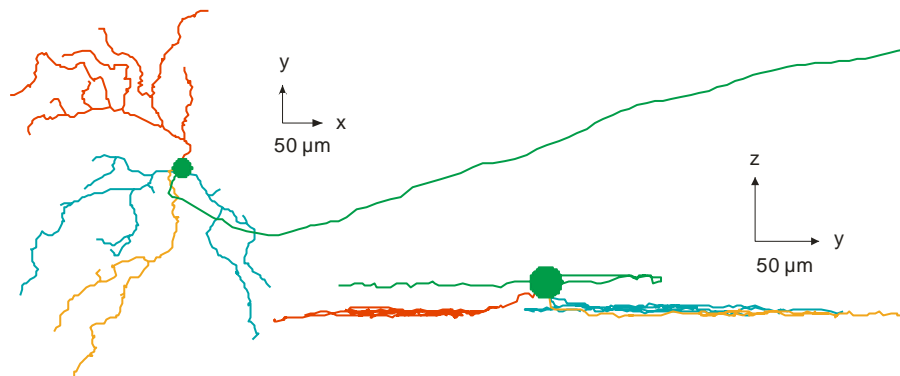


Fig. 2.6 Retinal ganglion cell #1 in x, y and y, z plane. Soma and axon drawn in green color. Changing diameters of the compartments are not included.

Ganglion cell #1

The x-, y-, and z-coordinates of 819 points with an average distance of 5.15 μm as well as the actual fiber diameters are describing this cell (Fig. 2.6). In x-direction the widest extension of the dendritic field is 340 μm, in y-direction the greatest distance of two dendritic points is 482 μm. The full expansion of the cell in z-direction is 36.5 μm.

This salamander ganglion cell has three dendritic trees which connect directly to the soma, and the entire dendritic field has 23 branching points. The average diameter of a dendrite is 0.83 μm, which is decreasing from the soma (mean value 1.4 μm) to the end (mean value 0.76 μm). The diameter of the actual traced mudpuppy soma is 24 μm, but to be a better approach for the human case sometimes a 10 μm soma is modeled. For the influence of the soma size on thresholds see Section 4.2.

The length of the axon emerges of the ganglion cell soma is 1.1 mm. Morphological studies of retinal ganglion cells in the mudpuppy identified a characteristic thinning of the axon that begins after the initial segment. Morphometric analysis of the thin segment revealed an average length of $74\mu\text{m}$ with a standard deviation of $22\mu\text{m}$ [Carras et al. 1992]. In the case of the ganglion cell #1 the thin segment is $67.53\mu\text{m}$ long, starts $44.6\mu\text{m}$ after the center of the soma, and has an average diameter of $0.5\mu\text{m}$, whereas the rest of the axon has an average diameter of $0.68\mu\text{m}$.

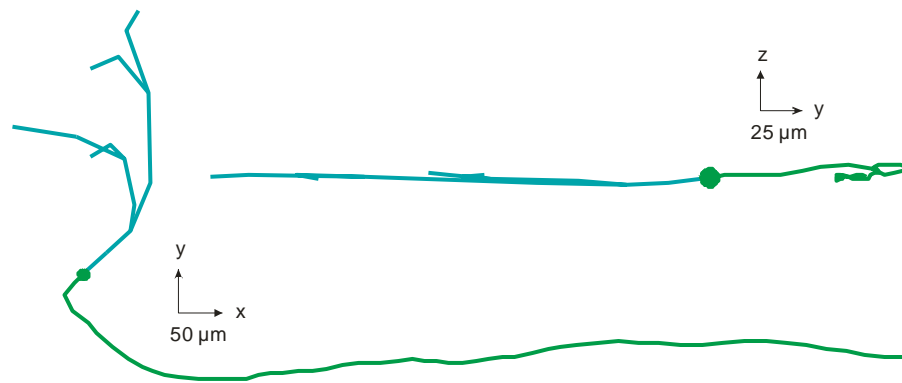


Fig. 2.7 Retinal ganglion cell #2 in x, y and y, z plane. Soma and axon drawn in green color. Changing diameters of the compartments are not included.

Ganglion cell #2

This cell (Fig. 2.7) was created, by cutting four main branches of the dendritic tree of a traced mudpuppy ganglion cell to simulate a smaller cell type, and in order to save computing time. Finally, it was only used for investigations, where the extension of the dendritic tree is of minor influence.

The ‘reduced’ retinal ganglion cell has 69 compartments with an average length on the dendrites of $53.86\mu\text{m}$ and an axonal compartment length of $19.3\mu\text{m}$. It has been left only one dendritic branch originating directly from the soma, with 3 branching points. The dimension of the dendritic tree in x -direction is $202\mu\text{m}$ and in y -direction $316.1\mu\text{m}$. The entire cell has a rather two-dimensional structure and extends in z -direction over $13.5\mu\text{m}$. For the soma of this cell the same applies as for soma of ganglion cell #1.

The thin segment of this ganglion cell starts $55.28\mu\text{m}$ after the center of the soma and it is $90.62\mu\text{m}$ long, with a diameter of $0.5\mu\text{m}$. The average diameter of the axon without the thin segment is $64\mu\text{m}$ and the entire length of the axon is about 1 mm.

Bipolar cell #1

The third cell is a bipolar OFF cell of a mudpuppy (Fig. 2.8), which is defined by 340 tracing points with an average distance of $3.58\mu\text{m}$. The soma diameter amounts to $14\mu\text{m}$. 7 dendritic trees connect directly to the soma; altogether they have 26 branching points.

The extension of the cell in x-direction is $154\ \mu\text{m}$, in y-direction $158.5\ \mu\text{m}$, and in z-direction $34\ \mu\text{m}$. The diameter of the dendrites amounts on average $1.57\ \mu\text{m}$.

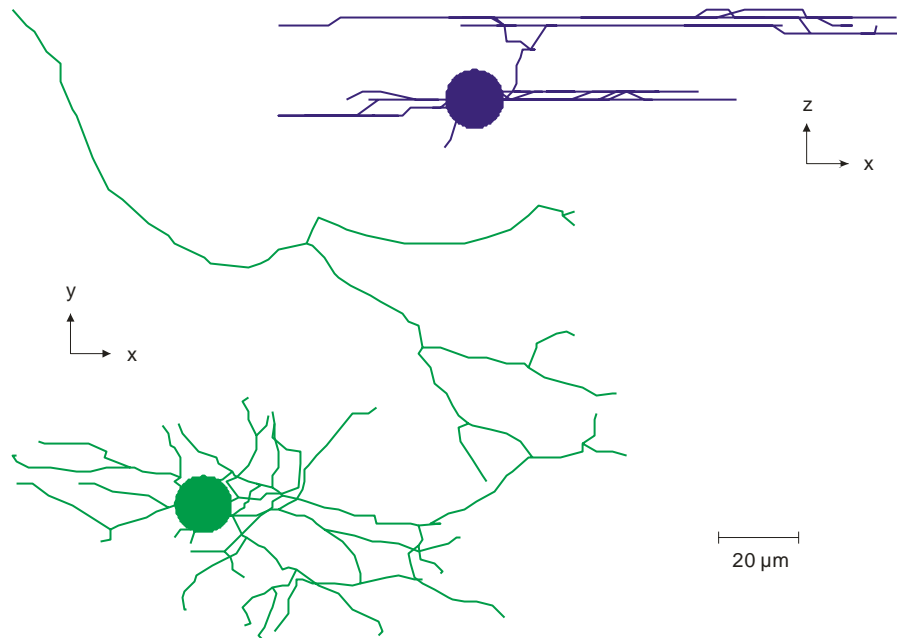


Fig. 2.8 Retinal bipolar cell #1 in x, y and x, z plane. Diameter of the compartments are not in scale.

Bipolar cell #2

The last cell (Fig. 2.9 left) is a very simple cat rod bipolar cell used mainly for investigations concerning the orientation of the bipolar cells in the retina. This cell is the only one which is not traced, but was reconstructed from a picture (Fig. 2.9 right).

14 compartments are sufficient to describe this cell. Their average length is $4.56\ \mu\text{m}$ and their average diameter is $1.41\ \mu\text{m}$. The soma is approximated by a sphere with radius $8.3\ \mu\text{m}$. The bipolar cell extends $52.3\ \mu\text{m}$ through the retina. The two dendritic branches have no bifurcations.

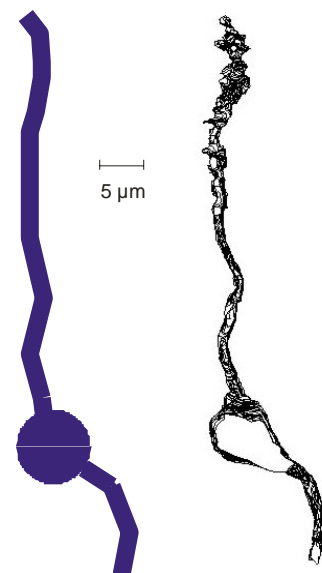


Fig. 2.9 Left: Bipolar cell #2
Right: Serial reconstruction of a cat rod bipolar cell.
[http://retina.anatomy.upenn.edu/cells/lab_cells.html]

3. Modeling

In this chapter the methods needed for the simulation are discussed. It describes how the physiological and anatomical properties of the eye and their reaction in the presence of an applied electric field are modeled. The chapter is divided into four sections. The first section is devoted to the electrical network model for the four target cells described in Section 2.3. A good representation depends essentially on an adequate membrane model [Resatz and Rattay 2003a, 2004]. Three of them are specified in the second section: a passive model for the bipolar cells and two active models for the ganglion cells. Particularly the Fohlmeister, Coleman, and Miller model is worth mentioning, since in literature there are very few membrane models available for special cell types [Fohlmeister and Miller 1997a, b]. Since a sophisticated electrode design is one of the goals of this work, great importance is attached to the volume conductor model. Two in principle different approaches are described in the third section. The last section is devoted to the implementation of the previously discussed models.

3.1 Electrical network model

Retinal cells consist of subunits with different electrical properties, e.g. in retinal ganglion cells the neural membranes are quite different in dendrites, soma, initial and thin segment of the axon and the rest of the axon. To simulate neural reactions, the subunits are further divided into several segments. The electrical properties of every segment are represented by an electrical circuit. The shapes of the segments are approximated by cylinders, except the soma, which is modeled as a sphere (Fig. 3.2). The resulting model is called a ‘compartment model’ and each part is called a compartment.

Thus every compartment has its individual shape, geometric and electric parameters. Electrically a compartment is represented as a single point in the center of the cylinder and sphere respectively. According to Fig. 3.1 the current to the central point of the n -th compartment (marked by crossed lines) consists of the following components: capacitive current ($I_{C,n}$), ion currents across the membrane ($I_{ion,n}$) and ohmic currents to the neighbors ($I_{R,n}$), i.e. applying Kirchhoff’s law results in

$$I_{C,n} + I_{ion,n} + I_{R,n} = 0, \quad (3.1)$$

or in more detail

$$\frac{d(V_{i,n} - V_{e,n})}{dt} C_n + I_{ion,n} + \frac{V_{i,n} - V_{i,n-1}}{R_n/2 + R_{n-1}/2} + \frac{V_{i,n} - V_{i,n+1}}{R_n/2 + R_{n+1}/2} + \dots = 0, \quad (3.2)$$

where V_i is the intracellular and V_e the extracellular potential (for calculation of V_e see Section 3.3), C denotes the capacity of cell membrane, I_{ion} is the ion current, which is computed from an appropriate membrane model (see Section 3.2) and $R/2$ represents the internal resistance between the center and the border of the compartment. Furthermore, n indicates the compartment number; $n-1$ and $n+1$ are arbitrary chosen numbers of the neighbor compartments. To choose an appropriate enumeration within the branching dendrite is a problem of adequate implementation (Section 3.4). The dots in equation (3.2) stand for terms similar to the previous ones that have to be added in cases of more than two neighbor compartments, e.g., at the soma or in other branching regions. In the case of just one neighbor element equation (3.2) has only three summands.

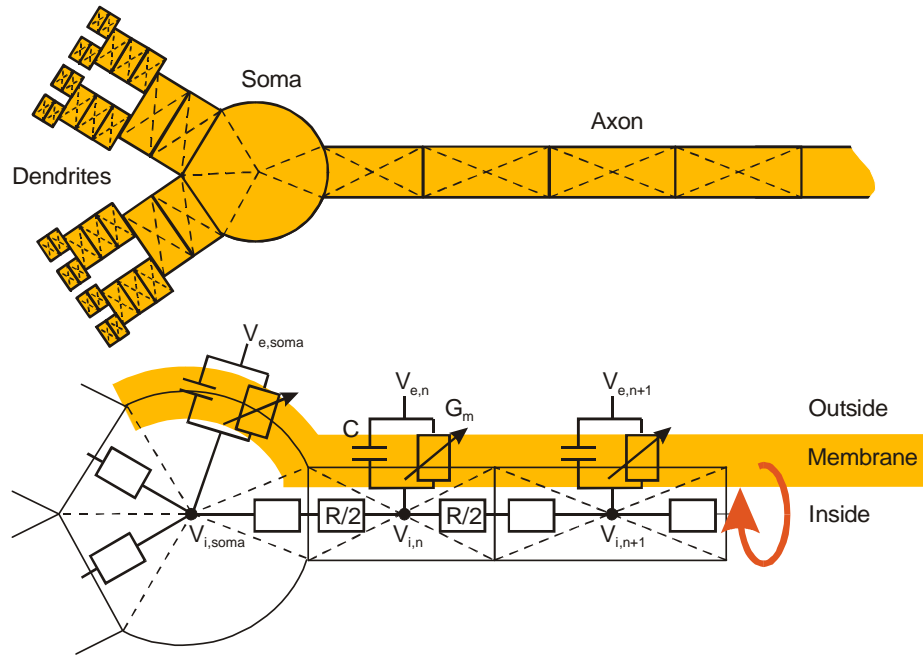


Fig. 3.1 Upper trace: Scheme of a neuron with subunits. Lower trace: Part of the simplified electrical network. G_m denotes the membrane conductance, which is only constant in compartments with passive membranes. Generally, the ohmic membrane current consists of different types of ion currents. The batteries resulting from different internal and external ion concentrations are not shown.

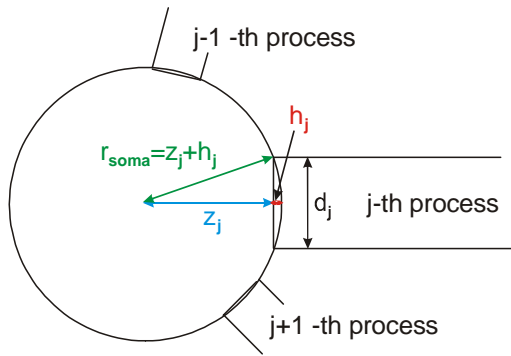
Introducing the reduced membrane voltage $V = V_i - V_e - V_{rest}$ (V_{rest} denotes the resting voltage across the membrane, and starting in the steady state $V(0) = 0$) leads to the following system of differential equations for calculating the time-courses of V_n in every compartment; compare [Rattay 1999]:

$$\frac{dV_n}{dt} = \left[-I_{ion,n} + \frac{V_{n-1} - V_n}{R_{n-1}/2 + R_n/2} + \frac{V_{n+1} - V_n}{R_{n+1}/2 + R_n/2} + \dots + \frac{V_{e,n-1} - V_{e,n}}{R_{n-1}/2 + R_n/2} + \frac{V_{e,n+1} - V_{e,n}}{R_{n+1}/2 + R_n/2} + \dots \right] \frac{1}{C_n}. \quad (3.3)$$

To be independent of geometrical parameters the equations of the membrane models are formulated for currents passing through 1 cm² of cell membrane. Thus, the ion currents I_{ion} become current densities i_{ion} (see Section 3.2), and it is convenient to transform equation (3.3). With A_n being the surface of the n -th compartment and c the specific membrane capacity, one obtains $C_n = A_n c$. For cylindrical compartments with diameter d and length Δx surface and resistance results in

$$A_n = d_n \Delta x_n \pi \quad \text{and} \quad \frac{R_n}{2} = \frac{2\rho_i \Delta x_n}{d_n^2 \pi}$$

(ρ_i is the intracellular resistivity). In case of the spherical soma (Fig. 3.2)



$$A_{soma} = 4r_{soma}^2 \pi - \sum_j 2r_{soma} \pi h_j,$$

where $h_j = r_{soma} - z_j$, and

$$z_j = \sqrt{r_{soma}^2 - (d_j/2)^2}.$$

Fig. 3.2 shows how h_j and z_j are computed. The somatic resistance to the border of the j -th process can be calculated with

Fig. 3.2 Calculation of the soma surface.

$$\frac{R_{soma,j}}{2} = \frac{\rho_i}{2r\pi} \ln \left(\frac{r_{soma} + z_j}{r_{soma} - z_j} \right).$$

Most of the electric parameters are based on whole-cell recording data which include the value for membrane capacitance (1 μF/cm²) and intracellular resistivity (110 Ωcm) [Coleman and Miller 1989]. These values are assumed to be uniform throughout the cell and were used in all simulations. The other parameters are specified in the context of the description of the specific simulation.

Compartment length

As mentioned above every compartment is electrically represented as a single point. Therefore the compartments have to be small enough so that the intracellular and the extracellular voltages can be represented by a mean value.

This means that from the numerical point of view, the length of a cylindrical compartment with diameter d is restricted by its space constant λ , with $\lambda = \sqrt{d/(4\rho_i g_m)}$, where g_m denotes the specific membrane conductance (λ gives the distance where V falls to V/e , i.e. V loses 63 % of its value). If the compartment length is below $\lambda/4$, the error compared to the continuous cable equation is of the order of 1 % [Rattay 1999].

The smallest process diameter of a retinal ganglion cell used in this thesis is 0.4 μm . This gives $\lambda \approx 674 \mu\text{m}$ ($\rho_i = 110 \Omega\text{cm}$, $g_m = 0.02 \text{ mS/cm}^2$ Greenberg et al. 1999) and consequently $\lambda/4 \approx 169 \mu\text{m}$. The maximal distance of two tracing points is about 34 μm for Ganglion cell #1 and 114 μm for Ganglion cell #2. Therefore, to ensure fine numerical solutions, it was possible to take the data points as the boundaries of the compartments. Also the dendrites of the two target bipolar cells are nowhere thinner than 0.4 μm . Assuming $\rho_i = 110 \Omega\text{cm}$ and $g_m = 0.0416667 \text{ mS/cm}^2$ [Coleman and Miller 1989] it follows $\lambda \approx 467 \mu\text{m}$ this implies $\lambda/4 \approx 117 \mu\text{m}$. The maximum compartment length for Bipolar #1 and Bipolar #2 is 12 μm , far below the required value.

For the sphere, which models the soma, also the question of the appropriate size arises. After Rattay [1999] the representation of the soma by a single spherical compartment is sufficient for a diameter less than 30 μm , if the extracellular voltage does not vary considerably along the compartment surface.

Natural situation of excitation

With the spatial model described above, it is possible to compute both the influence of an artificial electric field (which causes an extracellular potential V_e - for calculation see Section 3.3) as well as an injected stimulus that simulates synaptic ganglion cell excitation. In the natural situation the currents along the inside of the neuron are responsible for the propagation of the neural signals. Therefore, if the cell is immersed in a large volume of extracellular fluid, the extracellular resistance may be neglected. The pioneers in the field of nerve modeling used this simplification when they examined the propagating action potential, hence if no extracellular stimulation is applied it will be set $V_e = 0$ for all segments. (Clark and Plonsey examined the potential distribution on both sides of the membrane and found that only changes in order of some mV occur on the extracellular side when an action potential is passing [Clark and Plonsey 1968, Plonsey 1974].)

To simulate the effect of a current injection locally in the cell, a system of differential equations has to be solved, which is derived from (3.3) by neglecting the extracellular potential and by introducing the reduced voltage: $V_{e,n} = 0$ and $V_n = V_{i,n} - V_{rest}$. Assuming that the stimulus current I_{stim} is injected in the j -th compartment, the model is reduced to a system of equations of the form

$$\frac{dV_j}{dt} = \left[-I_{ion,j} + \frac{V_{j-1} - V_j}{R_{j-1}/2 + R_j/2} + \frac{V_{j+1} - V_j}{R_{j+1}/2 + R_j/2} + \dots + I_{stim} \right] \frac{1}{C_j} \quad (3.4)$$

and for all $n \neq j$:

$$\frac{dV_n}{dt} = \left[-I_{ion,n} + \frac{V_{n-1} - V_n}{R_{n-1}/2 + R_n/2} + \frac{V_{n+1} - V_n}{R_{n+1}/2 + R_n/2} + \dots \right] \frac{1}{C_n} \quad (3.5)$$

The dots again stand for terms, which have to be added in cases of more than two neighbors and in the case of the first or an end compartment the second and third summand respectively vanishes.

Hence the models of the retinal cells consist of systems of differential equations. The dimension of the system is determined by the number of compartments which were required to simulate the target neuron. For every active segment, that is the gating mechanisms of voltage sensitive channels are included, the ion current density ($i_{ion,n}$) is calculated with the help of a subsystem of differential equations; its dimension depends on which membrane model will be chosen. Three membrane models will be presented in the following section: two active models for the ganglion cells and a passive one for the bipolar cells.

3.2 Cell membrane models

Two basically different retinal cell types have been modeled: ganglion cells and bipolar cells. The great difference of these cells is the way how the signal transmission is performed. A retinal ganglion cell uses voltage sensitive ion channels to forward the information in form of spikes not only in the axon but also within the dendrites [Velte and Masland 1999, Vetter et al. 2000]. In contrast bipolar cells do not generate action potentials at all. They use electrotonic conduction, i.e. the direct flow of electric current along the membrane. Thus there is a continuous charge flow, not the all-or-nothing response seen in typical neuronal transmission. The release of neurotransmitters at the synapses is graduated in proportion to the amount of current flowing [Coleman and Miller 1989].

Thus a linear passive model is adequate to simulate the response of bipolar cells to an applied electric field, whereas for the simulation of spiking ganglion cells a nonlinear active model is needed.

The most famous active membrane model of Hodgkin and Huxley (HH model) [Hodgkin and Huxley 1952, Rattay 1990] can easily be adapted to simulate a retinal ganglion cell axon. With a passive dendrite membrane such a semi-active model is a good approach with relatively low computational effort.

A sophisticated membrane model includes the most important ion channels which characterize the cell membrane. Sodium, potassium, chloride, calcium and calcium dependent potassium channels belong to the most prominent channel types involved in the excitation processes. An active membrane model has to be

tested carefully, because the properties of ion channels as well as their densities have great influence on the neural response. In this sense the Fohlmeister, Coleman, and Miller model (FCM model) for retinal ganglion cells is more complex [Fohlmeister et al. 1990, Fohlmeister and Miller 1997a, b] compared to the HH model where it is derived from. Nevertheless both active models have a similar behavior with regards to the electro-stimulation process. They belong to the same class of differential equations: They have a stable steady state; small disturbances produce small excursions of the states, but higher influences bring them against a pseudo limit circle from where the trajectories come back to the resting level.

The multi-compartment FCM model of the retinal ganglion cell takes into account different membrane compositions in dendritic tree, soma, axon hillock, thin axonal segment, and axon distal to the thin segment. Thus, modeling of the propagation of dendritic action potentials is also possible. To develop the FCM model a study of nerve impulse generation in ganglion cells of tiger salamander retina were carried out through a combination of experimental and analytical approaches. Whole cell recordings from ganglion cells were obtained using a superfused retina-eyecup preparation and studied with pharmacological and electrophysiological techniques [Fohlmeister and Miller 1997a, b]. The FCM model provides an accurate representation of impulse waveform and repetitive firing behavior.

The following description of the three retinal membrane models starts with the simplest one. As mentioned in the previous section they are formulated for 1 cm^2 of cell membrane and the currents in the equations (3.1)-(3.5) become current densities.

Linear passive model

The linear passive mechanism reduces each patch of membrane to a simple parallel RC circuit with a leak. In this case the term $I_{ion,n}$ in the equations (3.1)-(3.5) has to be substituted by $G_{m,n}V_n$, where G_m denotes the cell membrane conductance. For the modeling of the retinal bipolar cells a specific membrane conductance of $g_m = 0.0416667 \text{ mS/cm}^2$ is assumed [Coleman and Miller 1989]. The results obtained with the passive model are highly influenced by the local input resistance, and ignore nonlinear membrane properties.

Hodgkin-Huxley model

The Hodgkin-Huxley mechanism is the classic nonlinear description of unmyelinated axons. The model was developed from a homogeneous squid axon. It includes two specific currents: a sodium (I_{Na}), a potassium (I_K), and the less important ions are summarized into a nonspecific leakage (I_L) current. To describe the nonlinear gating mechanism of the ion channels, Hodgkin and Huxley introduced the stochastic variables m , n and h . In their model the sodium channel has two gates: an activation and an inactivation gate. m and h

denote the probabilities that these gates are open. The potassium ions has to pass only a single type of gate which is controlled by the probability n .

Again the reduced voltage is used $V = V_i - V_e - V_{rest}$ where V_i and V_e are the intracellular and extracellular potential respectively and V_{rest} is the resting voltage of the cell, which is -70 mV for squid axons. The equations to calculate the ion currents passing through 1 cm^2 cell membrane have the form:

$$i_{ion} = i_{Na} + i_K + i_L. \quad (\text{HH-3.6})$$

V_{Na} , V_K and V_L denote the voltages across the membrane, caused by different ion (sodium, potassium and leakage) concentrations at the inside and the outside of the cell. For the special values see Table 3.1.

$$i_{Na} = g_{Na} m^3 h (V - V_{Na}),$$

$$i_K = g_K n^4 (V - V_K),$$

$$i_L = g_L (V - V_L),$$

where g_{Na} , g_K and g_L represent the maximum conductance of sodium, potassium and leakage per cm^2 of cell membrane. m , h and n solve the first order kinetic equations:

$$\frac{dm}{dt} = [-(\alpha_m + \beta_m)m + \alpha_m]k, \quad (\text{HH-3.7})$$

$$\frac{dh}{dt} = [-(\alpha_h + \beta_h)h + \alpha_h]k,$$

$$\frac{dn}{dt} = [-(\alpha_n + \beta_n)n + \alpha_n]k,$$

where k denotes the coefficient for temperature and is given by $k = 3^{0.1(T-6.3)}$. Here T (in $^{\circ}\text{C}$) is the temperature in the simulation. The α 's and β 's are used to fit the ion conductances to the experimental data.

Sodium channel:

$$\alpha_m = \frac{2.5 - 0.1V}{e^{2.5 - 0.1V} - 1} \quad \beta_m = 4e^{-\frac{V}{18}} \quad (\text{HH-3.8})$$

$$\alpha_h = 0.07e^{-\frac{V}{20}} \quad \beta_h = \frac{1}{e^{3 - 0.1V} + 1}$$

Potassium channel:

$$\alpha_n = \frac{1 - 0.1V}{10(e^{1-0.1V} - 1)} \quad \beta_n = 0.125 e^{-\frac{V}{80}}$$

The HH model was originally used with $T = 6.3^\circ\text{C}$ ($k = 1$) according to the experimental temperature.

Table 3.1 Symbols, constants and units used in the HH model

V_{Na}	sodium voltage	115 mV
V_K	potassium voltage	-12 mV
V_L	leakage voltage	10.6 mV
g_{Na}	max. sodium conductance	120 mS/cm ²
g_K	max. potassium conductance	36 mS/cm ²
g_L	max. leakage conductance	0.3 mS/cm ²

In Table 3.1 the original Hodgkin-Huxley parameters are listed [Hodgkin and Huxley 1952]. The parameters are altered for some simulations to adapt the HH model to ganglion cell. These values are mentioned later in the context of the respective simulation.

Fohlmeister-Coleman-Miller model

The FCM model developed especially for the retinal ganglion cell is based on voltage clamp studies in tiger salamander and rat retina [Lipton and Tauck 1987, Lukasiewicz and Werblin 1988, Coleman and Miller 1989]. These studies have identified at least five intrinsic ion currents, which appear to play a role in generating nerve impulses. In the model are these specific ion currents and a leakage current (I_L) included, namely a sodium current (I_{Na}), a calcium current (I_{Ca}) and three types of potassium currents: the delayed rectifier I_K , $I_{K,A}$ (potassium A type), and the calcium-activated potassium current $I_{K,Ca}$. Five of these currents are modeled as voltage-gated like in the HH equations, whereas the sixth $I_{K,Ca}$ is modeled to respond to calcium influx. In addition a variable-rate calcium-sequestering mechanism was implemented to remove cytoplasmic calcium. The equation for the ion current density is given by:

$$i_{ion} = i_{Na} + i_{Ca} + i_K + i_{K,A} + i_{K,Ca} + i_L. \quad (\text{FCM-3.9})$$

The resting potentials in salamander ganglion cells range from -70 mV to -45 mV. For the purpose of this study, a resting potential of -65 mV was used to calculate the reduced membrane voltage. With the probabilities of the membrane gating processes m , h , c , n , a , and h_A , the ion current densities have the form:

$$i_{Na} = g_{Na} m^3 h (V - V_{Na}),$$

$$i_{Ca} = g_{Ca} c^3 (V - V_{Ca}),$$

$$i_K = g_K n^4 (V - V_K),$$

$$i_{K,A} = g_A a^3 h_A (V - V_K),$$

$$i_{K,Ca} = \bar{g}_{K,Ca} (V - V_K),$$

$$i_L = g_L (V - V_L),$$

where V_{Na} , V_{Ca} , V_K and V_L denote the ion (sodium, calcium, potassium and leakage) battery voltages across the membrane and g_{Na} , g_{Ca} , g_K , g_A , g_L the maximum conductances of sodium, calcium, potassium, potassium A type and leakage per cm^2 membrane (Table 3.2). The gating of $i_{K,Ca}$ is modeled as

$$\bar{g}_{K,Ca} = g_{K,Ca} \frac{([Ca^{2+}]_i / Ca_{diss}^{2+})^2}{1 + ([Ca^{2+}]_i / Ca_{diss}^{2+})^2}. \quad (\text{FCM-3.10})$$

Here $g_{K,Ca}$ represents the maximum conductance of calcium-activated potassium per cm^2 (Table 3.3). The calcium dissociation constant Ca_{diss}^{2+} is taken to be 10^{-3} mM/dm^3 [Coleman and Miller 1989]. The intracellular calcium ion concentration $[Ca^{2+}]_i$ is allowed to vary in response to i_{Ca} . Moreover, the inward flowing calcium ions are assumed to be distributed uniformly throughout the cell and the free intracellular calcium ions above a residual level, $[Ca^{2+}]_{res} = 10^{-4} \text{ mM/dm}^3$, are actively removed from the cell, or otherwise sequestered with a time constant τ . Thus, $[Ca^{2+}]_i$ satisfies equation:

$$\frac{d[Ca^{2+}]_i}{dt} = \frac{-s i_{Ca}}{2vF} - \frac{[Ca^{2+}]_i - [Ca^{2+}]_{res}}{\tau}, \quad (\text{FCM-3.11})$$

where F is the Faraday constant ($F = 9.64845 \cdot 10^4 \text{ C/M}$), s/v is the ratio of surface to volume of the concerning compartment, and the factor of 2 on v is the valency. For a spherical soma with radius $12 \text{ }\mu\text{m}$, and $\tau = 1.5 \text{ ms}$ equation (FCM-3.11) reads as:

$$\frac{d[Ca^{2+}]_i}{dt} = -0.000013 i_{Ca} - 0.666667 ([Ca^{2+}]_i - 0.0001).$$

V_{Ca} is modeled as variable according to the Nernst equation:

$$V_{Ca} = \frac{RT}{2F} \ln \frac{[Ca^{2+}]_e}{[Ca^{2+}]_i} + 65. \quad (\text{FCM-3.12})$$

In this well known equation R denotes the gas constant ($R = 8.31441 \text{ J/(M}\cdot\text{K)}$), T temperature in Kelvin, F the Faraday constant, the factor of 2 on F correspond to the valency of a calcium ion. $[Ca^{2+}]_e$ represents the extracellular

calcium ion concentration, which is 1.8 mM/dm³. The summand 65 results from the usage of the reduced membrane potential.

Similar to the Hodgkin-Huxley model the stochastic variables for the four channels with direct voltage dependent gating m , h , c , n , a , h_A , solve the first order kinetic equation:

$$\frac{dx}{dt} = -(\alpha_x + \beta_x)x + \alpha_x. \quad (\text{FCM-3.13})$$

In these differential equations the following constants - listed in order of the according ion channels - operate.

Sodium channel:

$$\begin{aligned} \alpha_m &= \frac{0.6(35-V)}{e^{0.1(35-V)} - 1} & \beta_m &= 20e^{(10-V)/18} \\ \alpha_h &= 0.4e^{(15-V)/20} & \beta_h &= \frac{6}{e^{0.1(45-V)} + 1} \end{aligned} \quad (\text{FCM-3.14})$$

Calcium channel:

$$\alpha_c = \frac{0.3(52-V)}{e^{0.1(52-V)} - 1} \quad \beta_c = 10e^{(27-V)/18}$$

Potassium channel:

$$\alpha_n = \frac{0.02(25-V)}{e^{0.1(25-V)} - 1} \quad \beta_n = 0.4e^{(15-V)/80}$$

Calcium-activated potassium channel:

$$\begin{aligned} \alpha_A &= \frac{0.006(-25-V)}{e^{0.1(-25-V)} - 1} & \beta_A &= 0.1e^{(35-V)/10} \\ \alpha_{h_A} &= 0.04e^{(-5-V)/20} & \beta_{h_A} &= \frac{0.6}{e^{0.1(25-V)} + 1} \end{aligned}$$

The temperature is modeled at 22°C, according to the amphibian electrophysiological experiments.

Table 3.2 Symbols, constants and units used in the FCM model

V_{Na}	sodium voltage	100 mV
V_K	potassium voltage	-10 mV
V_L	leakage voltage	3 mV
g_L	max. leakage conductance	0.005 mS/cm ²
τ	time constant of calcium removal	1.5 ms

Noticeable is the brief time for the calcium removal which is probably much too short to reflect mechanism for the sequestering and removal of cytoplasmic free calcium, and may reflect instead a component of electrical gating of $g_{K,Ca}$.

As mentioned above the FCM model includes representation of the dendritic tree, soma, initial and thin segment of the axon, and rest of the axon. On each of these parts of the ganglion cell the five ion channels are distributed in varying densities, simulated by varying the value of g_{Max} (mS/cm²) for each channel. These values are listed in the following table:

Table 3.3 Channel densities at soma, dendrite, and axon in mS/cm ²					
g_{Max}	Soma	Dendrite	Axon initial	Axon thin	Axon rest
g_{Na}	70	40	150	100	50
g_{Ca}	1.5	3.6	1.5	0	0
g_K	18	12	18	12	15
g_A	54	36	54	0	0
$g_{K,Ca}$	0.065	0.065	0.065	0	0

The densities listed in Table 3.3, and the values of Table 3.2 are identical to those proposed by Fohlmeister et al. [Fohlmeister and Miller 1997b].

3.3 Volume conductor models

In applications of electrical stimulation, electrodes are positioned in a geometrically and electrically more or less complex volume conductor containing cell bodies, dendrites, and axons in close proximity. When a stimulus is applied within the eye, cells and fibers over an unknown volume of tissue are activated, resulting in direct excitation as well as trans-synaptic excitation/inhibition from stimulation of presynaptic axons and cell bodies. Fundamental knowledge of interactions between the applied currents and the neurons of the retina is limited, and this void will impair the development of save and effective future devices.

In order to contribute to the solution of this problem the approach of investigating a target cell embedded in a volume conductor is used. The distinct models differ in the number of included inhomogeneities and electrode configurations. All models neglect the presence of the target cell when the extracellular potential is calculated.

Thus to investigate the influence of different electrode designs, the extracellular potentials V_e has to be calculated, which serve as the input data for

the electrical network model; i.e. for equation (3.3). Two basically different mathematical approaches for calculation of the extracellular potentials are used:

1. analytical solutions for V_e are available in the case of a monopolar or dipolar point source and disk electrode in an infinite homogenous medium,
2. for a more complex model, which takes inhomogeneities of the eye into account and includes sophisticated geometries of the electrodes the extracellular potential is numerically calculated based on the finite element method.

These two approaches will be discussed in detail later, first the influence of an applied electrical field to the target cell will be discussed from a more theoretical point of view.

Activating function

The following summands of equation (3.3) describe the influence of the extracellular potential on the n-th compartment:

$$f_n = \left[\frac{V_{e,n-1} - V_{e,n}}{R_{n-1}/2 + R_n/2} + \frac{V_{e,n+1} - V_{e,n}}{R_{n+1}/2 + R_n/2} + \dots \right] \frac{1}{C_n}, \quad (3.15)$$

which is the formulation of the activating function for neurons of arbitrary shape [Rattay 1999]. The physical dimension of f is V/s or mV/ms. If the neuron is in the resting state before a stimulating current impulse is applied, this form of the activating function represents the rate of membrane voltage change in every compartment that is activated by the extracellular field. Regions with positive activating function are candidates for spike initiation, whereas negative activating function values cause hyperpolarization. Changes in extracellular voltages, in the geometry and membrane capacity, as well as the occurrence of branching elements, cause irregularities in the graph of f .

Within a long homogeneous fiber, the activating function becomes proportional to the second derivative of the extracellular potential along the axon. The activating function is a powerful tool for obtaining a first impression – with a small computational effort – of the influence of an applied electric field on the target cell [Rattay 1986, 1989, Coburn 1989, Basser et al. 1992, Garnham et al. 1995].

The target cell embedded in an infinite homogeneous medium

Assuming that the target cell is embedded in an infinite homogenous medium makes sense, because of the short distances between the electrode and the target cell, and the relatively small retinal cells compared to the dimensions of the eye. The electrical characteristics of the medium in which the current travels are linear, homogenous and unaffected by the presence of the neuron. Extracellular potentials are applied uniformly to the circumference of each compartment. As

mentioned above analytical formulas for the calculation of the extracellular potential can be provided for two kinds of electrodes.

In the first case the electrode is modeled as an ideal point source. If so, the extracellular potential of an arbitrary point at distance r from the electrode is

$$V_e(r) = \frac{\rho_e I_{el}}{4r\pi}, \text{ and } V_e = 0 \text{ for } r \rightarrow \infty, \quad (3.16)$$

where I_{el} denotes the electrode current, and ρ_e the extracellular resistivity ($\rho_e = 57 \Omega\text{cm}$, is the resistivity of 0.9 % saline, which is similar to the resistivity of vitreous body [Geddes and Baker 1967]). r is computed as the distance between the position of the electrode and the center of each compartment.

In the second case the electric field is caused by an equipotential metal disk electrode in a semi-infinite medium. The extracellular potential under the electrode is calculated by:

$$V_e(r, z) = \frac{2V_0}{\pi} \arcsin \frac{2a}{\sqrt{(r-a)^2 + z^2} + \sqrt{(r+a)^2 + z^2}}, \quad (3.17)$$

here r denotes the radial and z the axial distance from the center of the disk in cylindrical coordinates for $z \neq 0$ [Wiley and Webster 1982]. V_0 is the potential and a is the radius of the disk.

The target cell embedded in a finite inhomogeneous medium

In this approach the potential distribution is computed with the finite element software FEMLAB, which makes possible a substantially more complex model with elaborate electrode configurations and consideration of inhomogeneities.

The first model included representations of the entire eye and even structures outside the eye with five different conductivity media [Resatz 2001, 2002b], as they where:

1. aqueous humor, vitreous body, and retina (which were considered as a single volume, since they have nearly the same conductivity);
2. sclera;
3. structures outside the eye (which were lumped together as one effective conductivity);
4. lens;
5. cornea.

But a comparison of the computed extracellular potential of the above model and of a simplified model obtained by taking only a patch of retina and sclera into account showed that this attempt was unnecessarily too complex. The difference of the results was smaller than the error made by the modeling and by the numerical evaluations. Besides, the smaller model accelerates the computations significantly.

Table 3.4 Parameters for the FEMLAB model

Structure	Dimension in μm	Specific resistance*
Sclera	$2000 \times 2000 \times 200$	10
Retina	$2000 \times 2000 \times 200$	1
Electrode carrier	$2000 \times 2000 \times 100$	1000

Figure 1: Schematic diagram of the computational domain for the finite element analysis. The diagram shows a 3D model of the eye and implant. The top part shows a cross-section of the eye with dimensions: 1000 μm width, 1000 μm depth, and 200 μm height. The bottom part shows a 3D view of the eye with layers: Implant, Retina, Sclera, and Symmetry plane. The eye is divided into regions with $V=0$ (blue), $V=1$ (green), and $V=-1$ (green). An electrode is shown on the Retina. A coordinate system (x , y , z) is shown in the top left.

Moreover it should be mentioned that the piece of aqueous body layer between the implant and the retina which has a thickness of about 20 μm , depending on the respective simulation, is treated like a piece of retina with the

same specific resistance. The electrodes are modeled as active dipoles. Their intrinsic geometry is mentioned in context of the description of the particular simulation.

3.4 Implementation

As described in the preceding sections the excitation process of the retinal cells is simulated in a two step procedure. In the first step the extracellular potential along the neural structure is calculated. In case of a target cell embedded in an infinite homogeneous medium this is accomplished either with MATLAB (MATrix LABoratory) or with ACSL (Advanced Continuous Simulation Language). In the case of a target cell embedded in a finite inhomogeneous medium the extracellular potential computed with FEMLAB (Finite Element Modeling LABoratory). In the second step the target cell is represented by a compartment model. The implementation of this model is done in both programming languages MATLAB and ACSL.

MATLAB program

MATLAB is a high-performance language for technical computing and represents the state-of-art in software for matrix computation. The basic data element of this interactive system is an array that does not require dimensioning. Thus, makes a simple handling of the input-data possible, which are given as an ASCII file.

First the ASCII file is converted in a MAT-file that saves MATLAB workspace and looks like a matrix. The columns of the matrix include the x-, y-, and z-coordinates of the target cell, the diameter of each compartment (and the soma radius respectively) and the branching information of the dendritic tree. This information is numerically coded in a single number in the following way: 0 stands for the soma; 1 for a neighbor element of the soma; 2 means linear proceed in the sense that the predecessor is the previous element and the successor is the next element in the list; 3 is a branching point and 4 the end. The numbering of the compartments starts at the dendritic branches, then the compartment of the soma is listed, and finally there are the compartments of the axon beginning from the soma. The enumeration makes no qualitative difference between dendrites and axon.

In a next step two vectors are produced, which contain in each branching point the number of the preceding and the succeeding compartment. This information is needed for the evaluation of the right hand side of the system of differential equations describing the model, i.e. equation (3.3). In these equations it is necessary to know at each point the number of the variable of the predecessor and of the possible successors (that can be more than one).

Apart from computations with a traced target cell the MATLAB program can also produce an artificial cell. This cell optionally possesses the following neural structures: a dendrite without ramifications, a soma, and an axon. After creating the artificial cell it is treated in the same way as the traced cells.

Besides parameters of the target cell the MATLAB program requires as input data:

- o information whether intracellular and/or extracellular stimulation is used;
- o in the case of intracellular stimulation: number of the compartment which is stimulated;
- o in the case of extracellular stimulation of a target cell embedded in an infinite homogeneous medium: the decision whether the electrode is a dipole or monopole, a point source or disc, in addition the location of the electrode(s) must be indicated;
- o in the case of extracellular stimulation of a target cell embedded in a finite inhomogeneous medium: the potential distribution for the target cell imported from FEMLAB;
- o the stimulus current and the parameter of the time dependent stimulation pulse trains, as they were: initiation time, period, pulse width;
- o membrane model used in the simulation;
- o duration of the simulation.

Having the extracellular potential and the activation function calculated using the input data, the nonlinear system of differential equations of order 1 (3.3) for the membrane voltage can be set up. As solver in this program the MATLAB function `ode23` is used. `ode23` is an implementation of an explicit Runge-Kutta (2,3) pair of Bogacki and Shampine [1989].

The whole MATLAB program contains the following files:

1. `RGC1.mat`, `RGC2.mat`, `BP1.mat`, `BP2.mat`: data files for the traced cells as described above;
2. `head.m`: starting file of the program, m-file call, and specification of the output;
3. `start.m`: initiates initial values;
4. `dataTRACE.m`: data processing for the traced target cells;
5. `dataARTIF.m`: data generation and processing for the artificial target cell;
6. `calcAKTIV.m`: computation of the activating function;
7. `sonachb.m`: supplies data about size and location of the neighbor compartments of the soma;
8. `calcVE.m`: computation of the extracellular potential in the case of a point source or disk electrode in an infinite homogeneous medium;
9. `calcION.m`: calculation of the membrane currents for the selected model;
10. `DGL.m`: contains the differential equations of the model, i.e. equation (3.3) and the computation of the stimulating signal;
11. `plot_v.m`, `plot_f.m`; `plot_ion.m`: visualization of the values for the extracellular potential, the activating function, and the ion currents.

The MATLAB program is very comfortable for plotting and small investigations like variation of parameters and for comparing the behavior of different retinal cells in an applied electric field. But unfortunately it is much too slow for threshold investigations. Thus extensive computations were carried out with the ACSL program.

ACSL program

ACSL was introduced 25 years ago as the first commercially available modeling and simulation language designed for simulating continuous systems.

Generation of the simulation code is a two step procedure in ACSL. The program defines the system being modeled; the runtime commands exploit this model (i.e. they change parameters, execute runs, specify plots etc.). The program is read by the ACSL translator, which translates it to a FORTRAN 77 compile file. The FORTRAN code is then compiled, linked with the ACSL runtime library, and executed, finishing at an ACSL runtime prompt. At this point, ACSL is waiting for runtime commands, which can be entered by reading a command file. The results are written into a file and can be plotted and/or printed in the command file.

ACSL has been developed expressly for the purpose of modeling systems described by time dependent, nonlinear differential equations. As mentioned above the models are compiled, which offers tremendous speed advantages over interpretive simulation languages. The simulations run as fast as the hardware will permit.

This is the main reason why for threshold investigations the MATLAB program is converted in an ACSL program. From the MATLAB program the following data are imported in the ACSL program as txt-files:

1. d.txt: diameter and radius of the cylindrical compartments and soma respectively (which comes just from the data file);
2. dx.txt: computed length of the compartments and diameter of the sphere respectively;
3. vor.txt, nach.txt: branching information;
4. zmp.txt: distance z_j (see Fig. 3.2) between center of the soma and the neighboring compartments;
5. sodent.txt: number of the compartments which are neighbors to the soma;

Apart from the additional tool of the automatic threshold computation the ACSL program has exactly the same features as the MATLAB program.

The principal structure of an ACSL program is shown in Table 3.5. Particularly, because of the included sort algorithm, it has a very simple structure. The ACSL translator sorts the code in the DERIVATIVE section so that the outputs are calculated before they are used. But ACSL has also crucial disadvantages. Because of depending on FORTRAN 77 no dynamic fields are available. Thus for the simulation of different cells the program must be altered.

Also it is not easy to debug a program and to find errors, since the error messages are relatively nonspecific.

Table 3.5 Outline of an explicitly structured ACSL program		
PROGRAM		
⋮		Pre-INITIAL Section
INITIAL		
⋮		INITIAL Section: statements executed before the run begins. State variables do not contain the initial conditions yet.
END	! of INITIAL	
DYNAMIC		
DERIVATIVE		
⋮		DERIVATIVE Section: Statements which are to be integrated continuously (model equations can be found here).
END	! of DERIVATIVE	
DISCRETE		
⋮		DISCRETE Section: statements that are executed at discrete points in time.
END	! of DISCRETE	
⋮		DYNAMIC Section: statements executed each communication interval (subinterval for numerical integration).
END	! of DYNAMIC	
TERMINAL		
⋮		TERMINAL Section: statements executed after the run terminates.
END	! of TERMINAL	
END	! of PROGRAM	

As in MATLAB in ACSL the integration algorithm can be chosen (but it cannot be changed during a simulation run). From the mathematical point of view, this is the most critical step in the ACSL program. For most systems of differential equations the Runge-Kutta second order algorithm is recommend as the most efficient. In this thesis another integration algorithm is used because the Runge-Kutta algorithm often breaks down with an overflow. On the other hand, the required step size changes significantly during a simulation, because large values appear mainly during the stimulation period. That is why the Adams-Moulton algorithm is used.

The Adams-Moulton algorithm is an implicit integration algorithm. It is a variable step, variable order integration routine that is self-initializing. In general it attempts to minimize the step changing by always choosing a step size that divides evenly into the time-to-go to the next event and keeping the per-step error in each state variable below an allowed value. This desired value is obtained by

taking the maximum of the corresponding absolute allowed error, and the relative allowed error multiplied by the maximum absolute value of the state so far. The order of integration starts at one and then changes dynamically as the program progresses. The step size also changes dynamically as the integration routine attempts to take the largest possible step consistent with the allowed error bounds (for further information see [Breitenecker et. al. 1993]).

FEMLAB program

For investigations concerning the elaborate electrode design the extracellular potential is calculated with finite element software FEMLAB. FEMLAB is an interactive environment for modeling scientific and engineering applications based on partial differential equations. It is a complete package that covers all facets of the modeling process.

For the calculations of this thesis FEMLAB 2.3 was used, which is the first engineering tool for partial differential equations based multiphysics modeling in an interactive environment - MATLAB. The underlying mathematical structure with which FEMLAB operates is a system of differential equations that can be represented in three ways: weak form, general form, and coefficient form. Lastly mentioned was implemented here, since it is suitable for linear or nearly linear problems.

When solving the differential equations that describe a model, FEMLAB applies the finite element method. It runs that method in conjunction with adaptive meshing and error control as well as with a variety of numerical solvers. The basic flow of actions, in the process of modeling, defining, solving, and postprocessing the problem using the graphical user interface, is indicated by the way the toolbar buttons and the menus are ordered from left to right.

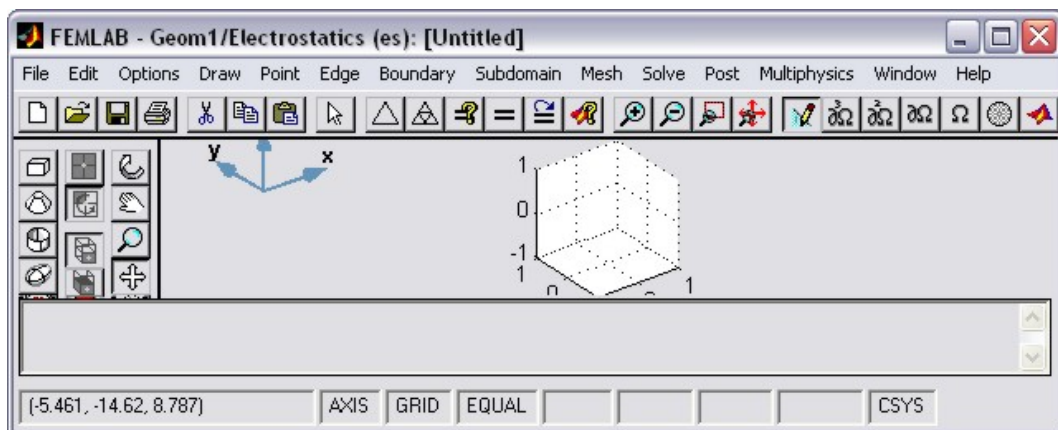


Fig. 3.4 Screenshot where the graphical user interface of FEMLAB is visible.

In this environment the model is created and manipulated by choosing one of several predefined physics modes (electrostatics, linear stationary) in the *Model Navigator*, where one work with familiar scientific laws and relationships. Also the space dimension 3D is specified here.

In electrostatics, the scalar electrostatic potential V is related to the electric field density \vec{E} by $\vec{E} = -\nabla V$ and, using one of Maxwell's equations, $\nabla \cdot \vec{D} = \rho$, and the relationship $\vec{D} = \epsilon_0 \epsilon_r \vec{E} + \vec{P}$, where \vec{P} is the polarization vector, we arrive at the equation

$$-\nabla \cdot (\epsilon_0 \epsilon_r \nabla V - \vec{P}) = -\nabla \cdot (\epsilon \nabla V - \vec{P}) = \rho,$$

where ϵ is the permittivity and ρ is the space charge density (here $\rho = 0$ for all cases). ϵ_r and ϵ_0 denotes the relative permittivity (see Table 3.4) and the permittivity of vacuum (8.854×10^{-12} Farad/meter) respectively. The permittivity of vacuum is a universal constant that, in electrostatics, gives the relation between the electric charge and the electric field. The relative permittivity is a material property that describes the relation between the electric field, \vec{E} , and the electric displacement, \vec{D} , in a material.

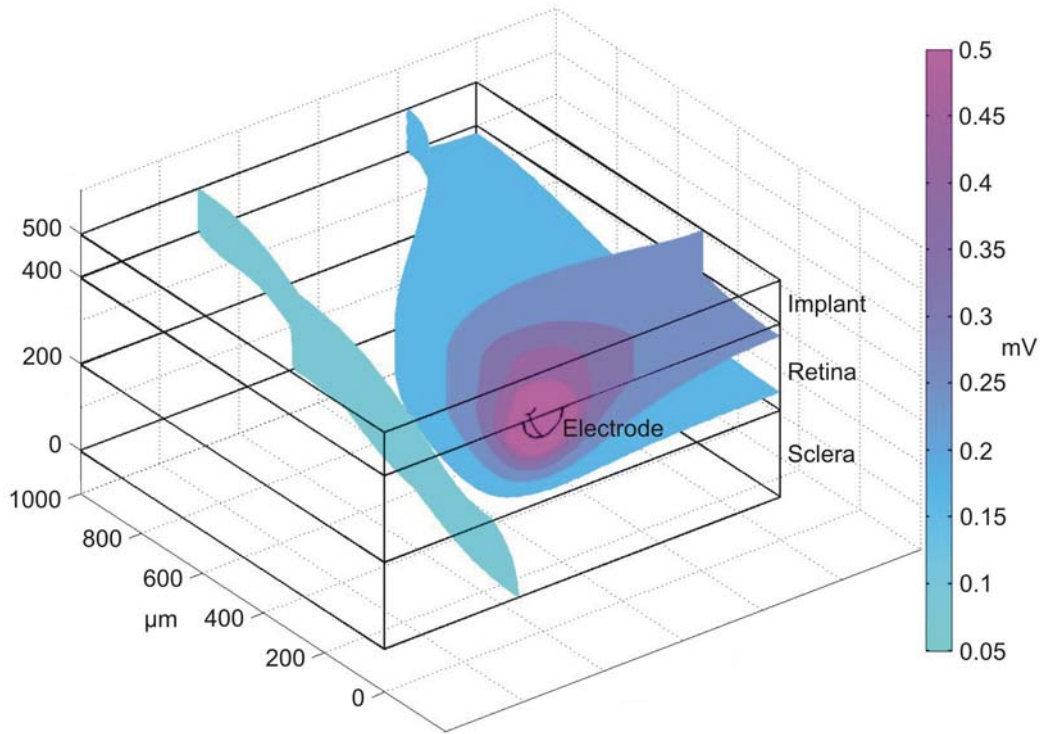


Fig. 3.5 Example of a FEMLAB calculation. The figure shows an isosurface plot of the computed electric potential.

After the overall settings of a FEMLAB session are chosen in the Model Navigator, the modeling starts in the *Draw Mode* where the geometry is defined. In order to ensure an efficient and fast processing the model is not implemented in the full dimensions as listed in Table 3.4, but symmetry characteristics were considered (shown in Fig. 3.3). Thus a block with a base area of $1000 \times 1000 \mu\text{m}$ and a height of $500 \mu\text{m}$, consisting of the 3 different layers, is sufficient.

The next step is performed in the *Boundary Mode*, where the boundary conditions of the model are specified in the boundary settings dialog box. The boundary conditions for electrostatic problems can be of Dirichlet or Neumann type. For Dirichlet conditions, the electrostatic potential V is specified on the boundary. For Neumann conditions, the surface charge density $-\vec{n}\vec{D} = \rho_s$ is specified on the boundary. Here the charge 1 mV is assigned to the electrode and one side area gets the charge 0 mV (Fig. 3.3). The remaining sides of the modeled block are occupied with Insulation/symmetry. This boundary condition is used for defining a zero surface charge ($\rho_s = 0$), but can also be used as a symmetry boundary condition. It is the default value on internal borders, and as such it specifies a continuous normal component of \vec{D} .

In *Subdomain Mode*, the parameters in the differential equations are specified. Since both the values for the space charge density and for the polarization vector are zero, here only the permittivity is interesting. The resistance is the reciprocal of the permittivity. The values for the specific resistance for the three modeled materials are listed in Table 3.4.

In the *Mesh Mode* the geometry is meshed using tetrahedrons. Now the modeling is finished and the problem can be solved. Finally the visualization settings are made in the *Post Mode*. Also the surface charge of the electrode is calculated here.

To compute the electric potential along a neural structure ‘Export FEM structure as ‘fem’’ has to be selected from the file menu. Then the value of the potential can be accessed in each point from MATLAB by the command `posteval`. Using a straightforward transformation helps to find the potentials for those geometric parts that are not directly calculated with FEMLAB because of the symmetry simplification. For the example of Fig. 3.3 this is done by reading the computed potential for the absolute values of the target cell coordinates, and multiply them by the sign of the x-coordinate.

4. Influence of the cell geometry on the excitation process

Localized retinal electrical stimulation in blind volunteers results in more or less discrete round visual percepts corresponding to the location of the stimulating electrode. The success of such an approach in order to provide useful vision depends on elucidating the neuronal target when stimulating the retina with electrodes at its surface. This section provides a detailed analysis of the influence of the cell geometry on the excitation process to determine if the electrodes preferentially stimulate ganglion cells directly below them or passing fibers from distant ganglion cells, and to clarify if other retinal cell types, like the bipolar cells for instance, contribute to the excitation process.

In the first section an investigation with the help of the activating function should enlighten the influence of the fundamental cell elements, dendrite, soma, and axon, on the excitation process. After that the threshold values for an electrode moving above an artificial cell as a function of soma size are calculated and analyzed. This question arises because the traced mudpuppy cell bodies are about twice as large as an average human ganglion cell soma. The third section includes in the investigations the distance between the electrode and the stimulated neural target elements, and the fourth section deals with a special morphological property of the retinal ganglion cells: the thin segment, which plays a crucial role in the nerve impulse initiation in the natural situation. By the means of traced ganglion and bipolar cells the fifth and last section of this section tries to answer the question: Which neural elements are excited by electrical stimulation? An answer is given by the cell geometry [Resatz and Rattay 2004].

4.1 Preliminary studies with the activating function

The incipient investigation with the help of the activating function enlightens in a first approach the effects that arise from a very simple geometry of the cell, a straight structure consisting of dendrite, soma and axon, to clearly differentiating them from other phenomena in extracellular stimulation. On the level of the activating function studies concerning the influence of an applied electric field on each compartment are concrete and easy to perform, because the equation is very simple and the effects are directly readable. However it is not

surprising that thresholds and generally complex phenomena which occur in the course of the cell's excitation process are inadequately represented by the activating function, as it does not include membrane properties.

The following simulations are done for several straight structures of 2000 μm length (in Fig. 4.1 a selected section of 800 μm is displayed). The length of the cylindrical compartments is always 10 μm . The electrode is modeled as a point source located 40 μm above the target structure in an infinite homogeneous medium, and the stimulating current is 1 μA .

In the first trace of Fig. 4.1 the typical activating function (equation (3.15)) for an 1 μm thick fiber is shown. If one includes the specific membrane capacity and internal resistance

$$C_n = d_n \Delta x_n \pi c \text{ and } \frac{R_n}{2} = \frac{2\rho_i \Delta x_n}{d_n^2 \pi}$$

(d_n and Δx_n diameter and length of the n -th compartment, c specific membrane capacity, ρ_i the intracellular resistivity) in equation (3.15), the activation function has the following form:

$$f_n = \frac{d_n}{2c\rho_i(\Delta x)^2} \left[\frac{d_{n-1}^2}{d_{n-1}^2 + d_n^2} (V_{e,n-1} - V_{e,n}) + \frac{d_{n+1}^2}{d_{n+1}^2 + d_n^2} (V_{e,n+1} - V_{e,n}) \right]. \quad (4.1)$$

Thus the values of the function are nonlinearly influenced by the compartment diameter and linearly by the electrode current that is multiplicatively included in the extracellular potential V_e . In the following analysis the activating function is regarded as continuous function ($\Delta x \rightarrow 0$). The borders between the depolarizing and hyperpolarizing regions, which is given for straight fibers by an angle of 70.5° [Rattay 1986, 1990], are marked by dotted lines in Fig. 4.1. The zeros of the function, that enclose a region of 56.6 μm referring to the fiber, remain constant for all investigations, because the position of the electrode is all the same in the left column and the right column of Fig. 4.1 respectively. The cut off at the minimum of the graph is a consequence of the compartment size.

The effect of a fiber diameter thinning is shown in the second trace of the figure. It differs if the diameter change is on the right hand side (left column in Fig. 4.1) or on the left hand side (right column in Fig. 4.1) of the electrode position. If the electrode is above the thick part of the fiber (case C) the absolute values of the three activating function extrema are doubled relative to the upper trace, because the diameter of the fiber is doubled under the electrode. Equation (4.1) shows that, if $d_{n-1} = d_n = d_{n+1} = d$, then the activating function is linear with respect to d . Therefore the absolute values of these primary extrema (there are also new extrema besides those which already appear in the first row) remain constant for all investigations shown in the right column of Fig. 4.1, because the electrode is always positioned over a 1 μm thick piece of the fiber.

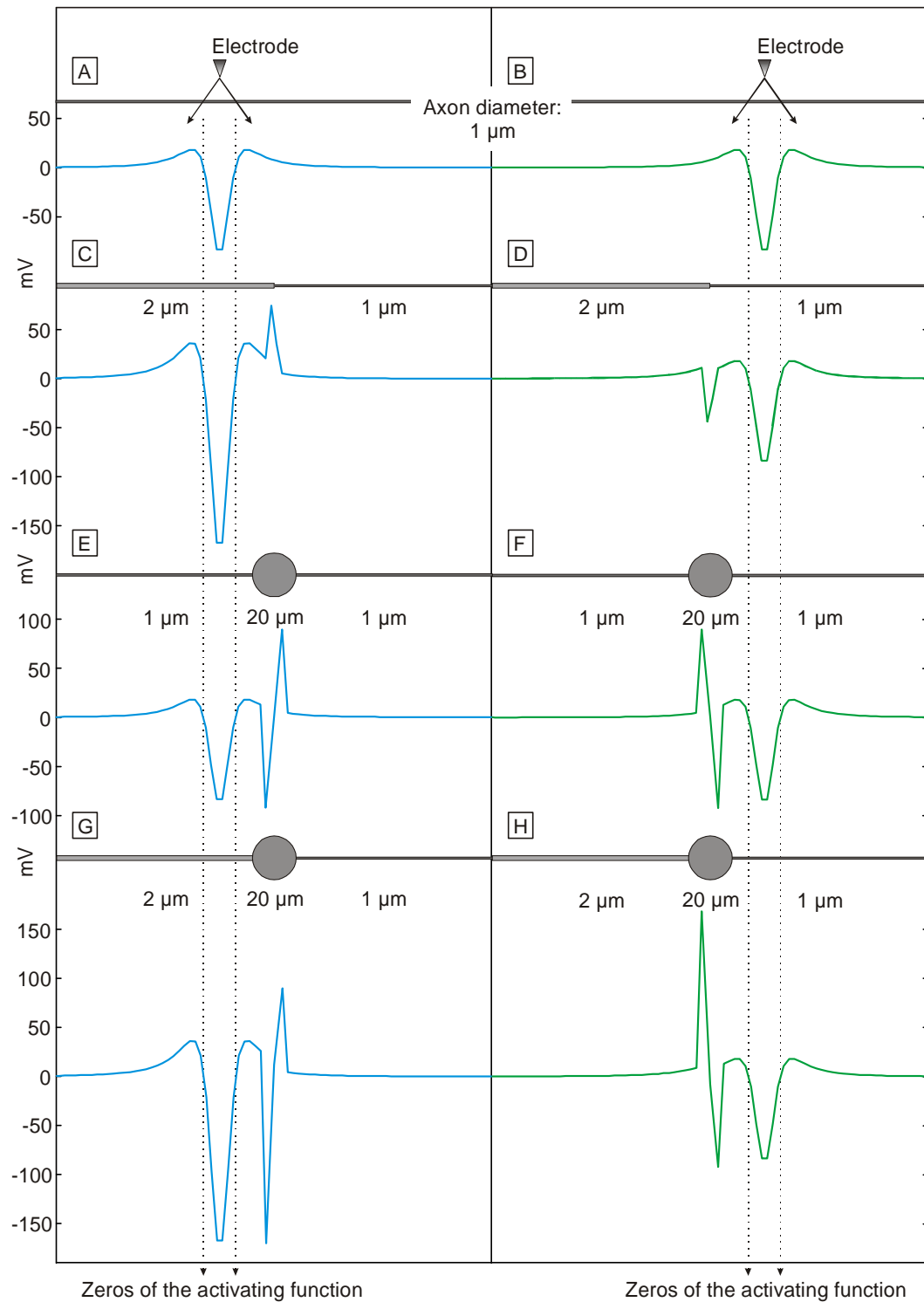


Fig. 4.1 Activating function for two electrode positions (left column and right column respectively). The first trace shows the classic activating function, which is the second difference quotient of the extracellular potential along the axon. Second trace shows the influence of bisecting of the fiber diameter. Third and bottom trace includes a soma in the model latter with a twice as thick dendrite than axon.

The diameter change produces additional extrema of the activating function, which do not appear in the first trace of Fig. 4.1. Attention should be paid to the fact that the nonlinearity, caused by the different diameter sizes of neighbor compartments, affects only these two compartments, which are numbered i (diameter 2 μm) and $i+1$ (diameter 1 μm) in the following. In case C the electrode is located over the thick (2 μm) piece of the fiber and here f_i and f_{i+1} are positive, because

$$(V_{e,i-1} - V_{e,i}) > 0 \text{ and } (V_{e,i} - V_{e,i+1}) > 0$$

are the dominant terms in equation (4.1) by the reason that they are weighted with the factor 0.5, whereas

$$(V_{e,i+1} - V_{e,i}) < 0 \text{ and } (V_{e,i+2} - V_{e,i+1}) < 0$$

are multiplied with a value smaller than 0.5. The maximum is attained at f_i .

The reversed situation is diagrammed in Fig. 4.1 D. Here the electrode position over the thin segment induces negative values for f_i and f_{i+1} , because

$$(V_{e,i-1} - V_{e,i}) < 0 \text{ and } (V_{e,i} - V_{e,i+1}) < 0.$$

But the absolute values for f_i and f_{i+1} are the same as in the previous case. Thus the minimum is attained at f_i corresponding to the last thick compartment before the thinning.

The third trace of Fig. 4.1 shows the influence of including a soma in the model. Now three compartments are involved in the irregularities, but effects are similar to those in the upper trace. If the electrode is on the left side of the soma, the first diameter change after the electrode from the thin fiber to the thick soma causes a large minimum and the change from the soma to the fiber diameter produces a maximum in the activating function (case E). With the electrode on the right side of the soma (case F) the situation is mirror-inverted.

Finally the bottom trace shows the activating functions for the two electrode positions and the simplest model of a cell including a dendrite, a soma and an axon. The dendrite at the left side is twice as thick as the axon connected on the right hand side to the soma. All phenomena discussed above are combined here. With the electrode above the dendrite the absolute values of the activating function (case G) are doubled and with them also the absolute value of the left soma extremum is enlarged, it stays enlarged even if the electrode moves over the thinner axon, because this phenomenon is characterized by the diameter relation of dendrite and soma. Beside of these differences the fourth trace looks like the third.

At the parts of the fiber where the activating function is positive the fiber is stimulated. Here an electrode current of 1 μA is applied and since the function is linear with respect to this variable, it is obvious that a homogenous fiber is

easier to excite with a negative current, because then the graphs in Fig. 4.1 are reflected at the x-axis and consequently the new maximum is much larger than the two maxima in the actual first trace.

The thinning of the second trace causes additional extrema which generate a further location on the fiber where in the case of an active membrane, for example, an action potential could be induced. With the electrode over the thicker part of the fiber the new maximum is the driving force of positive stimulation (case C). Since the additional extrema in case D are smaller than the primary extrema (already seen in B), it needs extra support for them to be crucial for the excitation process, which could be different membrane properties for instance. These phenomena will be the target of further investigations on effects of the thin segment in retinal ganglion cell axons (Section 4.4).

If a soma is included in the model the situation becomes much more difficult. Two additional extrema arise compared to the original activating function and in the case of Fig. 4.1 they have contrary algebraic signs. As in a real cell dendrite and axon have different membrane kinetics further investigations are necessary to ascertain, which peak is the ‘winning’ term, that initiate a spike. This and further studies about the influence of a soma on the excitation process is the topic of the next section.

4.2 Variation of the soma size

Studying the influence of soma size on the excitation process is necessary, due to a special characteristic of the traced target cells that are used for the investigations in following sections of this thesis. These retinal ganglion cells are mudpuppy cells, and as mentioned in Section 2.3, their nuclei contain a doubled set of chromosomes. Hence the cell bodies are relatively large. Actually they are about twice as large as the somata of human ganglion cells. Therefore it is interesting to know how the soma radius affects the threshold values as well as other properties of the excitation process, like the development and propagation of action potentials.

In the simulations of this section the electrode is modeled as a point source in an infinite homogeneous medium. The stimulus is a single 100 μs pulse for all investigations. Similar to the last row of Fig. 4.1 the target structure consists of a 500 μm long dendrite, a soma, and a 1000 μm long axon attaches. The diameter of the dendrite is 2 μm in agreement with the middle diameter of a retinal ganglion cell dendrite. The axon diameter is 1 μm also in accordance with anatomical knowledge [Bron et al. 1997]. In the following studies the soma radius varies in steps of 1 μm from 5 μm to 15 μm . The length of the cylindrical compartments forming dendrite and axon is 5 μm for investigations with an electrode distance of 20 μm in z-direction (see Fig. 4.2), and 10 μm for larger distances.

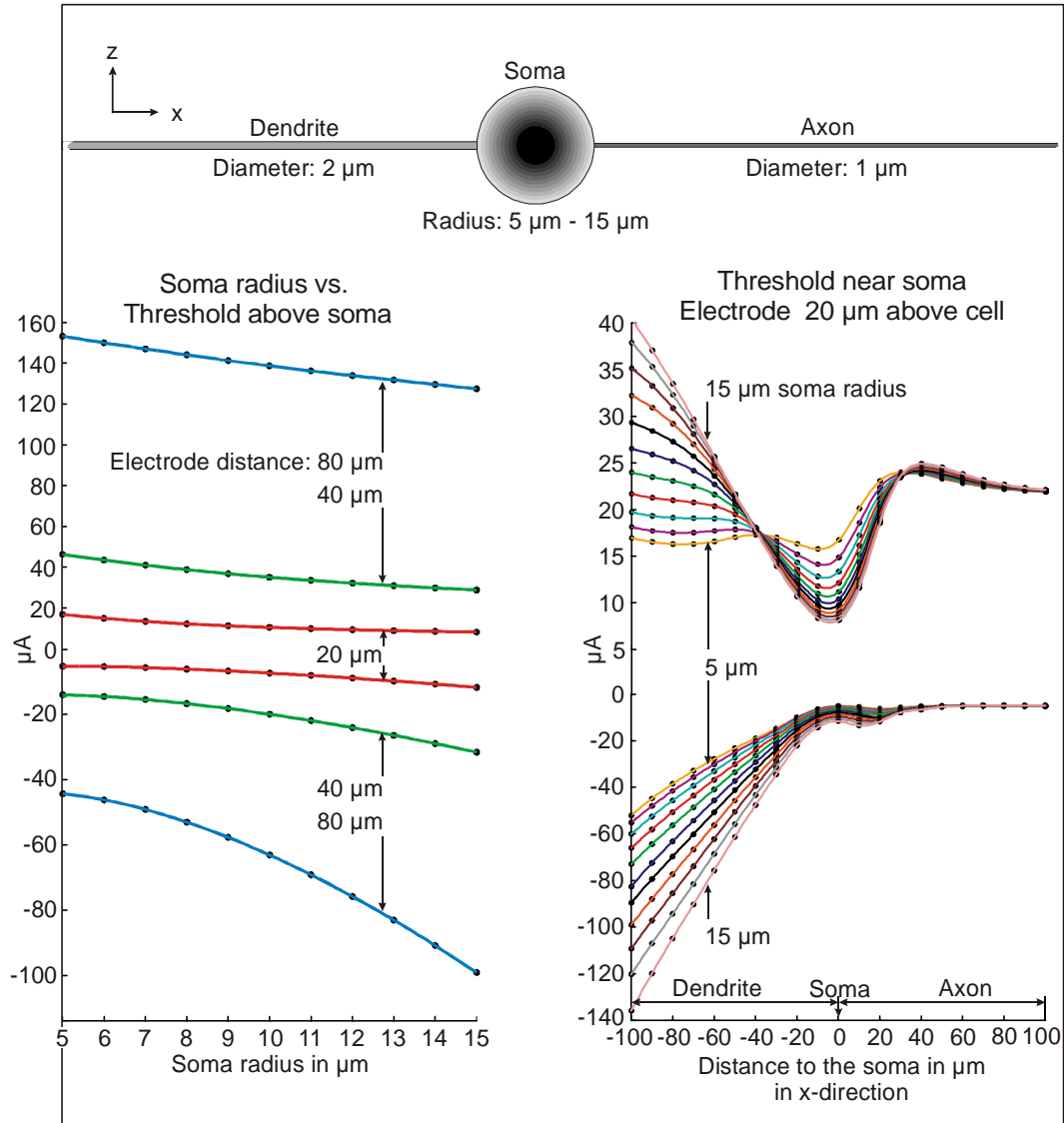


Fig. 4.2 The first row shows the target cell, with a schematic representation of the soma radius variation from 5 μm to 15 μm which is used in the models. The graph in the left column pictures the positive and negative thresholds for an electrode above the soma as a function of soma radius. In the right column the cathodic and anodic threshold values are plotted for an electrode moving 20 μm above the cell from 100 μm before the soma on the dendrite to 100 μm after the soma on the axon. Each curve in the graph represents a cell with a different soma radius. The stimulus duration is always 100 μs .

The dendrite and the rest of the target cell are modeled with different membrane kinetics. On the dendrite a linear passive model with a specific membrane conductance of $g_m = 0.02 \text{ mS/cm}^2$ is applied [Geddes and Baker 1967]. Soma and axon are modeled with the Hodgkin-Huxley mechanism (for model details see Section 3.2). For the plots of Fig. 4.2 a cubic spline data interpolation is used to smooth the graphs.

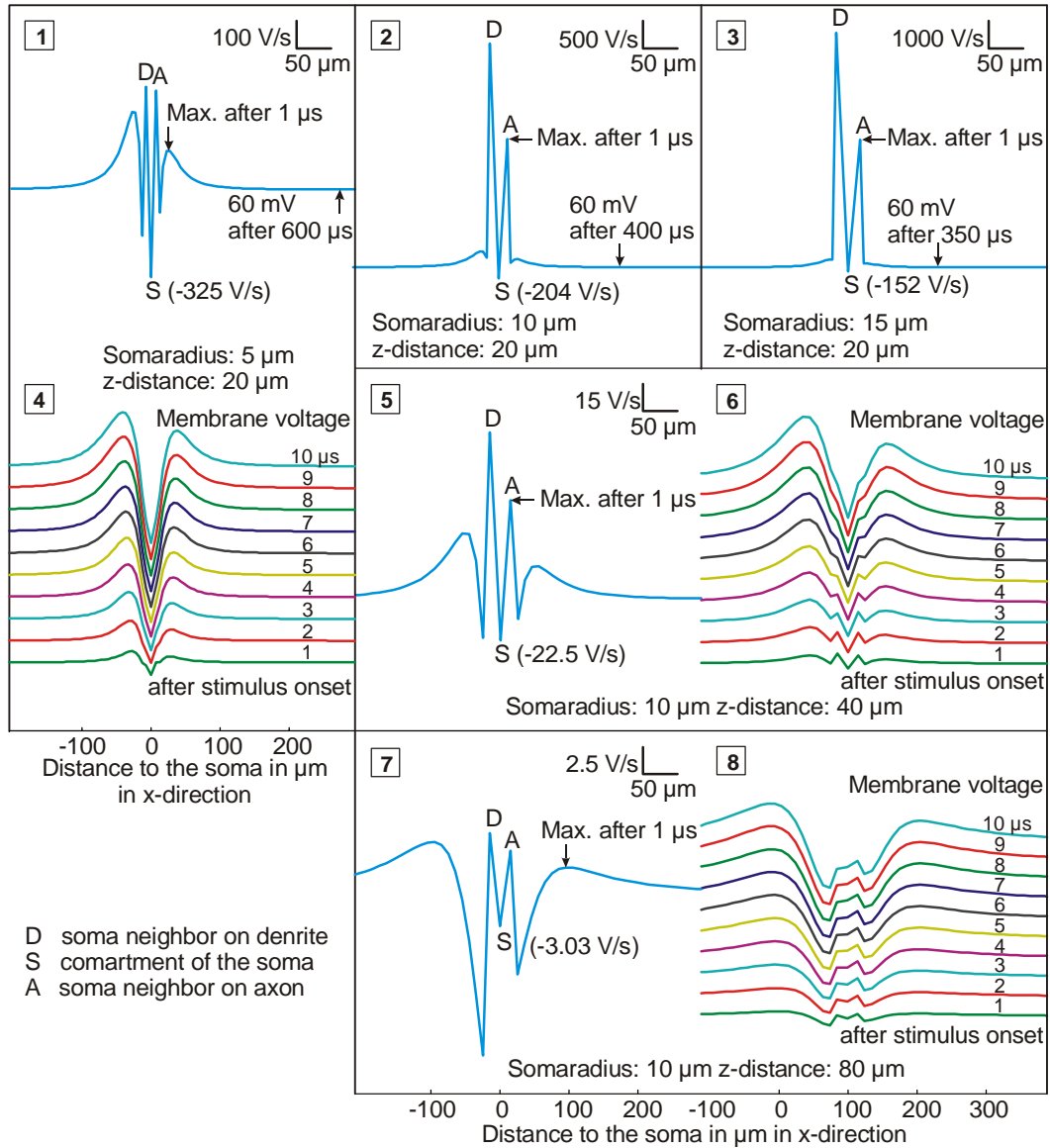


Fig. 4.3 Activating function and excitation profiles for an electrode position above the soma, and positive stimuli. For the activating functions shown in the pictures 1, 2, 3, 5, and 7 the stimulus is $1 \mu A$. In the first row the electrode is fixed $20 \mu m$ above the soma over cells with a radius of $5 \mu m$ (1), $10 \mu m$ (2) and $15 \mu m$ (3), respectively. Pictures 2, 5, and 7 show the graph of the activating function for a cell with a soma radius of $10 \mu m$ and an electrode distance of $20 \mu m$ (2), $40 \mu m$ (5), and $80 \mu m$ (7). The capital letters D, S, and A mark the compartments of the soma neighbor on the dendrite, the soma (value of the activating function enclosed in brackets), and the soma neighbor on the axon respectively. Additionally the location of the maximum membrane voltage after $1 \mu s$ stimulation is tagged by an arrow, and likewise marked is the initial site of excitation in the pictures 1, 2, and 3. Pictures 4 (same model as in 1), 6 (same model as in 5), and 8 (same model as in 7), show the membrane voltages for a stimulus current on the respective threshold ($16.7 \mu A$, $35 \mu A$, and $139 \mu A$) between $1 \mu s$ and $10 \mu s$ after stimulus onset in steps of $1 \mu s$.

The first investigation concerns the thresholds with negative and positive stimulus for varying soma size (left column of Fig. 4.2). Here the point source is

located 20 μm , 40 μm , and 80 μm respectively above the cell body. Regarding the graph for the negative threshold values, one notices that the curves for the different electrode distances look rather similar. Indeed, the simulation demonstrates the linear dependence: the threshold values for 40 μm z-distance are the result of multiplying the 20 μm values with 2.72, and a further multiplication with 3.16 delivers the thresholds for 80 μm distance up to small deviations (two times the last digit doesn't follow the prediction of the linear model - the thresholds are calculated for three digits exactly).

In case of negative stimulation the excitation process is rather simple, which will be explained by inverting the activating function in Fig. 4.3. The pictures **1**, **2**, **3** of Fig. 4.3 show the activating functions for electrodes 20 μm over the respective somata (the stimulus current in all activating function graphs is 1 μA ; i.e. the minima become positive with negative stimulation). The soma radius varies from 5 μm over 10 μm to 15 μm , but independently of this the minimum in the activating function caused by the cell body (marked by a **S** in the pictures of Fig. 4.3) is the driving force of the excitation process. As the absolute value of this extremum becomes smaller if the soma is larger, the cell becomes more difficult to excite.

As mentioned above the cathodic stimulation situation differs a little bit if the electrode distance is large. Pictures **2**, **5**, and **7** of Fig. 4.3 show the activating functions for a cell with a soma of 10 μm radius and an electrode distance of 20 μm , 40 μm , and 80 μm , respectively. Here it is remarkable that in the case of the 80 μm distance the soma compartment achieves not the absolute minimum of the function. But the values of the compartments adjacent to the neighbor compartments of the cell body (marked in Fig. 4.3 by **D** and **A** for the dendritic side and the axonal side, respectively) are lower. These two minima are caused by the regular activating function without soma influence. But determining for the excitation process is still the soma, because 28 μs after stimulus onset the membrane voltage of the cell body is higher than that of the axon, and 20 μs later this value is the absolute maximum. The influence of the dendritic arbor decreases fast because of the passive cell membrane properties.

The location of the compartment, that is the driving force of excitation, varies much more in the case of a positive stimulus current, and this phenomenon influences the thresholds. The largest and the smallest threshold value differ with negative stimulation about 56 % for each investigated electrode distance. With a positive electrode current the difference is 51 % for a distance of 20 μm , 38 % for 40 μm , and 17 % for 80 μm displacement of the electrode. This effect is caused by diverse origin points of the action potentials (Fig. 4.3).

In Fig. 4.3 the maximum membrane voltage after 1 μs positive stimulation, with a stimulus current on threshold, is marked by an arrow in the graph of the respective activating function. Soma and axon are favored regarding the excitation because of their active Hodgkin-Huxley membrane. Arrows in pictures **1**, **2**, and **3** show that independent of the increasing soma size always a maximum of the

activating function over the axon is the origin point of the action potential. This maximum grows with enlargement of the somata (see scale bars in Fig. 4.3). Thus increasing soma size means more excitable with positive currents in contrast to the situation for stimulation with a negative current.

For a soma radius of 5 μm and an electrode 20 μm above the cell body with a stimulus intensity at threshold (16.7 μA) picture 4 shows the membrane voltage from 1 μs to 10 μs after stimulus onset in steps of 1 μs . After 1 μs not only the dominant maximum, which is an element of the regular activating function for a homogenous fiber without soma influence, but also the influence of the still larger maximum of the axonal soma neighbor compartment in the activating function is seen (lowest line in picture 4). The development of the action potential runs similarly for a cell with a soma radius of 10 μm or 15 μm (pictures 2 and 3), apart from the fact that in these cases the axonal soma neighbor becomes dominant as the driving force in the excitation process.

The situation differs again if the electrode is positioned 40 μm above the soma. In picture 6 of Fig. 4.3 the membrane voltage in the part of the cell around the soma (radius 10 μm) is shown from 1 μs to 10 μs . The electrode z-distance is 40 μm and the stimulus intensity at threshold 35 μA . 1 μs after stimulus onset the axonal neighbor compartment of the soma has the highest value, but nevertheless the axonal maximum that is further away from the soma wins fast at height and becomes the driving force for the production of an action potential. In picture 8 the graphs of the membrane voltages for an electrode 80 μm above the soma and at threshold current of 139 μA are plotted. Here, already after 1 μs , the most right maximum has the highest value, but it needs more than 1200 μs till the membrane potential reaches the value of 60 mV somewhere on the axon. Such long duration of the excitation process at threshold is a property of the HH model that is similar to the FCM dynamics, but it is not seen in the membrane models of myelinated mammalian axons.

The *initial site of excitation* is the location on the axon (measured from the boundary of the soma) where the membrane potential first crosses 60 mV on its way to produce an action potential (stimulus intensity at threshold). The maximum membrane voltage after 1 μs and the initial site of excitation is marked by an arrow in pictures 1, 2, and 3 in Fig. 4.3 for a positive stimulus. With increasing cell body radius the initial site moves nearer to the soma, and with it the *initial time of excitation* becomes shorter, that means the time (measured from stimulus onset) when the membrane potential first crosses 60 mV on its way to produce an action potential with a stimulus intensity at threshold shortens.

As the electrode moves further away from the cell body the initial site of excitation moves also further away from the soma along the axon, and the initial time becomes longer. Therefore it is impossible to mark these values in pictures 5 and 7. All these effects can be observed in a similar way with negative threshold stimulation, but generally the initial site becomes closer to the soma and the initial time shorter. This is also reflected by the mean values, which are 383 μm and 872

μs with positive stimulation, but only 89.7 μm and 667 μs with negative stimulation.

In the next investigations the electrode is moved along the cell and the influence on the thresholds is studied. The right column of Fig. 4.2 shows the thresholds for different soma sizes and an electrode 20 μm above the cell axis varying in steps of 10 μm from 100 μm before the cell body on the dendrite to 100 μm after the soma on the axon. Regarding the graphs it is eye-catching that with both positive and negative stimulation a larger soma causes a higher threshold over the dendrite. The further away from the cell body the more difficult it is to excite the dendritic structure, which is not surprising because of the passive dendritic membrane.

However there is a restriction for positive stimulation. Approaching on about 40 μm distance to the soma on the dendrite the consequence of direct soma stimulation described above takes control and now cells with smaller somata are more difficult to excite in this region. This phenomenon occurs earlier if the z-distance of the electrode increases, with an electrode 40 μm above the dendrite, larger somata are easier to excite already about 50 μm away from the soma, and with an electrode of 80 μm above the cell the distance increases to 70 μm .

Generally in the case of a positive stimulation the axonal soma neighbor determines the excitation process for an electrode above the dendrite and the soma. As long as the x-coordinate of the electrode is so large that the dendritic soma neighbor compartment comes not in the influence of the 'homogenous fiber activating function minimum' the situation is analogous Fig. 4.1 G. There the dendritic soma neighbor is a minimum and the axonal soma neighbor is a maximum of the activating function. With larger soma radius both extrema increase but the minimum more than the maximum. Therefore in such a case a larger soma radius causes a higher threshold. If the electrode moves along the dendrite nearer to the soma both soma neighbors become maxima (see Fig. 4.3 in contrast to Fig. 4.1 G) and now a larger soma radius causes a lower threshold.

With negative stimulation the activating function maximum for a homogenous fiber is the driving force of excitation. Thus the passive membrane properties on the dendrite and a large soma cause high thresholds. Up to a certain point negative excitation is even harder than positive. This point depends on the soma radius and is nearer to the dendritic end of the cell if the soma is smaller. For the situation shown in the right column of Fig. 4.2 the cross-over point for the negative and the positive threshold graph is 36 μm from the center of the soma on the dendrite for a cell body radius of 5 μm . For a cell with a soma radius of 15 μm this point moves to the axon 13 μm away from the soma center.

The absolute minimum threshold value for an anode 20 μm above the neural structure is for a 5 μm – 10 μm soma radius in 20 μm distance from the soma center on the dendrite (28 % - 63 % below the value for a straight axon), and in the case of a larger cell body directly above the soma compartment. If the z-distance of the electrode is larger, there is a similar situation as a function of soma

radius, but the location of the minimum values departs from the cell body along the dendrite. Thus when the electrode distance is 40 μm the minimum values are about 20 μm to 30 μm away from the soma (38 % - 51 % below the value for a straight axon), and if the electrode distance increases to 80 μm the minima are in a distance of about 50 μm to 60 μm from the soma (about 45 % below the value for a straight axon). (Note that these observations are based on the 10 μm grid evaluation and 100 μs square pulses.)

Negative stimulation produces minima directly above the axon 60 μm to 100 μm from the soma center. Both increasing z-distance and soma radius moves the minima away from the soma, but all things considered the threshold values do not differ a lot in some distance of the cell body, when the electrode is moved along the axon, because of the nearly identical activating functions (i.e. the minima are less than 4 % below the thresholds of the rest of the axon), resulting in less than 10 % threshold variations as soon as the x-distance to the soma center is greater than 30 μm . This result is independent from the chosen soma radius and z-distance. For negative stimulation and small soma radius (5 μm - 6 μm) the appropriate cell body distance is 40 μm for a 10 % deviation. For a larger soma radius this value varies between 50 μm to 70 μm with increasing z-distance of the electrode from 20 μm to 80 μm .

In summary, for an electrode above the dendrite the thresholds depend heavily on the soma radius, but over the axon the influence of the soma size decreases fast. Thus with positive stimulation the deviation in thresholds caused by the radius is, in 30 μm distance of the soma center, less than 10 % for each electrode varying from 20 μm to 80 μm over axon. With negative stimulation the critical x-distance for less than 10 % variation has a stronger correlation to the z-distance of the electrode. For an electrode 20 μm over the neural structure a x-distance to the soma of 50 μm is the necessary, for an electrode 40 μm above 60 μm , and if the point source is 80 μm above the axon it has to be also 80 μm away from the cell body to decrease the soma size influence under 10 %. For an electrode directly above the cell body the threshold values differ after all about 24 % for positive stimulation and 42 % for a negative electrode current.

4.3 Investigations on the distance between electrode and target structure

In this section, in a first approach, some fundamental mechanism of stimulation should be clarified on the basis of a simple model. The influence of a cathodic or an anodic stimulus on the principle structures of the cell is investigated on the assumption of a variable electrode distance. Thus on the one hand it is meant that the electrode moves, but on the other hand the electrode

should be regarded on fixed position and then dendrite, soma, and axon have in the natural situation different distances according to the retina's architecture. Namely the axonal fiber layer is closest to the retinal surface, followed from cell body and dendrite layer. Consequently focal stimulation needs sufficient lower thresholds for structures close to the soma. Under this aspect we approach on the question, whether a focused stimulation is possible.

The methods of modeling are matched with the generality of the investigations. Thus as target cell a straight structure is selected that is as simply as possible. It consists of a dendrite, a soma, and an axon and corresponds to the structure investigated in the bottom trace of Fig. 4.1.

Similar as in the previous section the diameter of the dendrite is $2\text{ }\mu\text{m}$ and of the axon $1\text{ }\mu\text{m}$. To avoid effects from dendritic or axonal endings this time the total length of the cell is $3020\text{ }\mu\text{m}$, whereby $1000\text{ }\mu\text{m}$ to the dendrite, $20\text{ }\mu\text{m}$ to the diameter of the spherical soma, and $2000\text{ }\mu\text{m}$ to the axon are allotted. The cylindrical compartment length is again $5\text{ }\mu\text{m}$ or $10\text{ }\mu\text{m}$. Thus the number of 301 or 601 (if the electrode z-distance is reduced to $20\text{ }\mu\text{m}$) compartments, guarantees that the thresholds are independent of their size. The properties of the cell membrane and the volume conductor are adopted as they stand. The electrode position varies in z-direction, i.e. perpendicular to the axis of the neuron, from $20\text{ }\mu\text{m}$, over $40\text{ }\mu\text{m}$, $80\text{ }\mu\text{m}$, and $160\text{ }\mu\text{m}$ to $320\text{ }\mu\text{m}$. Stimulus duration is $100\text{ }\mu\text{s}$ for all investigations. The graphs of Fig. 4.4 are again smoothed with a cubic spline interpolation.

It is known that over a straight axon with constant diameter the thresholds raise linearly with the electrode z-distance in the case of near field stimulation (electrode close to the target structure), and changes gradually to a third power relation of the distance in the case of far field stimulation [Rattay 1990]. Figure 4.4 shows the threshold graphs for cathodic (multiplied with -1) and anodic stimulation plotted against the x-distance of the electrode from the soma. The z-distances of the point source are doubled for each curve from $20\text{ }\mu\text{m}$ to $320\text{ }\mu\text{m}$. Here in the dendrite - soma - axon system the situation is much more complex than with a fiber only, because the graphs change qualitatively with increasing electrode distance.

Nevertheless after some x-distance from the soma the situation becomes the same as in the case of a straight axon. As mentioned in the previous section the position on the axon, where the threshold aberration falls below 10 % for an electrode moving away from the cell body, depends on the z-distance of the electrode and whether the stimulus current is positive or negative. In the first case the critical distance is less than $30\text{ }\mu\text{m}$ if the electrode is nearer than $40\text{ }\mu\text{m}$ in z-direction. In the second case $50\text{ }\mu\text{m}$ distance from the soma are necessary for electrodes nearer than $80\text{ }\mu\text{m}$ to be under the 10 % deviation. For the investigated electrode z-distances which are further away than those discussed here, the influence of the soma on the threshold is less than 10 %, thus practically not of importance (Fig. 4.4). The reason of this effect can be understood by looking at

the activating function. In the case of anodic stimulation the relevant activating function maximum moves with increasing z-distance of the electrode in a linear relation along the axon, even when the electrode is over the soma (see pictures 2, 5, and 7 of Fig. 4.3).

So if the threshold deviations are under 10 % the theory for straight fiber stimulation is appreciable. Hence the threshold increase factor is for a cathodic stimulus 2.5 for moving the electrode z-distance from 20 μm to 40 μm , 3.2 for 40 μm to 80 μm , 4 for 80 μm to 160 μm , and 4.9 for 160 μm to 320 μm . For anodic stimulation and same z-distance jumps are the factors 2.3, 3.1, 4.2, and 5.5. These values follow the theoretical prediction, which postulate a linear relation for electrodes close to the fiber (i.e. double distance results in double threshold which means factor 2 here) and a cubic relation for great distances (i.e. factor 8 for double electrode distance).

Anodic thresholds over the axon are on average about three times larger than the absolute values of cathodic, nearly independent from the z-distance of the electrode. The graphs of Fig. 4.4 demonstrate that at least for a point source closer than 80 μm to the axon, negative stimulation needs lower thresholds than positive stimulation with an electrode half as far apart. The intersection point between these two graphs moves the nearer to the soma the smaller the z-distance of the electrode (bold circles in Fig. 4.4).

It is a fact that with positive stimulation the dendrite is easier to excite than the axon, while with negative stimulation the situation turns around [Rattay 1999]. Only if the electrode is in a short distance above the dendrite and far apart from the soma the thresholds for anodic currents are higher (Fig. 4.4 graphs for 40 μm and 20 μm z-distance of the electrode), because in this position the axonal soma neighbor, the driving point in the case of anodic stimulation, is far away from the homogeneous fiber activating function maximum. The more these two extrema come together the better for the excitation process. For every electrode z-distance there is an optimal position over the dendrite to support this effect, and this location is obviously closer to the soma the nearer the electrode moves to the cell. Thus the lowest anodic threshold for the investigations of this section moves from a 10 μm soma distance to the end of the dendrite with increasing electrode distance (Fig. 4.4).

As discussed in the previous section the single homogenous fiber activating function maximum determines the excitation process in the case of cathodic stimulation. This leads to smooth falling curves over the dendrite with a decreasing rise the closer the electrode moves to the neural structure. In Fig. 4.4 the intersection points between the graphs for negative and positive stimulus current are marked with bold circles. The region over the dendrite where anodic stimulation is easier than cathodic is nearer to the cell body when the z-distance of the electrode is smaller. Thus the necessary distance from soma center is only 14 μm if the electrode is 20 μm over the dendrite and increases to 157 μm if the z-distance increases to 320 μm .

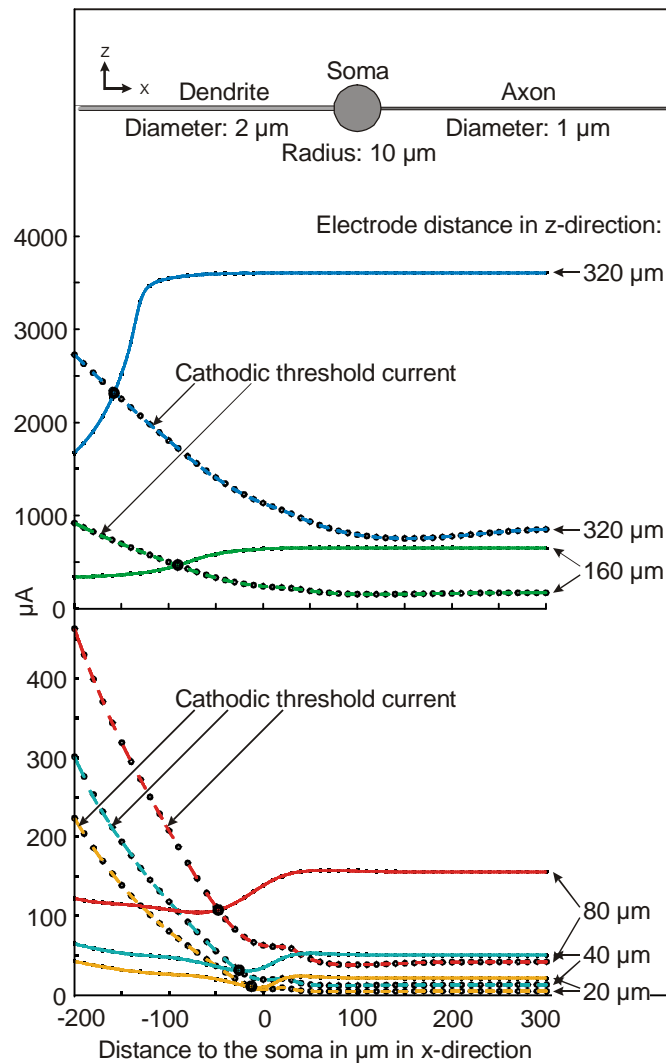


Fig. 4.4 The first row displays the target cell that is used for the investigations of this section. The pictures below show anodic and cathodic threshold curves for different z-distances of the point source (20 μm , 40 μm , 80 μm , 160 μm , 320 μm) as a function of x-distance between soma and electrode. Negative thresholds are multiplied with -1 to be comparable with the positive values. The scale factor differs for 160 μm and 320 μm to nearer positioned electrodes.

Next investigation concerns initial site and initial time of excitation. In the first row of Fig. 4.5 the graphs are shown for threshold stimulus current, and an electrode z-distance between 40 μm and 320 μm . Striking are the more or less large fluctuations of the curves, which are caused by the precision of the calculations. The thresholds are computed for three digits exactly, and therefore they are differently close to the exact value. These small interferences result in displacements up to 100 μm and more of the initial site of excitation accompanying with time fluctuations of hundreds of microseconds till the

membrane potential reaches 60 mV. This shows how sensitively the system reacts to disturbances on threshold.

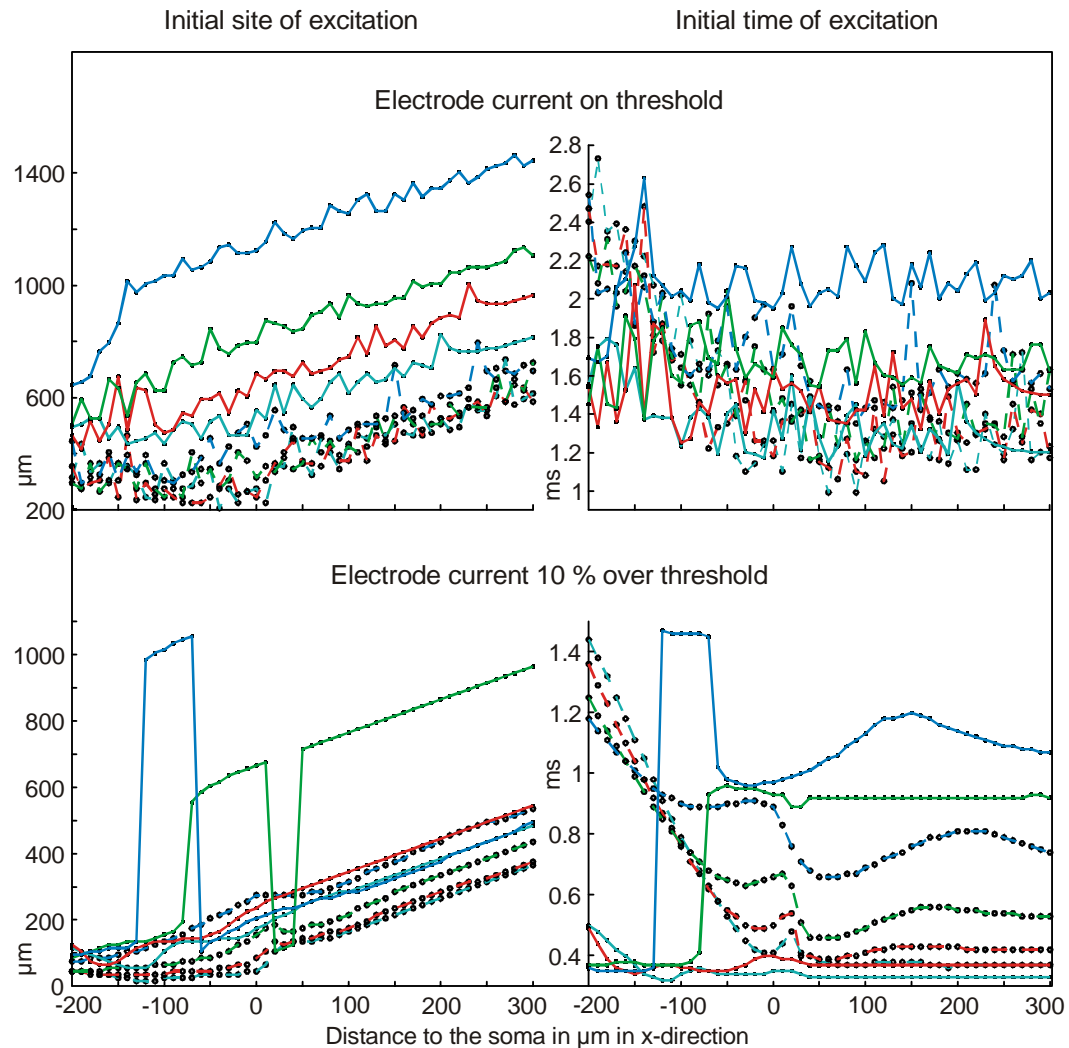


Fig. 4.5 The left column shows the graphs for the initial site of excitation. The right column shows the initial time of excitation. In the first trace these values are computed in respect of a stimulus current on threshold, for the graphs of the second trace an electrode current 10 % above threshold is used. Curves which belong to a cathodic stimulus are plotted with dashed lines. The color refers to the z-distance of the electrode: bright blue means 40 μm , red 80 μm , green 160 μm , and a dark-blue line indicates that the electrode z-distance for these calculations is 320 μm .

The graphs that illustrate the initial site of excitation in the left column of Fig. 4.5 show the same characteristics for both, stimulation on threshold and 10 % above: (i) generally, increasing z-distance of the electrode causes increasing distance from the soma for the initial site of excitation; (ii) with a cathodic stimulus the action potential originates nearer to the soma than with an anodic; (iii) for a point source over the dendrite 60 mV membrane voltage is achieved in some more or less fixed distance to the soma in the case of both negative and positive stimulation with 40 μm electrode z-distance; (iv) for all other electrode

positions the initial site of excitation moves down the axon in the same way as the electrode moves in x-direction.

Despite of all these similarities the initial site of excitation for a stimulus 10 % above threshold is in the case of cathodic stimulation in average 231 μm closer to the soma and in the case of an anodic stimulus 468 μm closer than for stimulation on threshold.

For stimulation 10 % above threshold the curves are relatively smooth (bottom trace Fig. 4.5), because point and time of excitation are here not as sensitive on small disturbances as on threshold. But nonetheless for 160 μm and 320 μm electrode z-distance and positive stimulation still large variations with small x-displacements of the electrode occur, namely, between 120 μm and 70 μm from the soma on the dendrite, with a z-distance of 320 μm the site of excitation varies about 900 μm compared to the values before and afterwards, and a similar behavior happens if the electrode z-distance is 160 μm .

To understand the irregularities in the initial site of excitation, Fig. 4.6 demonstrates the phenomena which appear between 130 μm x-distance of the electrode (left column, stimulus: 3630 μA) and 120 μm (right column, stimulus: 3810 μA) during the first 370 μs after stimulus onset (pictures A, B, D, and E), and the first microsecond (pictures C and E), respectively. In the first and the second trace the same situation is shown with the only difference that in the upper trace the membrane voltage curves for the 22 time steps are not shifted to get a better impression of the proportions. In the first trace the competing effects of anodic stimulation that are already mentioned above are clearly visible. On the one hand there is the first maximum after the soma, a sharp peak, which is generated by the first axonal compartment; on the other hand there is a second much smoother maximum which is caused by the homogenous fiber activating function. The lowest threshold demands that these two maxima coincide in one point. For an electrode over the dendrite the driving force is the axonal soma neighbor, but by moving the electrode over the axon its influence vanishes.

In the second trace of Fig. 4.6 this situation becomes obvious. For the electrode 130 μm apart from the soma the axonal soma neighbor compartment is the origin point of the action potential (picture B), but for an electrode only 10 μm nearer to the soma the, not very high but wide, homogenous fiber activating function maximum becomes dominant, although the high membrane potential of the soma neighbor supports the development of this action potential, too (picture E). Despite of all, after 370 ms the maximum membrane voltage is much lower in the second case (see first trace), and moreover two action potentials develop, which propagate in opposite directions (picture F). Thus it takes much more time and space till the membrane voltage reaches 60 mV, i.e. till the action potential which propagates to the brain is fully developed. If the electrode moves nearer than 70 μm (x-distance; z-distance of the electrode is still 320 μm) to the soma only a single action potential develops and the initial site of excitation is close under the electrode position again.

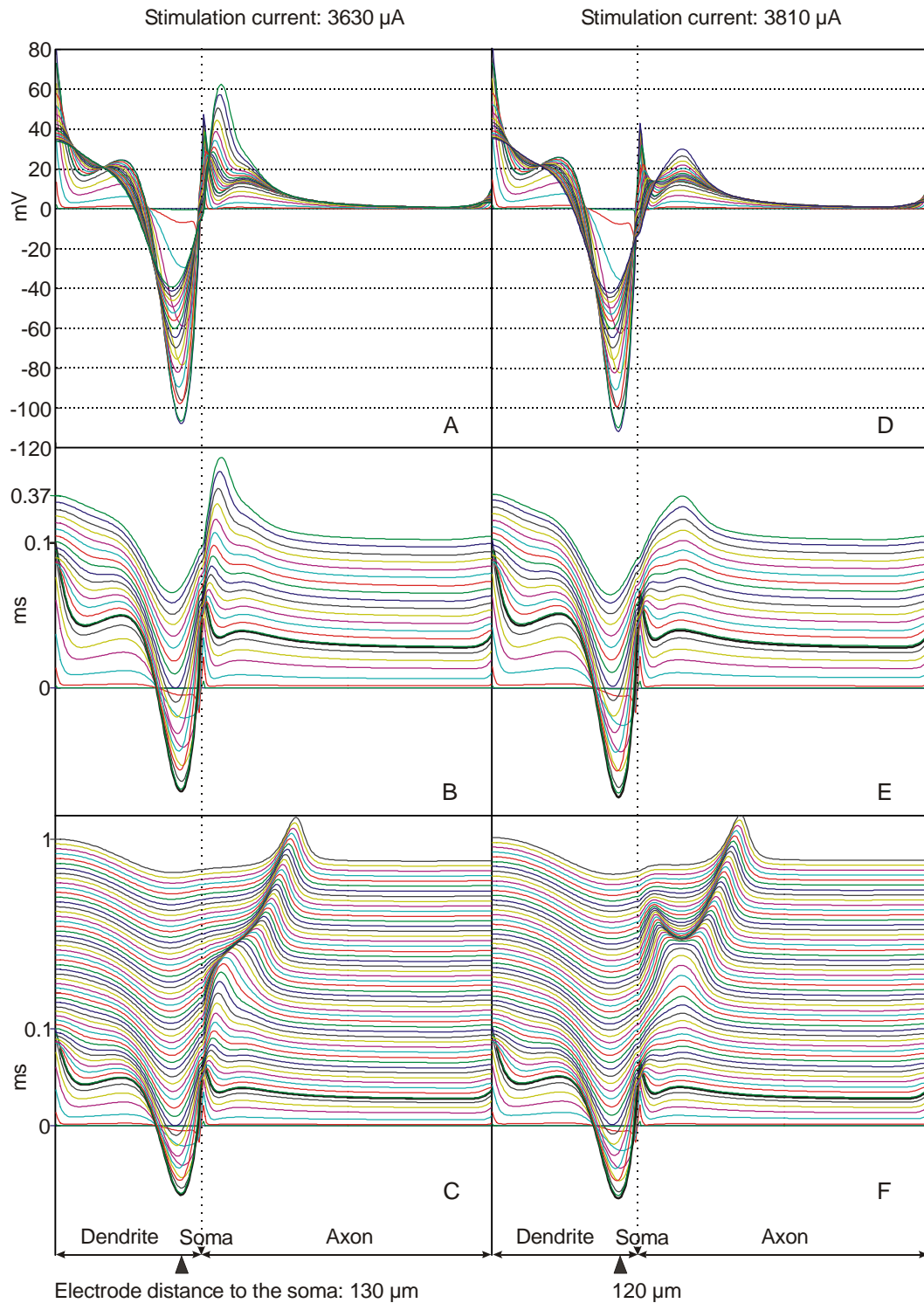


Fig. 4.6 Excitation process that causes the irregularities in initial site and time of excitation with an electrode x -distance to the soma of 130 μm (left column) and 120 μm (right column) over the dendrite (z -distance: 320 μm , stimulus: 10 % above threshold; c.f. Fig. 4.5 bottom trace). The membrane voltage versus x -distance is plotted till 370 μs (first and second trace) and 1ms (bottom trace) after stimulus onset. In the second and third trace the curves are shifted after every time step. The stimulus end after 100 μs is plotted bold in this and the following figures of the section.

A similar phenomenon can be observed for an electrode z-distance of 160 μm , but because of the shorter distance between the neural structure and the electrode the effect shown in Fig. 4.6 is shifted nearer to the soma. However here only one action potential develops and with moving the electrode over the axon the cell membrane potential of the soma neighbor compartment becomes a minimum (see Fig. 4.1 M), which weakens the driving maximum.

Figures 4.7 to 4.10 show the membrane voltage versus soma x-distance in steps of 10 μs from stimulus onset till 500 μs afterwards. For each column the electrode z-distance and current is fixed, and the x-distance varies in each trace from 100 μm before the soma on the dendrite to directly above the soma, and in the last trace the electrode is positioned 100 μm apart from the cell body on the axon.

Moving the electrode from the dendrite over the soma to the axon changes the characteristics of the excitation process for cathodic stimulation 10 % over the soma threshold essentially (Fig. 4.7 and Fig. 4.8). Whereas for a point source over the dendrite the stimulus is too weak to develop an action potential, it needs a relatively long time till the action potential produced by an electrode over the soma is fully developed. Stimulation with the same current over the axon leads to the emergence of an action potential mostly before the stimulus ends (marked by bold curves in Fig. 4.10), at least for not too large distances. For increasing z-distance the amount of depolarized membrane under the point source increases and alters the propagation mechanisms of the excitation. Thus, for an electrode over the axon, a current 10 % over threshold produces a single action potential if the electrode is 40 μm or 80 μm apart, and two in opposite directions propagating action potentials when the z-distance is 160 μm or 320 μm (Fig. 4.7 and Fig. 4.8 bottom trace).

For anodic stimulation with a current 10 % over the axonal threshold an action potential develops even if the electrode moves over soma or dendrite (Fig. 4.9 and Fig. 4.10). Whether one or two action potentials arise does not depend on the electrode x- or z-distance. Remarkable is only the strong cell membrane hyperpolarization in the case that the electrode is positioned above the dendrite, especially, when the electrode is close to the neural structure.

Finally, it should be discussed how these results affect the electrical stimulation of retinal ganglion cells. Regarding the situation with the axons overlying somata and dendrites, anodic stimulation seems the more promising way for selective excitation, because here the thresholds for the somata and especially for the dendrites are much lower than for the axons. But on the contrary the anodic thresholds are about three times higher than the cathodic ones and retina implants operate already close to the charge density safety limits. For the charge balanced biphasic impulses, it is possible that anodic stimulation is no object, because the anodic pulse will always be below threshold.

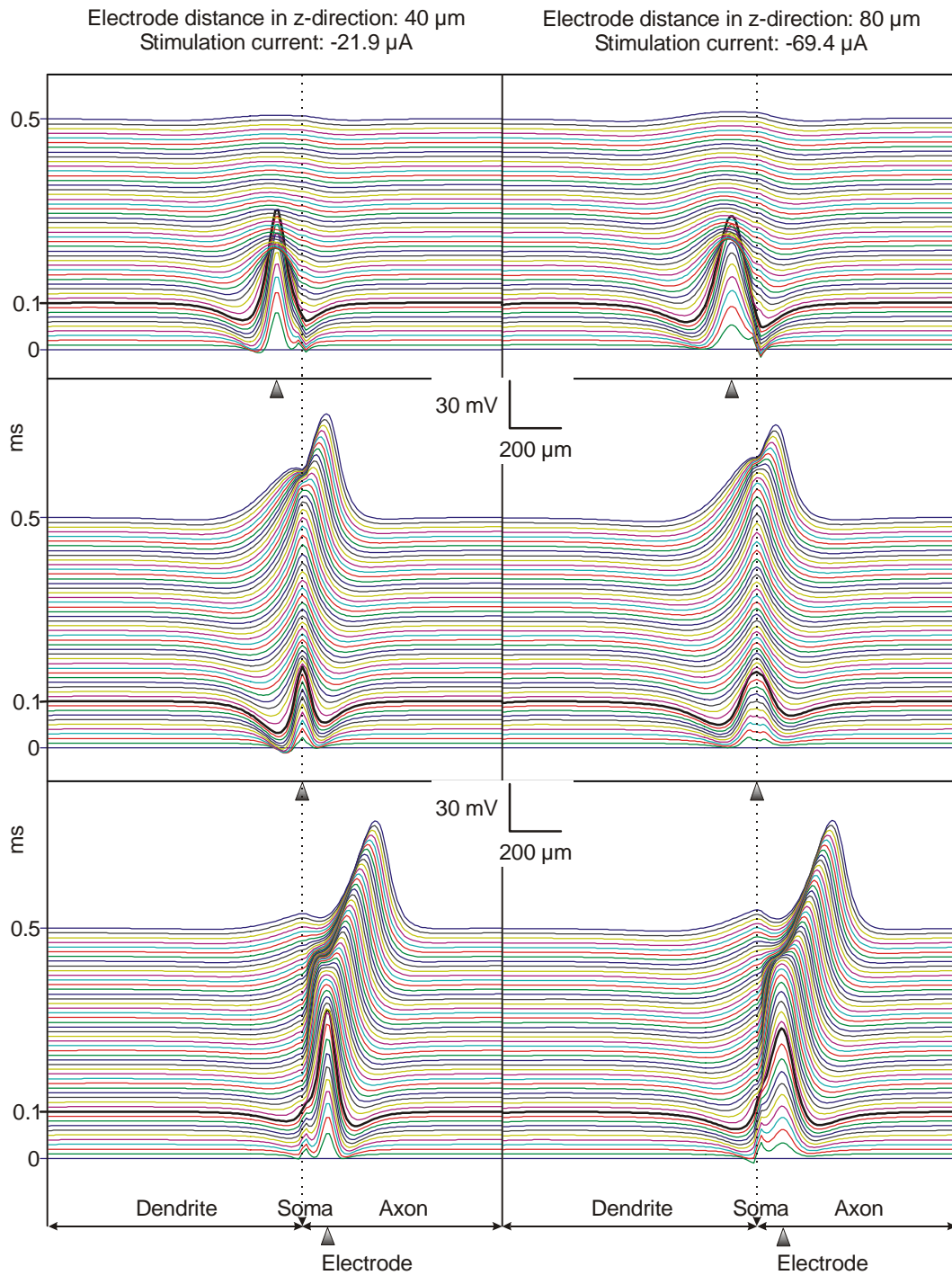


Fig. 4.7 Membrane voltage versus soma distance for a stimulus 10 % above the cathodic axonal threshold. For each column the electrode z-distance and current is fixed. The left column is calculated for an electrode 40 μm above the neural structure and a stimulus of -21.9 μA . The right column refers to a z-distance of 80 μm and a stimulus of -69.4 μA . In each trace the soma-electrode distance varies from 100 μm over the dendrite to the soma, and in the bottom trace the electrode is positioned 100 μm away from the soma over the axon.

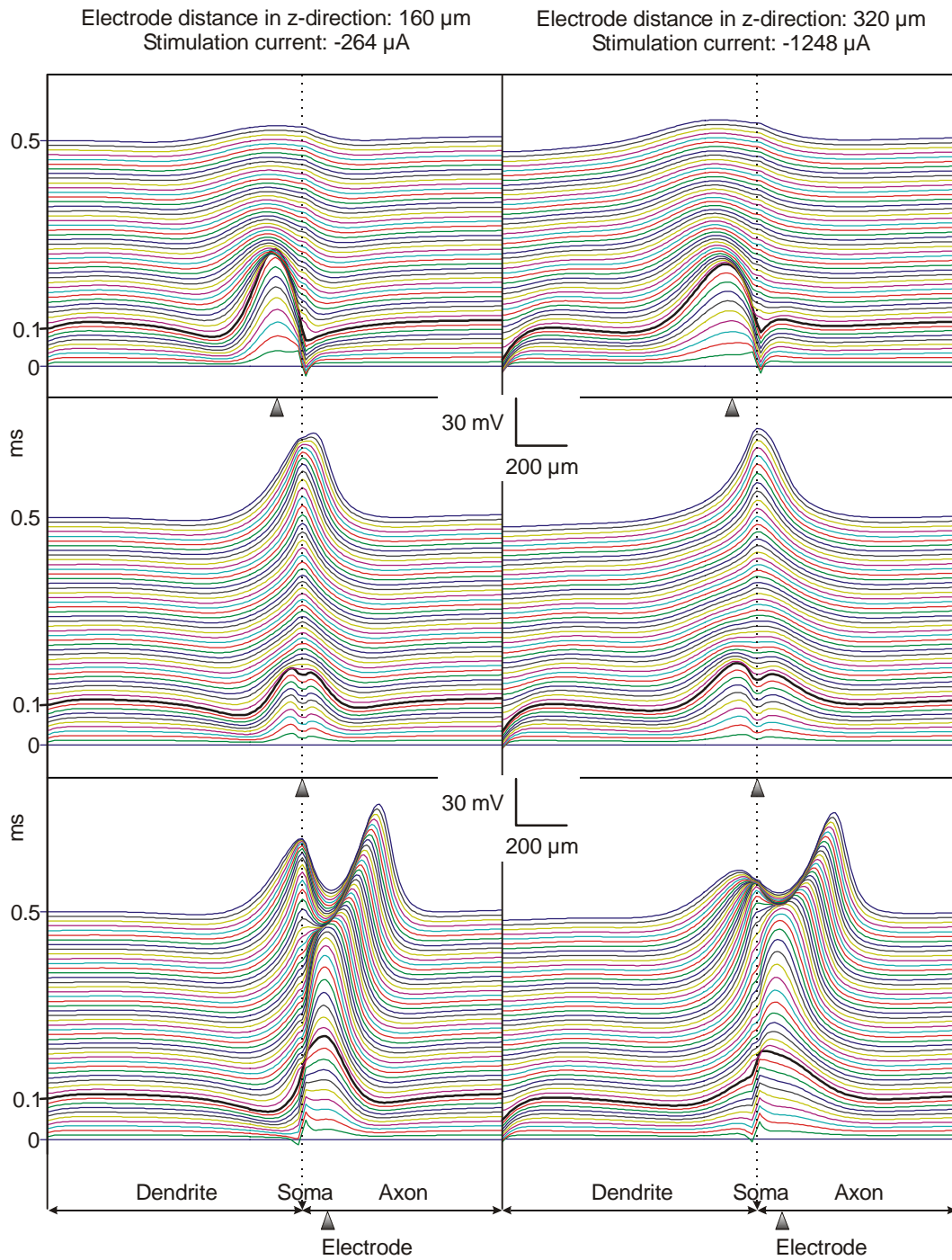


Fig. 4.8 Same situation as in Fig. 4.7, but now the electrode z-distance of the left column is 160 μm and the current is -264 μA and for the graphs of the right column the z-distance is 320 μm and the stimulus is -1248 μA .

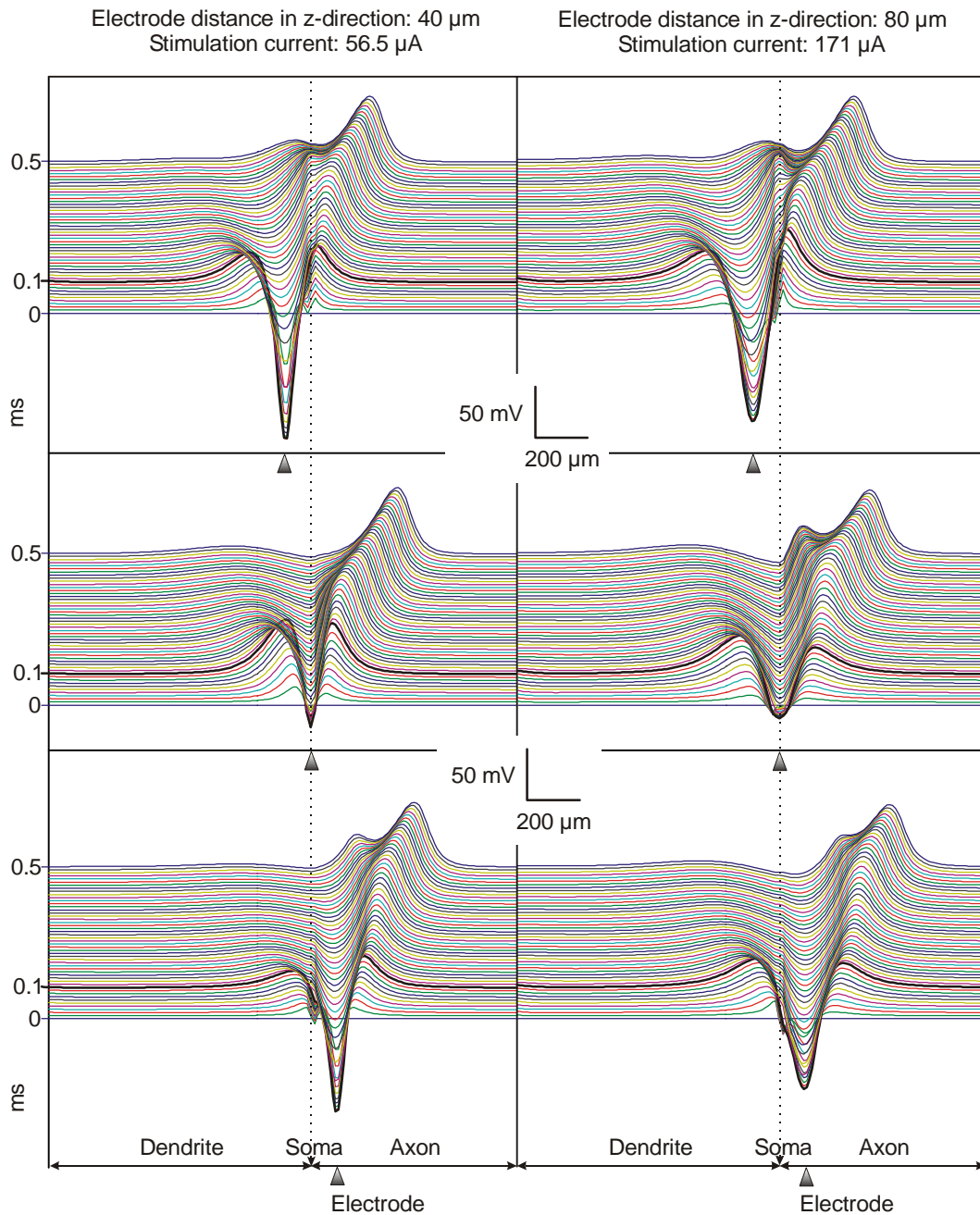


Fig. 4.9 Membrane voltage versus soma distance for a stimulus 10 % above the anodic threshold for an electrode 40 μm above the soma (left column), and 80 μm above the soma (right column). Again for each column the electrode z-distance and current is fixed. The left column is calculated for an electrode 40 μm above the neural structure and a stimulus of 56.5 μA . The right column refers to a z-distance of 80 μm and a stimulus of 171 μA . In each trace varies the soma-electrode distance as in the previous figures.

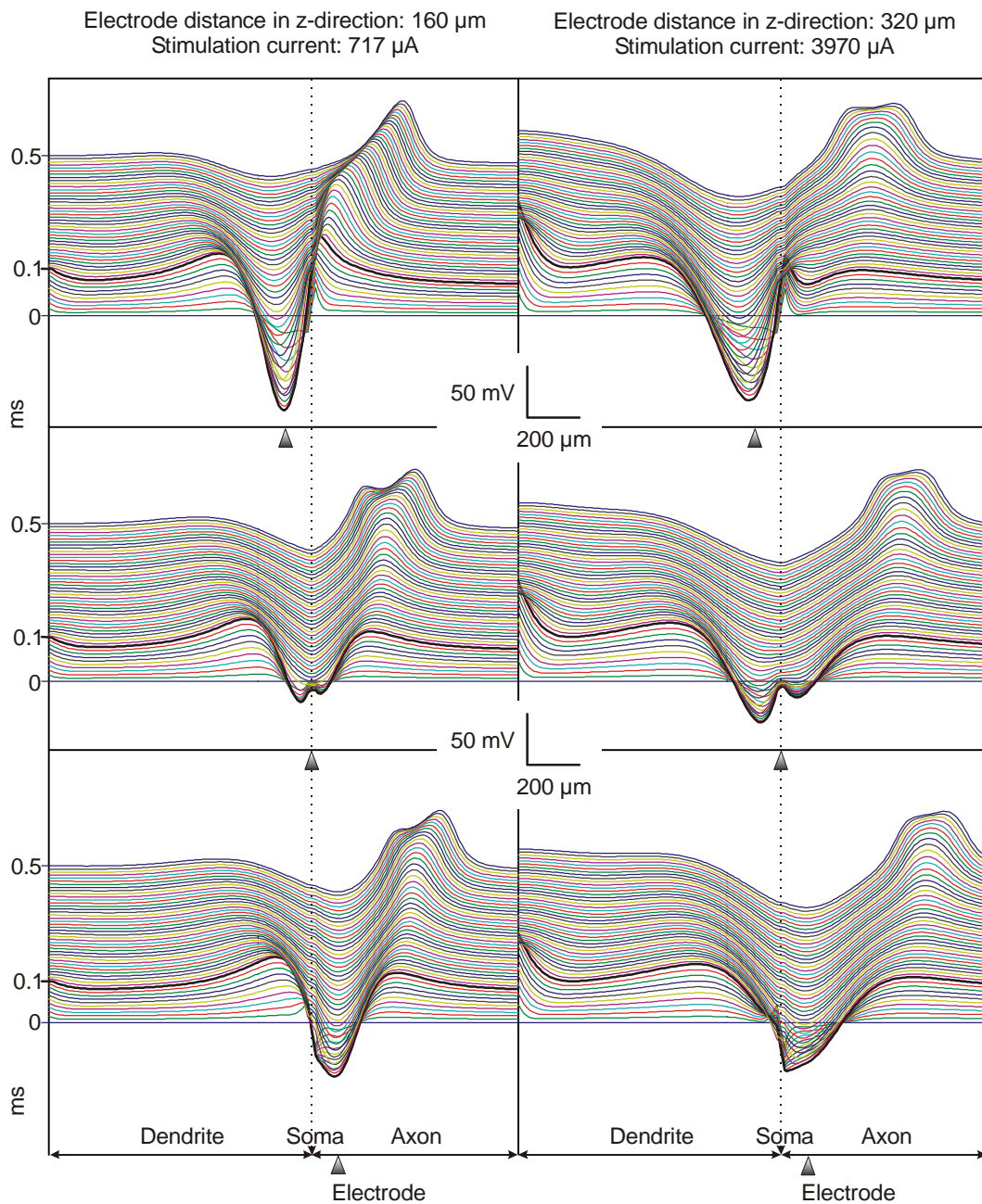


Fig. 4.10 Same situation as in the previous figure, but now the electrode z-distance of the left column is 160 μm and the current is 717 μA and for the graphs of the right column the z-distance is 320 μm and the stimulus is 3970 μA .

Now the question arises how many cells will be activated with a cathodic impulse. With a stimulus current at threshold, theoretically only a single ganglion cell will be stimulated. In human the threshold is found by increasing the current in small steps until the subject reports a visual perception. In this case it is not known how many ganglion cells are involved.

The presented results show that in the worst case, in the sense that a great deal of cells get excited, the threshold over the axon increases linearly with the electrode distance. An estimation of the axonal fiber layer area that is influenced by an active electrode, can give a rough estimation how many ganglion cells are excited (Fig. 4.11). Assuming a z-distance of 30 μm and a stimulus 10 % over threshold at most about 80 axons will be reached, i.e. at most about 80 cells will be excited. If the electrode distance is 100 μm about 760 axons will produce an action potential. That shows with increasing electrode z-distance the difficulty of selective stimulation increases. But this thought experiment includes a point source which is an unrealistic assumption. If a 10 μm disk electrode is used about 42 axons are additionally excited when the electrode is positioned 30 μm above the neural structure.

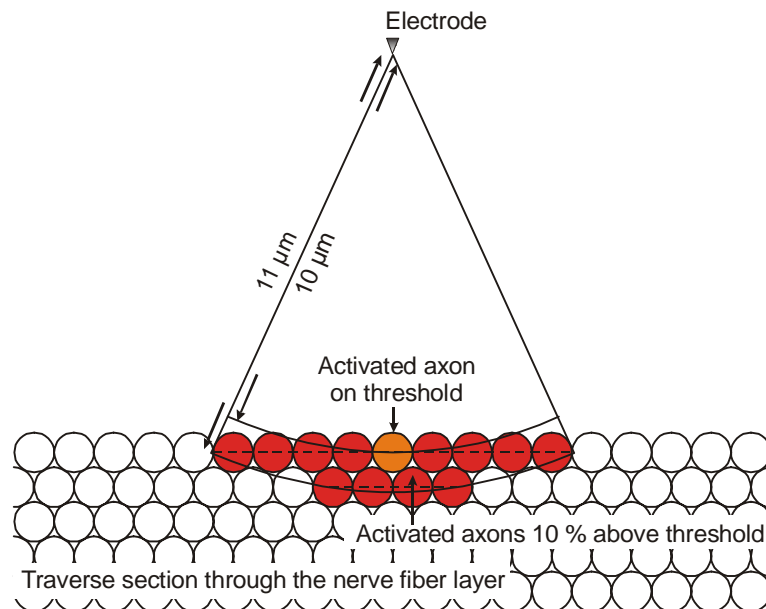


Fig. 4.11 The electrode 10 μm above the nerve fiber layer activates theoretically only one single ganglion cell with a stimulus current on threshold. With a stimulus 10 % above threshold 13 axons produce an action potential if a linear threshold rising with increasing distance is assumed.

The prediction of the excitation of 122 cells with a disk electrode 30 μm above the axonal fiber layer is naturally only a coarse estimation, but it shows the problem if these cells are scattered over a wide range of the retina. However the number of cells is also few enough to provide a crude spot-shaped perception, if they are located to some extent neighboring.

4.4 Influence of the axonal thin segment on the excitation process

Morphological studies of retinal ganglion cells in the mudpuppy (*Necturus maculosus*) and larval tiger salamander (*Ambystoma tigrinum*) identified a characteristic thinning of the axon that begins after the initial segment of the axon emerges from the ganglion cell soma or primary dendrite. Morphometric analysis of the thin segment revealed an average length of 74 μm with a standard deviation of 22 μm [Carras et al. 1992]. Electrophysiological experiments are consistent with the idea that the thin segment and cell soma are less excitable than the initial segment region, which appears to be the principal site of initiation of the nerve impulse. The initial segment is that portion of the axon that is bounded by the soma at its origin and the thin segment is the next towards the optic nerve.

The thin segment confines the site of impulse initiation to a relatively short portion of the axon and decreases the threshold for impulse initiation by decreasing the electrical load on the initial segment. In addition, the thin segment reduces the electrical shut that normally lowers the input resistance of the cell. The latter mechanism can enhance the sensitivity of retinal cells. This axonal site of impulse initiation may also be a feature of retinal ganglion cells of other species [Carras et al. 1992].

These effects of the thin segment in the natural excitation situation suggest that in the case of electrical stimulation the thin segment also plays a crucial role. If it is possible to stimulate a short portion of an axon selectively without activating bypassing axons, focal perceptions would be promoted. This hypothesis will be investigated here.

The model is in principle the same as in the previous section, a 50 μm , 70 μm , or 90 μm long thinning of the target cell's axon, in 30 μm distance to the soma. This thin segment is, in accordance with anatomical knowledge [Carras et al. 1992], half as thick as the rest of the axon, e.g. 0.5 μm (Fig. 4.12 top row). Again the Hodgkin-Huxley model is implemented, on one hand to allow comparison with the previous results, on the other hand to draw the attention solely on the morphological anomaly of the axon, because the FCM model uses different ion channel densities for the thin segment and the rest of the axon. Besides the Fohlmeister-Coleman-Miller model with the parameters used in this thesis is fitted to ganglion cells with a rather large dendritic tree and in the case of the target cell used here the FCM model supplies distorted results. Cubic spline interpolation is used to smooth the graphs of Fig. 4.12.

In the first experiment a current is injected in the soma to simulate a natural excitation process, and to investigate for the model used here the influence

of a thin segment on the electrode threshold. Intracellular 100 μs pulse stimulation of a cell without thin segment needs a minimum current of 2.51 nA to produce an action potential in the axon. The presence of an axonal thinning of 50 μm , 70 μm , or 90 μm lowers the threshold to 2.48 nA, 2.47 nA, and 2.44 nA, respectively. This equals a threshold decreasing of about 1 % - 2.5 %.

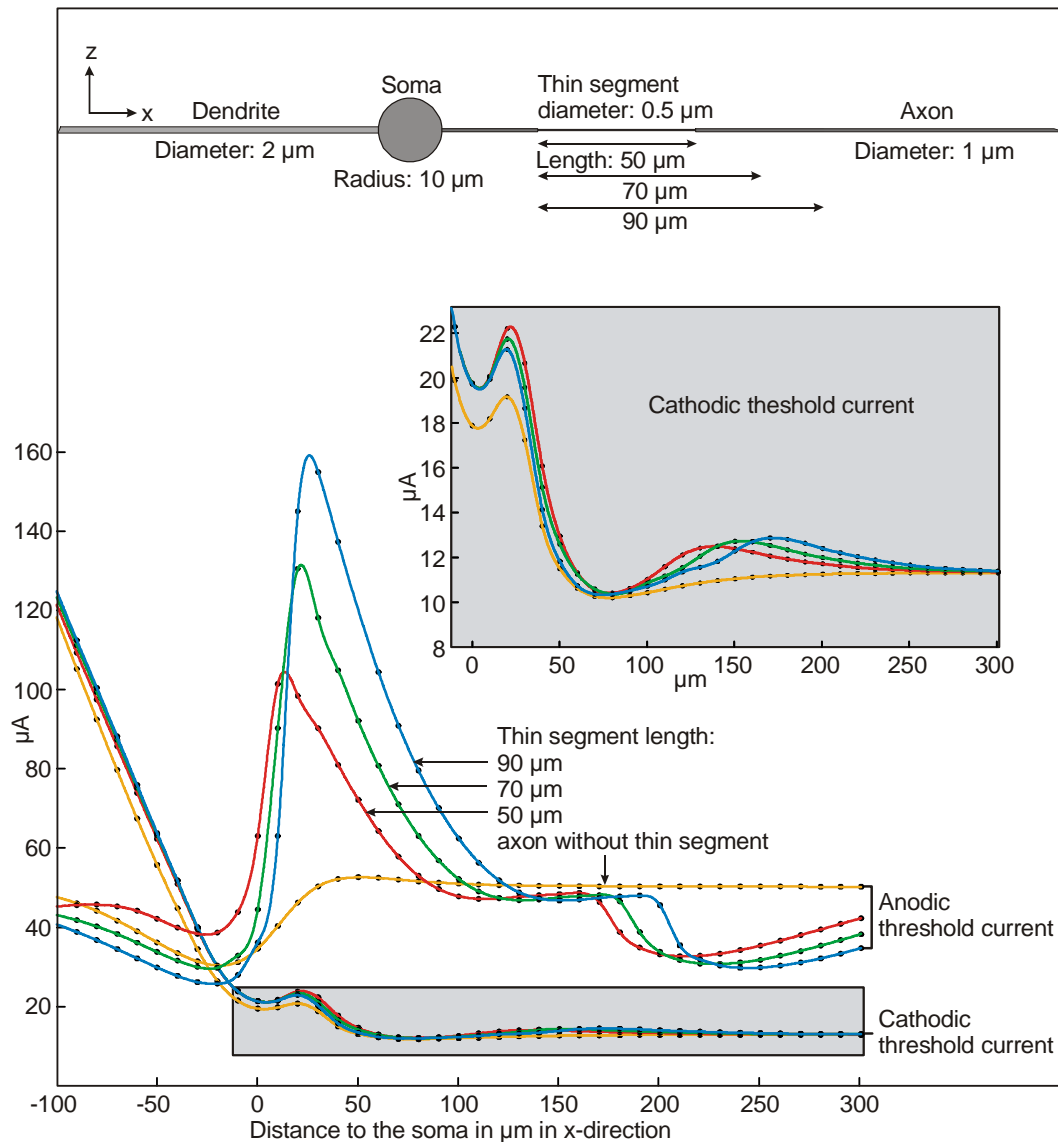


Fig. 4.12 First row describe the used target cells: a straight structure with a thin axonal segment 30 μm after the soma, of 50 μm , 70 μm , or 90 μm length, and a cell without thinning. Bottom trace shows cathodic and anodic thresholds vs. electrode distance from the soma. Curves corresponding to the cell without thin segment are yellow, with a 50 μm long thinning red, 70 μm green, and 90 μm blue. The insert zooms parts of the cathodic threshold graph.

Now the thresholds in the case of electrical stimulation are studied: The electrode is positioned over straight axons from further away somata and cell

bodies in a depth of about 30 μm . The axons emerging at these somata need less than 100 μm to choose the nerve fiber layer [Toris et al. 1995].

Including a thin segment in the axon simulation alternates the threshold graph for an electrode moving over the target cell in the case of an anodic stimulus essentially (Fig. 4.12). The yellow curve, for the model without axonal thinning, crosses two times every of the other curves, which represent axons with thin segments. With increasing length of the thinning the absolute maximum located over the initial segment increases. It is about two to three times higher than the threshold over an axon with homogenous diameter. But immediately at the end of the thin segment the threshold falls below the value for the homogenous fiber, and in about 130 μm distance from the soma it is 35 % to 40 % below the threshold for the model without thin segment.

This minimum would be a good candidate for selective stimulation, but the negative threshold is still 2.3 times lower. Thus, as mentioned above, cathodic stimulation remains the driving force of electrical stimulation. Unfortunately the curves for negative currents and models with thin segments are always above the curves for models without an axonal thinning. Beside the dendritic maximum there is also a threshold maximum for an electrode over the thin segment, but not as pronounced as in the case of an anodic stimulus. The minimum in about 80 μm distance of the soma occurs in every case, with and without thin segment, but in the second case it is followed by a higher maximum.

The results of this and the preceding sections correspond with previous outcomes, which were achieved by means of a traced retinal ganglion cell and the FCM model [Resatz 2002, Rattay et al. 2002]. These investigations show that selective stimulation of only a few ganglion cells directly under the electrode is not to be due, at least with a common electrode design. If the focal perceptions of the tested subjects [Humayun 2003, Rizzo 2003b] are not the consequence of rather closely located somata from the excited axons under the electrode, other retinal cell types must support the reported phosphenes. The first candidates are cells that extend from the outer plexiform layer to the inner plexiform layer: the bipolar cells, which are included in the investigations of the next section.

4.5 Which neural elements are excited by electrical stimulation?

The structures closest to the electrode don't have to be the most excitable ones in an externally stimulated neural network like the retina, even if these structures are axons which generally are assumed to be the most sensitive elements in functional electrical stimulation [Ranck 1975, Rattay 1999].

In this section the excitability of a retinal ganglion cell is compared with that of bipolar cells for a small ball electrode in a position typical for an epiretinal implant. There is only one type of rod bipolar cell, but many types of cone bipolar cells have been recognized in several mammalian species (see Section 2.1). The shapes of the bipolar cells differ concerning the size of the branching terminals and extensions of the dendritic trees. ON and OFF bipolar cells make synaptic contacts in different levels of the interplexiform layer, and thereby they have a different functional distance to the electrode. Especially the size and orientation of the dendritic terminal and its distance to the electrode seems to be of high importance for the electrical activation [Resatz and Rattay 2003a, Rattay et al. 2003].

Beside the ganglion cell #1 two rather extreme bipolar cell shapes are investigated: bipolar cell #1, without ramifications, and bipolar cell #2, with a large dendritic tree (for a detailed description of these cells see Section 2.3). In this simulation the ganglion cell soma is modeled with the diameter size of the traced mudpuppy soma: 24 μm . The membrane kinetics of the ganglion cell is computed with the FCM model, whereas the bipolar cells are simulated with passive membrane properties. Here a constant membrane conductance of $g_m = 0.0416667 \text{ mS/cm}^2$ is used as standard value [Coleman and Miller 1989]. Again the target cells are embedded in an infinite homogeneous medium. The electrode is modeled as a small ball electrode and a point source, respectively.

For the first investigation ganglion cell #1 and bipolar cell #2 are arranged as in the retina expected; the center of the retinal ganglion cell soma is 48 μm above the center of the bipolar cell soma. The spherical electrode with a diameter of 18 μm is located directly above the ganglion cell soma, with a center to center distance of 30 μm (Fig. 4.13 **A**). The target cells are stimulated with a current of 10 μA which is equivalent to a voltage of 50 mV for a 18 μm diameter ball electrode and $\rho_e = 57 \Omega\text{cm}$.

Why the structures closest to the electrode don't have to be the most excitable will be explained with help of the activating function (Fig. 4.13 **B**). The electrical field has a direct influence on every part of both retinal cells. As long as a stimulating pulse is applied the influence of the electric field is proportional to the activating function in every compartment. The first response of every compartment, i.e. the activating function, is shown (dotted line in Fig. 4.13 **B**) as a function of the cell's length coordinate.

Several zero crossings of the graph resulting from changes in curvature of the cell axis reduce the first stimulating effects, i.e., positive and negative slopes of the first transmembrane voltage response alternate within the very few compartments of this small bipolar cell. Within shortest time current redistribution smoothes the spatial voltage oscillations in regions small compared to the length constant λ (for definition see Section 3.1), which is in the order of 1 mm. This way a smoothing process changes the voltage slopes immediately after stimulus onset as a consequence of the increasing influence of the neighbored

compartments (Fig. 4.13 **C**). In Fig. 4.13 **C** and **D** the transmembrane voltages as functions of time are shifted vertically proportional to their compartment lengths.

In the following, linear analysis, i.e. passive membrane properties, will be applied to explain why the bipolar cell responds with 3.6 times stronger transmembrane voltage at the end of a 100 μ s pulse, although the bipolar cell has no compartment as close to the electrode as the ganglion cell (7.9 mV vs. 2.2 mV maximum value). The reason is the geometric orientation of both cells, at least in the region with high extracellular potential values, i.e. close to the electrode. The processes of the ganglion cell are tangential to the isopotentials, which means that a target compartment in that area has extracellular potential values similar to that of its neighbors. Therefore, the numerators of both activating functions are small in such cases (equation (4.1)). The activating function values for the 14 compartments of the bipolar cell are essentially greater compared to the activating function values for the soma and axon of the ganglion cell (right graph Fig. 4.13 **B**). But also after the smoothing process the slopes of the bipolar cell are essentially steeper than that of the ganglion cell.

Most bipolar cell types have branching terminals that include many process endings parallel to the surface of the retina (Fig. 4.14 top trace). This geometric orientation is similar to that of the ganglion cells. Therefore at the end of a 100 μ s pulse both cell types produce comparable membrane voltages. Moving an electrode over the retinal surface shows that even in this case the terminal endings of the bipolar cell reach the highest membrane potentials. In the center of Fig. 4.14 the highest value for each electrode is marked by a circle in the picture of bipolar cell #1. In the majority of positions it is the neuronal ending closest to the electrode. The lower right curve shows the maximum membrane voltage as function of electrode position. The irregularities are caused by the varying distance of the terminal endings.

Bipolar and ganglion cells react differently depending on the stimulus duration. Stimulating the ganglion cell with a constant -7 μ A current generates a slow response, i.e. three spikes within 500 ms (left lower picture in Fig. 4.14). The bipolar cell of Fig. 4.14 reaches a maximum transmembrane voltage of 2.7 mV after 3.9 ms.

Finally, taking the results of this and the previous sections concerning the influence of the cell geometry into account, the following fundamental question will be discussed: Which neural elements are excited by electrical stimulation?

The first candidates are the retinal ganglion cells, which are positioned directly under the electrode. With the FCM model it is possible to initiate propagating spikes in dendrites with strong stimuli. Some of these spikes degenerate at branching points both for extracellular and intracellular stimulation. For a cathode over the dendritic tree the threshold is at least 2 times higher than for a cathode over the axon (see Section 5.2 and [Resatz 2002]).

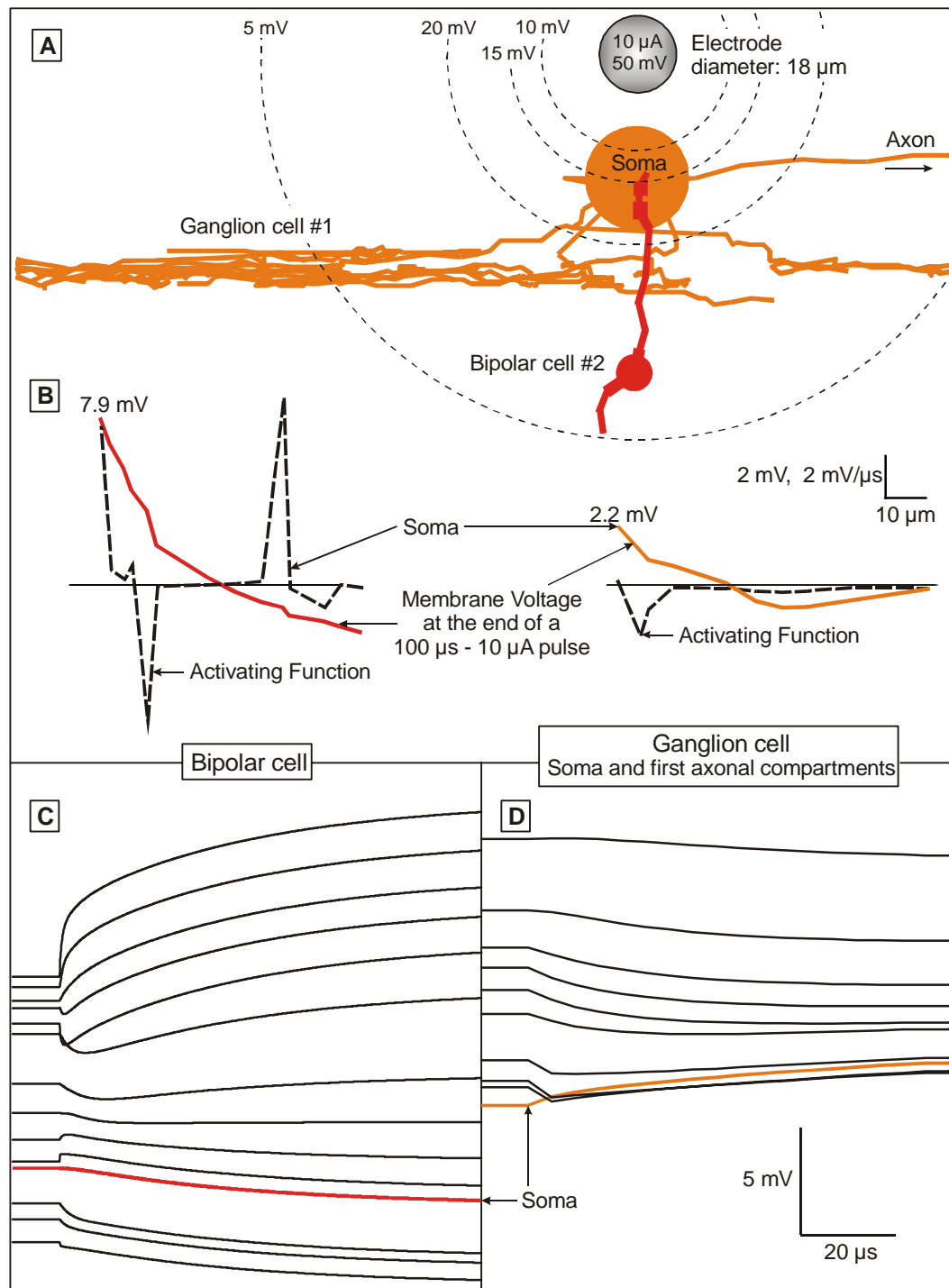


Fig. 4.13 Comparison of the excitation of a retinal ganglion cell (orange) and a connected bipolar cell (red) when stimulated from a small ball electrode (A). Transmembrane voltage at the end of a cathodic 100 μs stimulus and activating function for the bipolar cell and the first axonal part of the ganglion cell demonstrate that the largest membrane response have not to be expected in the compartments closest to the electrode (B). Membrane voltage as functions of time for the compartments shown above is plotted in the bottom trace (C, D). Note that the vertical scale bar in (B) is for both: transmembrane voltage (mV) and activating function (mV/ μs).

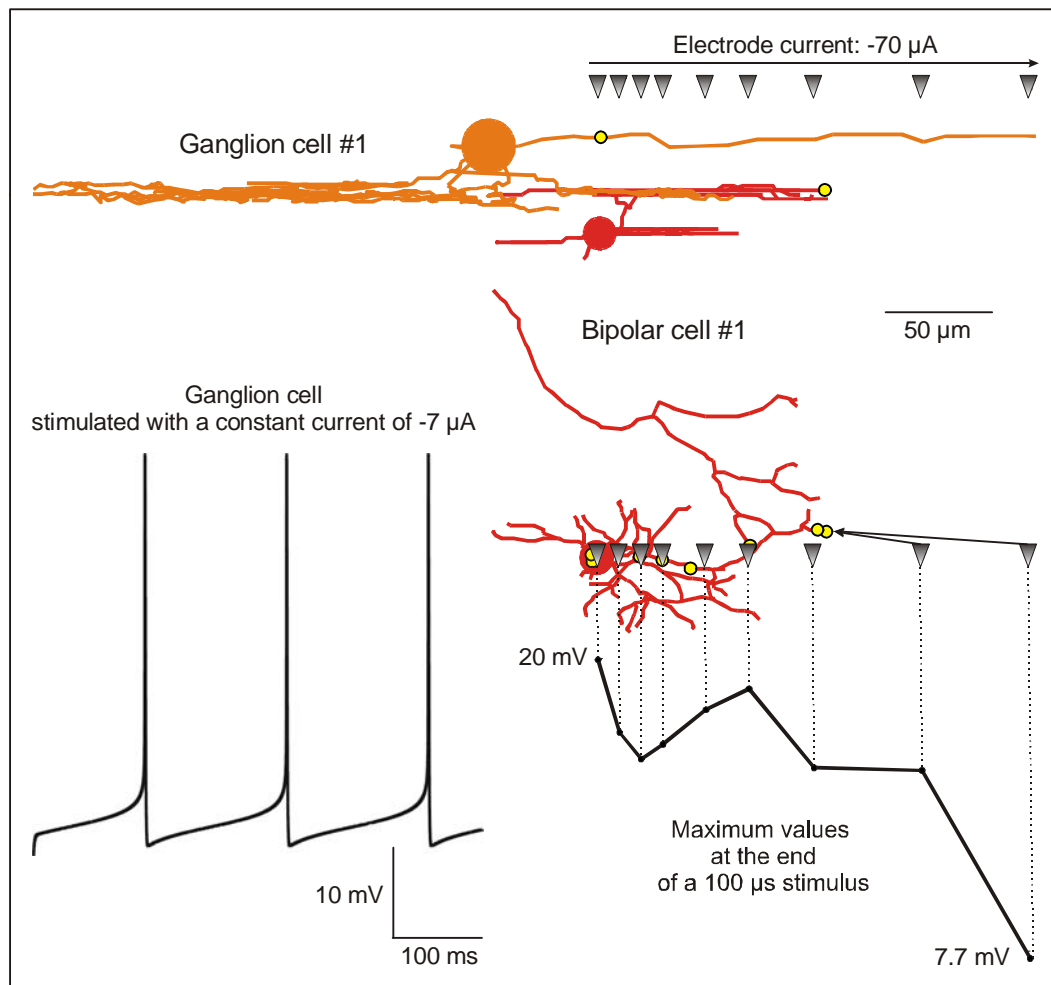


Fig. 4.14 Comparison of the excitability of a ganglion cell (orange) and a bipolar cell with a large terminal (red). Electrode position (marked by triangles) is varied along a line parallel to the retina surface. The ganglion cell is easiest to excite for an electrode above the beginning of the regular axon structure (end of the thin segment) which is marked by a circle. The maximum membrane voltage of the bipolar cell is reached at a terminal ending marked by a circle in the first trace drawing. The right picture in the center shows a top view of the bipolar cell and the electrode positions. Circles mark the most excited compartments at the end of a $100 \mu\text{s}$, $-70 \mu\text{A}$ pulse (ganglion cell threshold). Usually, the ending closest to the electrode reaches the maximum voltage. Reduction of the $100 \mu\text{s}$ pulse threshold to 10% constant current results in 6 spikes/s (lower left picture). Lower right curve shows the maximum membrane voltage as function of electrode position. Irregularities are caused by the varying distance of the terminal endings.

The threshold value for an electrode above the soma is within the same range as for an electrode over the axon or by more than two times higher depending on the cell body's diameter (see Section 4.2). Easiest to excite with a cathodic stimulus is the portion of the axon at the distal end of the thin segment in about $80 \mu\text{m}$ distance from the soma, but the difference to the rest of the axon is for equal z-distance below 5%, thus it seems more likely that the axons passing close under the electrode are stimulated.

But there is another hope for selective stimulation: the retinal bipolar cells. For the investigated electrode position the strongest bipolar cell response to cathodic stimulation is expected at the dendritic endings. Cells with few terminal branches vertical to the retinal surface are most excitable for the assumed electric field, in some cases even more than retinal ganglion cell axons. Cell endings parallel to the retina surface are not sensitive to the electric field from a small ball electrode positioned close to the retina. Therefore the driving force at the synaptic endings for the bipolar cells of this type is similar to that of the ganglion cells, resulting in a similar transmembrane potential in the interplexiform layer. Note that the operating range of the graded potentials of the bipolar cells is essentially lower than the threshold voltage for a propagating spike in the ganglion cell [Werblin and Dowling 1969, Boycott and Wässle 1999, Rieke 2001]. Therefore, even the bipolar cells of the second type are expected to answer with neurotransmitter release before a spike is initiated directly in the ganglion cell.

As observed above bipolar and ganglion cells show quite different behavior when stimulated with long signals. The ganglion cell, simulated with the FCM model, is very sensitive to weak constant current stimulation. This provides the possibility to stimulate them directly without producing an additional input from the bipolar network. Bipolar cells reach the maximum membrane voltage a few milliseconds after stimulus onset, but short stimulation pulses are expected to cause a small amount of neurotransmitter release in spite of remarkable membrane voltage. Greenberg and coworkers expect more support from the bipolar network and in the following rounder percepts for stimuli longer than 0.5 ms [Greenberg 1998, Weiland et al. 1999]. This hypothesis was tested with nearly 100 trials by Rizzo and his colleges in volunteers with epiretinal electrodes, but unfortunately it could not be proved [Rizzo et al. 2003b]. All things considered, if one wants to stimulate the bipolar cells, the subretinal approach seems to be the more promising technique.

5. Investigations on the stimulus pulse duration

Long stimulation pulses, that activate the bipolar cell network, could be one alternative to achieve focal perception. Thus it is necessary to investigate the influence of different stimulus durations on the excitation process. Unfortunately the passive bipolar cell membrane model is too simple for elaborate strength-duration investigations; therefore the main focus of this section is on the retinal ganglion cells. Beside their particular answer to increasing pulse durations, which is investigated in the first two sections, also the safe charge limit for spherical electrodes of different size is discussed.

5.1 Stimulus strength versus pulse duration

The strength-duration curve gives the threshold current, required to stimulate excitable tissue, in dependence of the pulse duration. Two important quantities characterize this curve: the *rheobase* and the *chronaxie*. The rheobase is the minimal strength of an electrical stimulus of indefinite duration that is able to cause excitation of muscle or nerve tissue. Thus theoretically the rheobase is the threshold current for an infinitely long stimulus. The practicable method however is to measure respectively simulate about 300 ms. The chronaxie is defined as the shortest duration of an effective electrical stimulus having a strength equal to twice the rheobase. Chronaxie was the most important measurement to characterize the excitability of nervous and muscular tissue because its dependence on electrode-tissue distances is rather poor compared to stimulus pulse strength [Ranck 1975].

Based on measurements for a wide variety of excitable tissues Weiss showed that these two quantities, rheobase (b) and chronaxie (c) define a linear strength-duration relationship for charge; the formulation for current is: $I = b(1 + c/d)$, where d is the stimulus pulse duration (Fig. 5.1) [Weiss 1901, Lapicque 1909, 1926].

The concept of describing the excitability of a tissue with chronaxie and rheobase impresses with its simplicity, unfortunately, it is not unrestricted applicable. For example, the definition of rheobase has to be modified if a cell fires spontaneously. Furthermore the simulations of this section show that the

relationship between threshold current and pulse duration is much more complex and can not be fitted with a smooth hyperbolic curve. Increasing pulse duration has not always to result in lower threshold currents, that is, in some cases the rheobase is not the minimum threshold current.

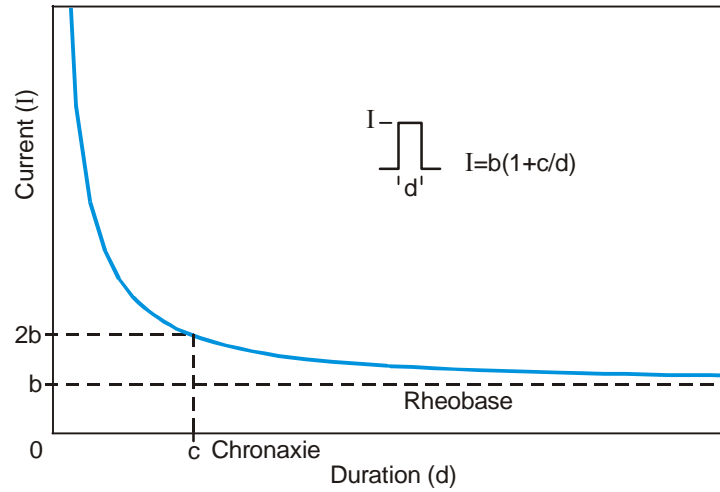


Fig. 5.1 Weiss's hyperbolic strength-duration curve for the current.

Two target cells are used for the simulations of this section: retinal ganglion cell #2 (see Section 2.3) and a straight dendrite - soma - axon structure (Fig. 5.2) with a 70 μm long axonal thin segment starting 30 μm from the soma boundary. The ganglion cell #2 membrane is always modeled with FCM kinetics. The straight target cell is simulated either with the HH model including a passive dendrite or with the FCM model. The volume conductor is an infinite homogenous medium with monopolar point source positioned in z-direction 30 μm above the axis of the target structure either directly above the soma or 200 μm away from the soma center along the axon.

The physiological processes in the retina proceed rather slowly therefore it is not surprising that the Fohlmeister-Coleman-Miller model is not appropriate to investigate short pulse durations. These simulations are done only with the Hodgkin-Huxley model (Fig. 5.2), whereas for stimulus durations from 0.1 ms up to 100 ms the FCM model is also used (Fig. 5.3).

The strength duration graphs calculated with the FCM model and the HH model in the case of anodic stimulation have the expected form (Fig. 5.2 and Fig. 5.3): the curves are monotonic decreasing with increasing slope (that is less negative). Anodic stimulation results in higher thresholds than cathodic for each stimulation length (Fig. 5.2). But surprisingly both graphs for cathodic stimulation calculated with Hodgkin-Huxley membranes show absolute minima for pulse durations less than 1 ms. For an electrode above the axon the lowest calculated threshold value belongs to a stimulus length of 0.6 ms. This is 12 % below the values for pulse durations of 10 ms and more, thenceforward the thresholds remain constant. Even more pronounced is this minimum for an electrode above

the soma. Here the lowest threshold is found for a 0.8 ms pulse, that is 17 % below the values for the long pulses.

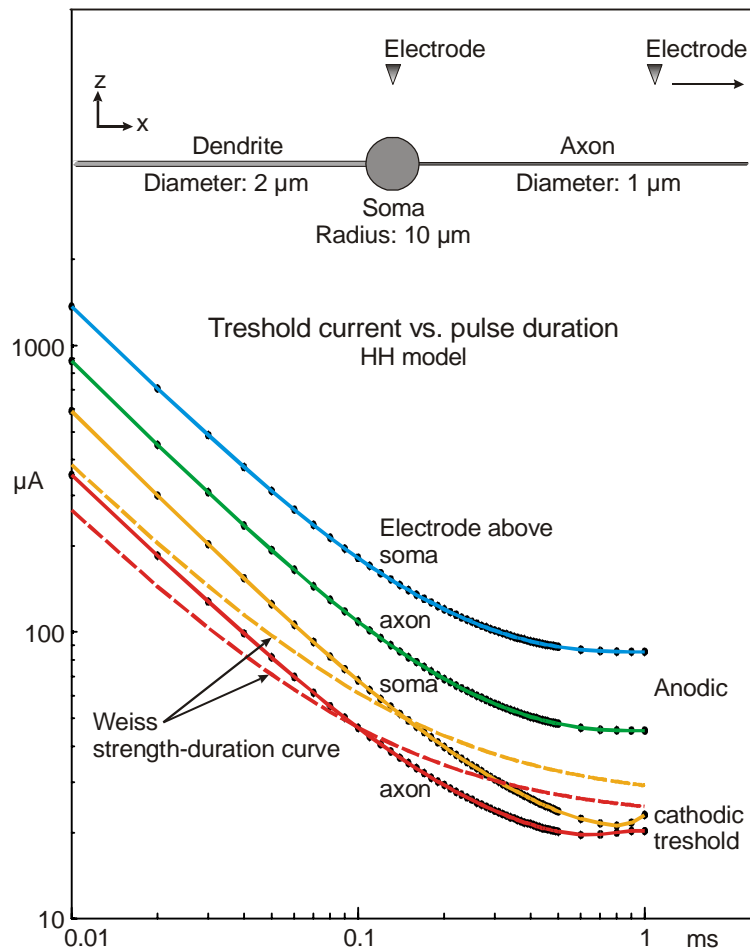


Fig. 5.2 Target cell with dendrite, soma, and axon. Axonal thin segment of 70 μm length and a diameter of 0.5 μm , starting in 35 μm distance of the soma center is not shown. In the second investigated case the monopolar point source is positioned above the axon in 200 μm x-distance of the soma (not in correct position shown, because only 123 μm of the axon is displayed, whereas the simulated length is 2000 μm). Both the electrode above the soma and the electrode above the axon are located 30 μm in z-direction above the center of the underlying compartment. The threshold (in μA) versus stimulus pulse duration (in ms) graph has a logarithmic scale. Note the minima in the curves for cathodic stimulation at a 0.6 ms pulse for an electrode above the axon and at 0.8 ms for an electrode above the soma.

This phenomenon occurs only with extracellular stimulation in spatial structure. Note that a propagating action potential necessary for perception is used as excitation criterion. The influence of short and long stimulation pulses on the excitation process are essentially different: in the short pulse case the action

potential develops after determination of stimulus, in the long pulse case development happens during applied current (Fig. 5.4). In this special situation the current hinders the propagation of the action potential when the stimulus is too weak.

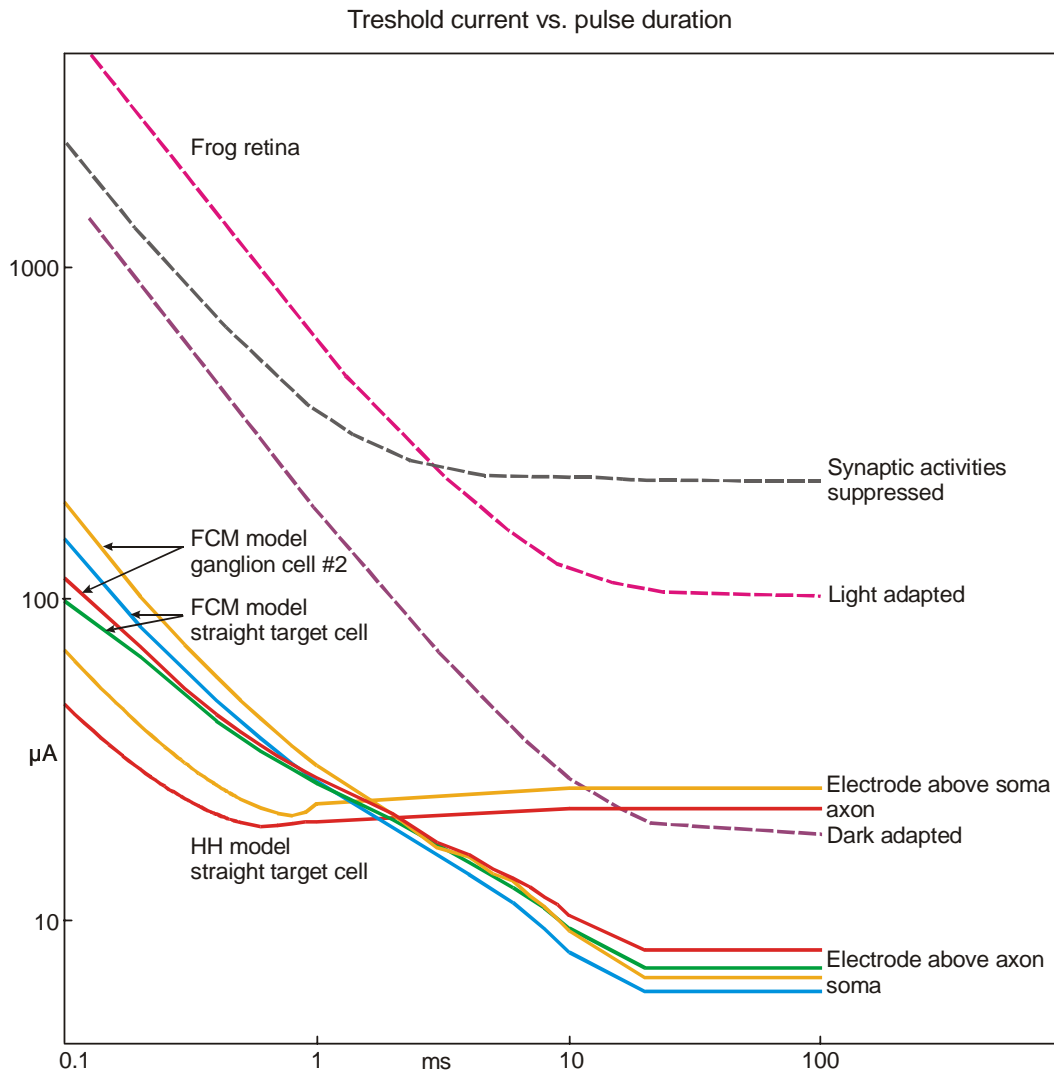


Fig. 5.3 The physiological recordings are from the frog retina [Greenberg 1998]; these graphs are drawn with dotted lines. The synaptic activities were suppressed with cadmium. The curve resulting from measurement of a light adapted retina fits well with calculations of the FCM model in shape. The absolute values differ, because the electrode distances of the physiological recordings are unknown, for the models it is $30\text{ }\mu\text{m}$ in z-direction. Admittedly the chronaxie for the isolated ganglion cells without synaptic input is essentially shorter, but not as short as the chronaxie of the models with the HH membrane.

After the onset of the stimulus current the compartment below the electrode depolarizes but other compartments in some distance hyperpolarize (see Section 4.1). Near threshold it is not the compartment under the electrode – especially if it is the large soma compartment – that develops a full spike (e.g. the

membrane potential exceeds 60 mV), but usually in some distance from the electrode along the neural structure after more than 1 ms the action potential reaches full extent (Fig. 5.4 A, B). If the current is still applied when the excitation propagates from the compartment under the electrode, it has to overcome the hyperpolarized membrane regions, and this can fail (Fig. 5.4 C, D). So it is possible that no action potential develops even if the compartment under the electrode reaches a higher membrane voltage for a longer stimulus than for a shorter superthreshold one. This explains the surprising observation why threshold values can be lower for shorter pulse durations.

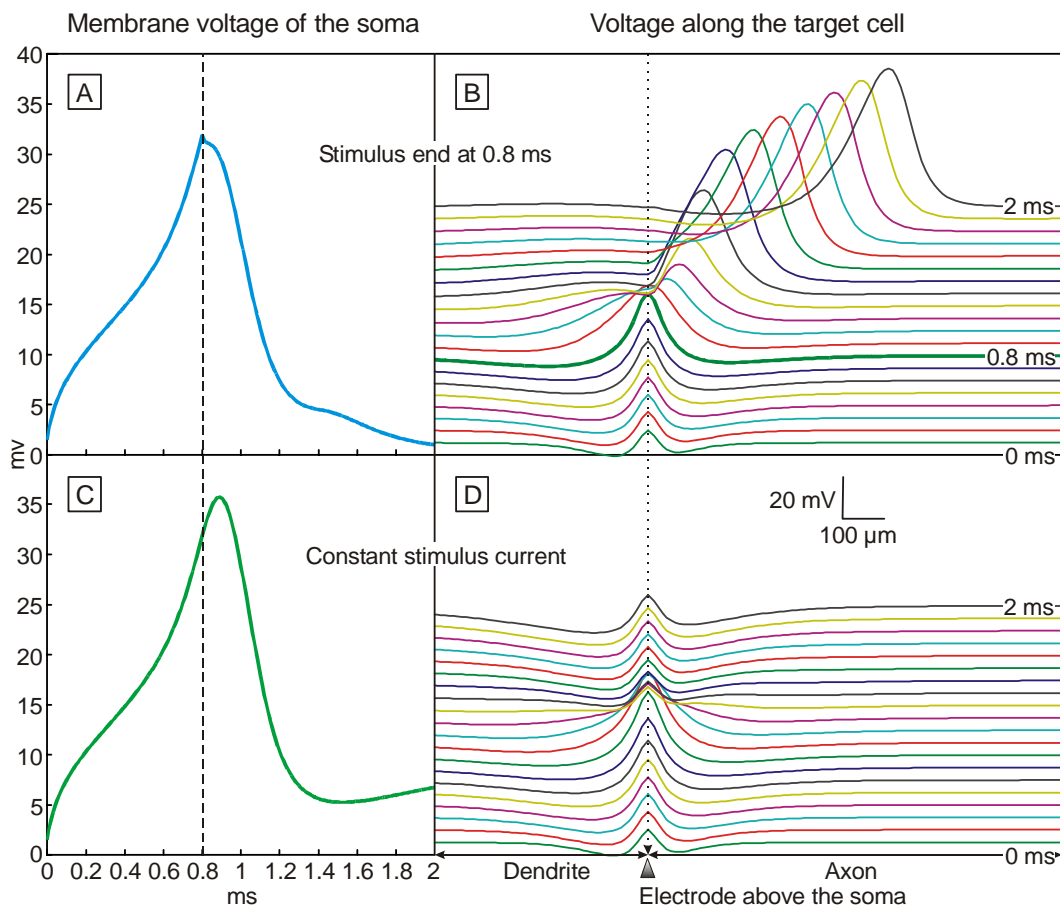


Fig. 5.4 Same sub-rheobasic stimulus current ($-4.03 \mu\text{A}$) used for a pulse of 0.8 ms and 2 ms initiates a propagating action potential in the first case (B), but not in the second (D). The membrane voltage development of the soma compartment situated directly under the electrode is identical till 0.8 ms, afterwards it reaches a higher voltage value in the case of a constant stimulus, nevertheless it remains subthreshold (A, C). The reason is that regions hyperpolarized by the applied current antagonize the propagation of the excitation.

For a cathodic stimulus and Hodgkin-Huxley membrane properties the rheobase and chronaxie are $26 \mu\text{A}$ and 0.14 ms , respectively, for the electrode above the soma, and $22 \mu\text{A}$ and 0.11 ms for the electrode above the axon. These chronaxie values are about 6 times lower than for the curve based on

electrophysiological recordings of a frog retina, where the synaptic activities are suppressed with cadmium (Fig. 5.3). The chronaxie for these measurements amounts to 0.73 ms, which is again nearly 6 times lower than the values for an electrode over the axon modeled with the FCM model (4.1 ms). Regarding the chronaxie, electrical stimulation of the frog retina with suppressed synaptic activities would be best simulated with cell membrane kinetics somewhere between the HH and the FCM model.

Unfortunately, the distance between electrode and frog retina in the physiological recordings is unknown, therefore the absolute threshold values are incommensurable with the results of the simulations. But the chronaxie of the light adapted retina fits very well with the simulations using the FCM model (Fig. 5.3, ganglion cell #2 and straight target cell). Here the chronaxie for an electrode above the axon is on average 4.1 ms, and the chronaxie for the light adapted frog retina is 4 ms.

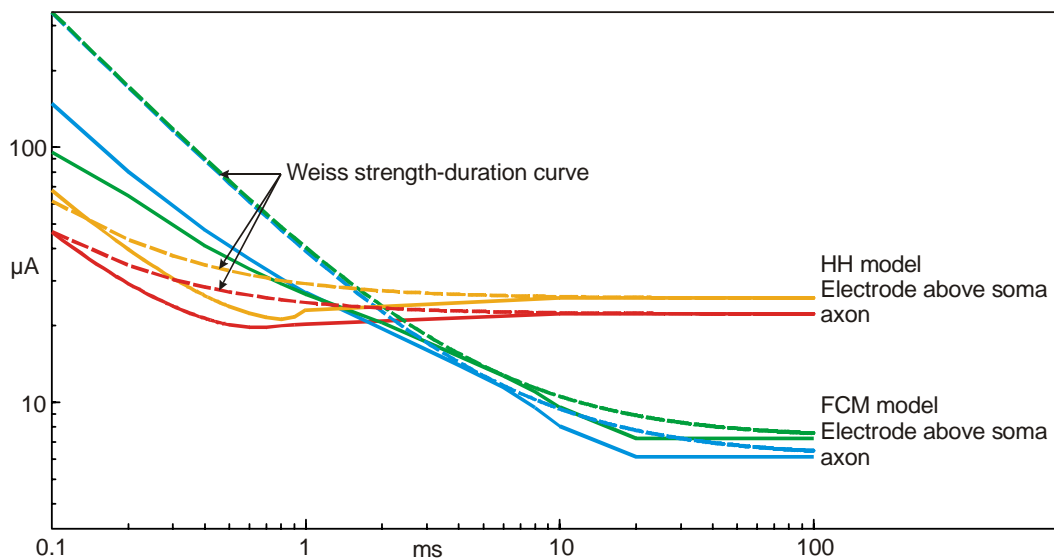


Fig. 5.5 Comparison of the simulation results with the Weiss strength-duration curve calculated with chronaxie and rheobase of the respective model.

Depending on cell type and neuronal substructures the measured chronaxies vary over a large range [Ranck 1975] and they seem to depend essentially also on the species. Recently Jensen and coworkers reported 0.14 ms for an electrode near the soma in an isolated rabbit retina [Jensen et al. 2005], which is identically with the result for the HH-model. Surprisingly his recordings deliver a higher value for an electrode above the axon (0.43 ms), which indicates a different relation of membrane properties for soma and axon than of the models used here.

The Weiss strength-duration curves are calculated for the rheobases and the chronaxies of the simulated models (Fig. 5.2 and Fig. 5.5). A comparison shows that the simulated strength duration curves are much more complex. In fact

it cannot be expected, that the highly nonlinear membrane kinetics resulting in complex excitation processes are describable with a simple hyperbolic graph. Changing the membrane properties from HH-type to FCM-type alters the threshold values essentially. While the HH curves intersect their Weiss curves in the chronaxie point, the FCM curves have only an osculation point and remain below otherwise.

The simulations show that the strength duration curves are not smooth, additional minima besides the rheobase appear as well as irregularities in the slopes. The same phenomena can be observed with physiological recordings of different tissue [Jensen et al. 2005, Grill et al. 2005, Kuhn et al. 2004]. The concrete relation between stimulus strength and pulse duration depends essentially on the model: species, electrode characteristics and position, stimulus waveform, tissue inhomogeneity, and temperature are determining factors and have to be taken into account.

5.2 Neural geometry and pulse duration

In the previous section the threshold current as a function of pulse duration was investigated with different membrane models. Now the influence of the neural elements of a retinal ganglion cell - dendrite, soma, axon, and their geometric specifics - will be examined. For this purpose a traced cell with a large dendritic tree is used.

Ganglion cell #1 with FCM membrane properties is the target cell for this section. The electrode, modeled as a point source in an infinite homogenous medium, was moved in the (x-y)-plane in 30 μm z-distance of the soma center. On 25 electrode positions with a distance of 50 μm each, the cathodic threshold is calculated for 50 μs , 100 μs , and 200 μs stimulus duration, respectively.

The lowest value is always found for the electrode nearest to the axonal thin segment, which is about 16 times lower than the highest value, obtained in greatest calculated distance to the cell (electrode in the first trace, left column of Fig. 5.6). Generally the region with the lowest thresholds is above and near the axon (see also [Resatz 2002]). This observation fits very well with the extracellularly recorded ganglion cells in retinas isolated from rabbits [Jensen 2003 et al.].

At first sight, for the three investigated durations doubling of the pulse length results in a threshold decreasing of about 44 % (Fig. 5.6). A closer look shows that the change in threshold current by doubling the stimulus length depends on the position of the electrode, i.e. the excitation of different neuronal structures respond differently to variation of stimulus duration.

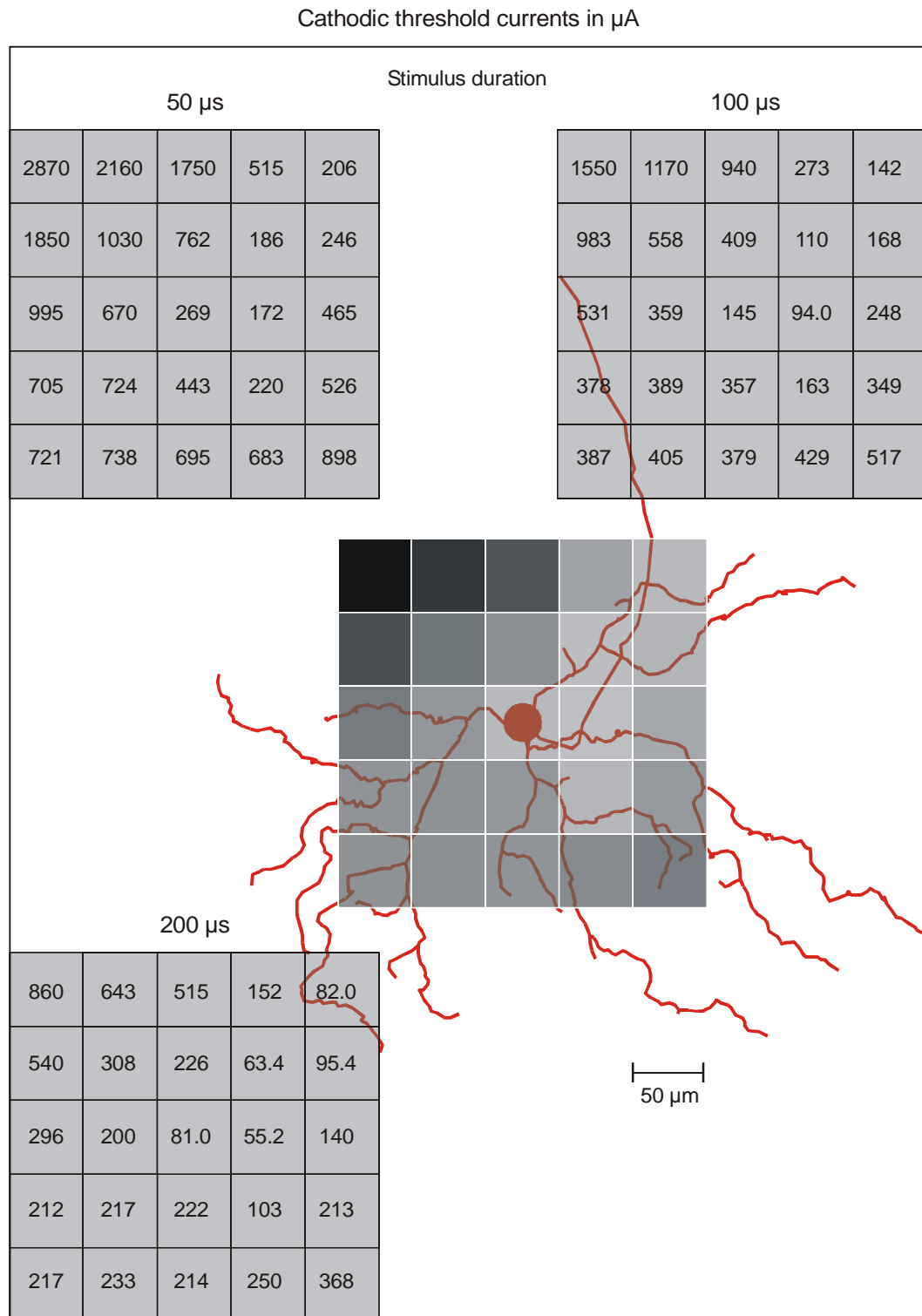


Fig. 5.6 25 threshold calculations in a two dimensional quadratic array of $250\ \mu\text{m}$ side length around the cell body. The height of the electrode is held fixed in $30\ \mu\text{m}$ z -distance above the soma center. The lowest threshold is found for all three stimulus durations ($50\ \mu\text{s}$, $100\ \mu\text{s}$, and $200\ \mu\text{s}$) for the electrode near the axonal thin segment; right beside the electrode above the soma. The shading in the central array corresponds to the thresholds of $100\ \mu\text{s}$ pulses.

To illustrate the matter Fig. 5.7 shows the threshold currents as disk areas. The values are normalized with respect to the electrode above the soma. The disks for the three stimulus durations are plotted with equal center, which refers to the position of the electrode.

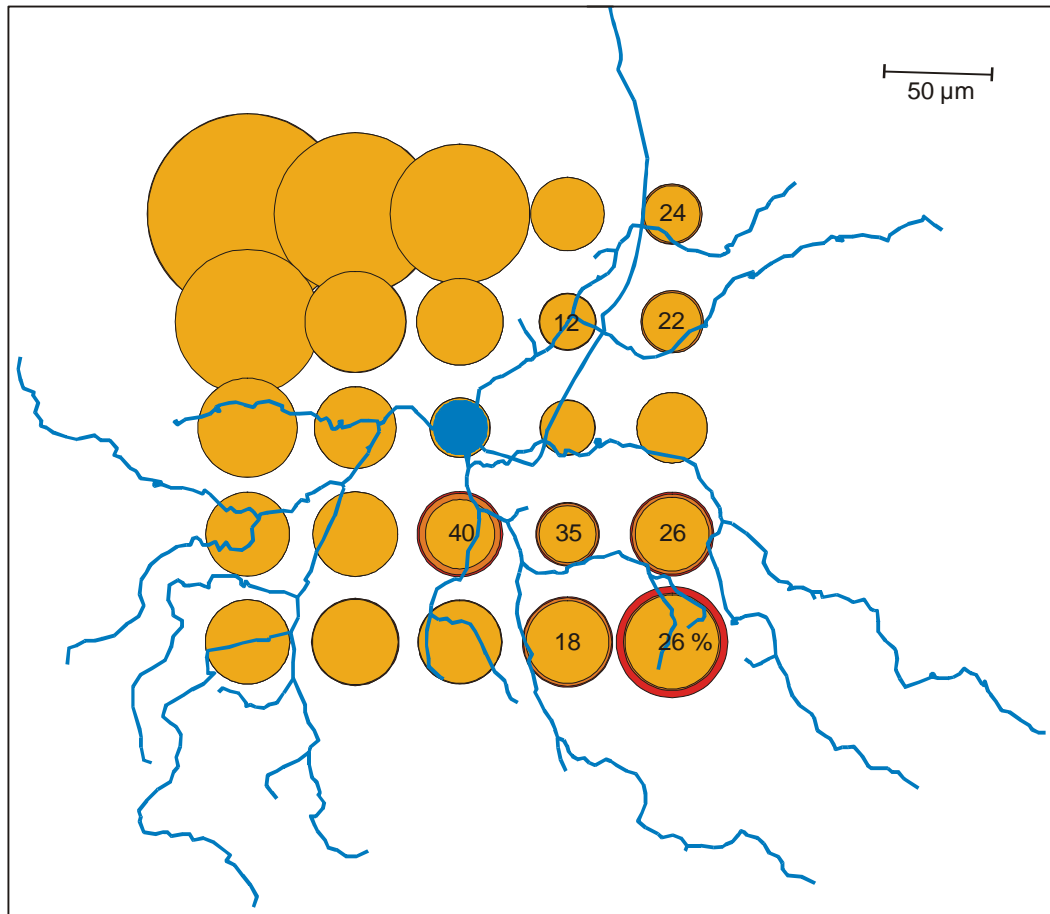


Fig. 5.7 The calculated threshold values are normalized with respect to the electrode above the soma for each of the three stimulus durations, and plotted as disks with corresponding area. Thresholds for a stimulus duration of 50 μ s are drawn with yellow disks, 100 μ s with orange, and 200 μ s with red. Note that the threshold variations for different stimulus lengths depend on the position of the electrode. Differences of more than 10 % are given explicitly.

It can clearly be seen that some structures need disproportional high effective stimulation currents for increasing pulses. For one electrode near the soma (fourth trace, third column in Fig. 5.7) the greatest step in threshold increasing happens when the stimulus duration alter from 50 μ s to 100 μ s, for another electrode the greatest step occurs for increasing the pulse from 100 μ s to 200 μ s (fifth trace, fifth column in Fig. 5.7). Noteworthy is that in the second case the electrode is located close to two dendritic endings. The neural geometry near the electrode seems to be the important factor for this phenomenon and not the different membrane properties of dendrite, soma, and axon which determine the general behavior. Ramifications, curvature, and endings of the neural structure

have influence on the proportion of threshold changes for stimulus duration variations.

5.3 Safe charge density limit

The required energy for effective stimulation is one of the great problems in retina implant development, since all existing clinical studies show that the safe charge density limits for long term stimulation are difficult to achieve.

Safe charge-injection limit determinations have been made primarily in brain tissue, and although it seems reasonable to use them as estimates for the retina, actual charge density safe limits for the retina are unknown [Margalit et al. 2002]. In addition, the stimulus paradigms used to determine safe limits (typically experiments were performed across several hours on 1 day) do not closely mimic what the retina would be exposed to with long-term stimulation by prosthesis.

It is necessary to know the chemical reversibility of reactions involving electrode materials in order to avoid tissue and device damage. Chemical reversibility requires that a pulse of opposite polarity will chemically reverse all processes occurring at an electrode subjected to an electrical pulse, and that H_2 and O_2 evolution as a result of electrical current will be prevented. But completely reversible charge injection is, for several reasons, not obtainable [Loewenstein et al. 2004]. Hence, some degree of potentially destructive chemical reactions will occur. The goal is to minimize these reactions. Judicious selection of electrode materials, electrode geometry, and stimulus parameters can reduce the amount of charge that is injected into the tissue.

It was shown that electrical stimulation-induced neural injury is dependent on current amplitude and pulse repetition rate, but more importantly on *charge density* and *charge per phase* [McCreery et al. 1988, 1990, 1997]. The charge per phase is defined as the integral of the stimulus current over half (one phase) of one cycle of the pulse duration. Charge density is defined as charge per phase divided by the electrochemically active surface area of the electrodes. From these definitions, it can be understood that very small electrodes can produce very low threshold currents, yet unacceptably high charge densities. Since charge density is responsible for the damage of tissue and electrodes, there is a theoretical limit to how small the electrodes can be [Tehovnik 1996, Brown et al. 1977]. Also, the total charge delivered to the tissue can not be ignored, even though the charge density can be within safe limits [Agnew et al. 1986, McCreery et al. 1990].

Experiments to determine safe charge-injection limits for a variety of materials have been performed in neural tissue. For platinum, a limit of 0.1 mC/cm^2 has been proposed [Rose and Robblee 1990]. Oxidized iridium has a significantly higher limit ($1\text{-}3 \text{ mC/cm}^2$) [Humayun et al. 1996, 1999a, Harpster et al. 2000]. There is some evidence, however, that the product of charge density and

charge per phase determines the safe charge-injection level [McCreery et al. 1990].

As noted in the ‘Introduction’ (Section 1.1), thresholds in humans with retinitis pigmentosa vary between 0.28 mC/cm^2 to 2.8 mC/cm^2 with an epiretinal microelectrode array directly on the retinal surface [Loewenstein et al. 2004].

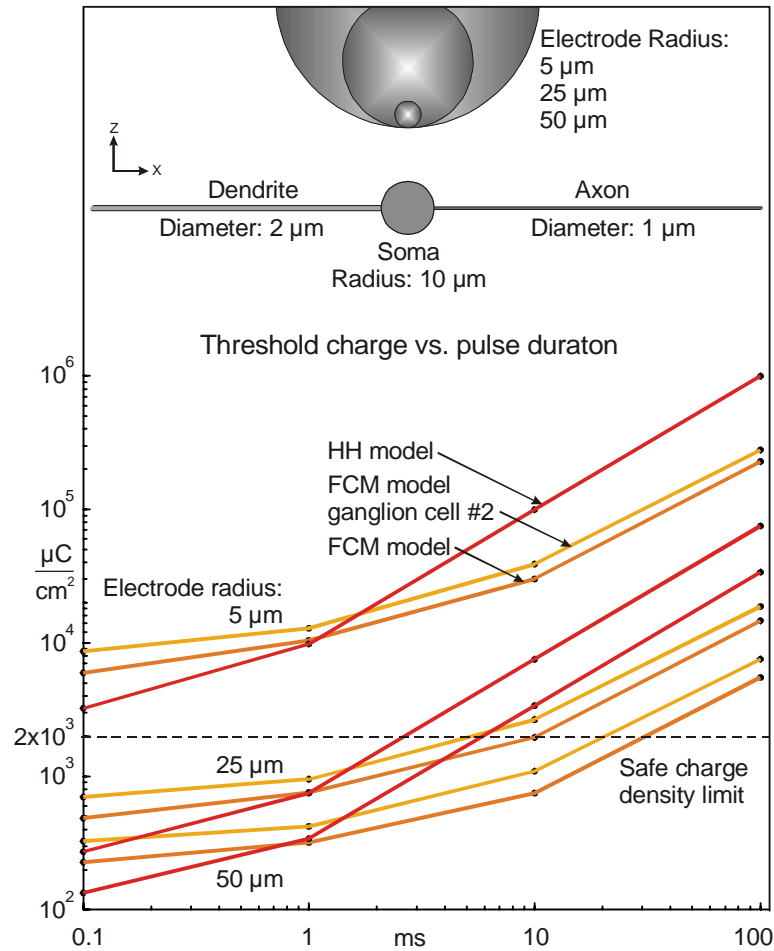


Fig. 5.8 Target structure used in two of the three models with the position and size of the electrodes. The third target cell, retinal ganglion cell #2, is plotted in Fig. 2.7. The threshold versus pulse duration graphs show that the small electrode of $10 \mu\text{m}$ diameter work effectively always above the safe charge density limit, even for short pulses. The electrode of the next size under-run the limit at least for pulse durations shorter than about 6.5 ms. Only the largest electrode with a diameter of $100 \mu\text{m}$ is safe even for long pulses.

Membrane models and target cells used for the simulations below are the same as in Section 5.1. Three spherical electrodes with different radius ($5 \mu\text{m}$, $25 \mu\text{m}$, and $50 \mu\text{m}$) are positioned in an infinite homogenous medium above the soma. To obtain a useful model where the diameter could be easily changed, the distance between the electrode border and the soma center is held fixed with 30

μm for all three spheres, i.e. the z-coordinates of their centers differ (Fig. 5.8). For realistic assumptions the electrode may be imagined as a hemisphere and the volume conductor as a half space with an isolated border. This is an equivalent model which does not alter the results.

Variations of the electrode size result in a shift of the threshold charge versus pulse duration curves (Fig. 5.8). The shift factor depends somewhat on the model. The required amount of threshold charge for models using a HH membrane is lower for short pulse durations than for the simulations with the FCM model. But generally, at a stimulus duration of about 1.5 ms the situation reverses and the FCM membrane is easier to excite.

Small electrodes would be preferable for retina implants, but the simulations as well as the clinical experiments show that there are limitations. A ball electrode of 10 μm diameter exceeds the safe charge density limit even for short pulses (Fig. 5.8). Averaged on the values for the different models, pulses shorter than 6.5 ms are safe for spherical electrodes with 50 μm diameter or larger. Electrodes with a diameter of 100 μm are safe up to 21 ms pulse durations.

Rizzo and coworkers reported that percepts could not be reliably elicited with 50 μm diameter disk electrodes using safe charges in blind patients. With two larger electrodes (100 μm and 400 μm) only the normal-sighted patient had thresholds at charge densities below the long term safety limit, if it is calculated as the product of charge density and charge per phase according to the suggestions of McCreery and coworkers [McCreery et al. 1990]. In blind patients, thresholds always exceeded these levels, although some were close to the limit [Rizzo et al. 2003a].

The problem with big electrodes is not only that focal stimulation is harder to perform, but also that an array large enough to create an image (e.g. 25×25 electrodes) becomes too big for the restricted dimensions of the eye. Furthermore placing the electrodes in direct contact with the retina, either subretinally or epiretinally, has a high risk of causing cell damage from heating.

6. Effective electrode configuration for selective stimulation

The quality of visual perception with retinal prostheses strongly depends on the local selectivity. Electrode arrays at the surface of the retina should excite exclusively cells within a local area but they are expected to co-stimulate bypassing axons originating from ganglion cells of the outer regions. Therefore, the aim of this section is to develop an effective electrode configuration for focal stimulation with an epiretinal implant.

The possible influence of electrode geometry on selective stimulation of a target retinal ganglion cell by avoiding co-activation of passing axons is analyzed. In the following an approach of Grumet is refined, who concluded from theory and preliminary experiments that long stimulating elements parallel to the main directions of bypassing axons are appropriate for this task [Grumet 1994]. The presented results reflect the evolving insight from small disk electrodes, via rectangular electrodes (Section 6.2), to sophisticated implant geometry (Section 6.3) [Resatz and Rattay 2003b, Rattay and Resatz 2004]. But in a first step the target is the optimization of the electrode geometry concerning the dipole distance (Section 6.1).

6.1 Dipole distance

Sometimes neuroprosthesis operate in a dipole mode where both electrodes effectively stimulate the same target neuron, which is generally not the case if the electrode distance is too large. As already mentioned in Section 5.3, a problem with small electrodes is the high charge density required even for short distance stimulation, e.g. epiretinal stimulation in human application needs a charge density close to the theoretical safe limit of 2 mC/cm^2 [Rizzo et al. 2000, Loewenstein et al. 2004]. Computer simulations of this section support optimization of electrode geometry and distance concerning stimulation with low charge densities, and focused stimulation, e.g. it is shown that a dipole distance in order of magnitude of $150 \text{ }\mu\text{m}$ needs minimum threshold current for dipole stimulation with small electrodes $30 \text{ }\mu\text{m}$ above the target structure.

The influence of increasing dipole distances is investigated with retinal ganglion cell #2 and two hemispheric electrodes in a semi-infinite medium, and

also with a straight axon and three different electrode configurations. These stimulating electrodes in form of disks or hemispheres with 10 μm diameters are mounted in central position on an insulating plate ($2000 \mu\text{m} \times 2000 \mu\text{m} \times 100 \mu\text{m}$). The 200 μm thick retina (resistivity $\rho = 57 \Omega\text{cm}$ for all simulations [Geddes and Baker 1967, Doslak et al. 1980]) is assumed to be between the electrode carrier and the 200 μm thick sclera with the tenfold specific resistance of the retina. The target structures are positioned 30 μm below the electrode centers.

Except for the semi-infinite medium the potential distribution is always calculated with the finite element software FEMLAB for different dipole distances and applied to compartment models of the target cells. For monopolar stimulation or dipoles with distances greater than 400 μm a semi-infinite medium approach is a good fit for the region close to electrode (Fig. 6.1).

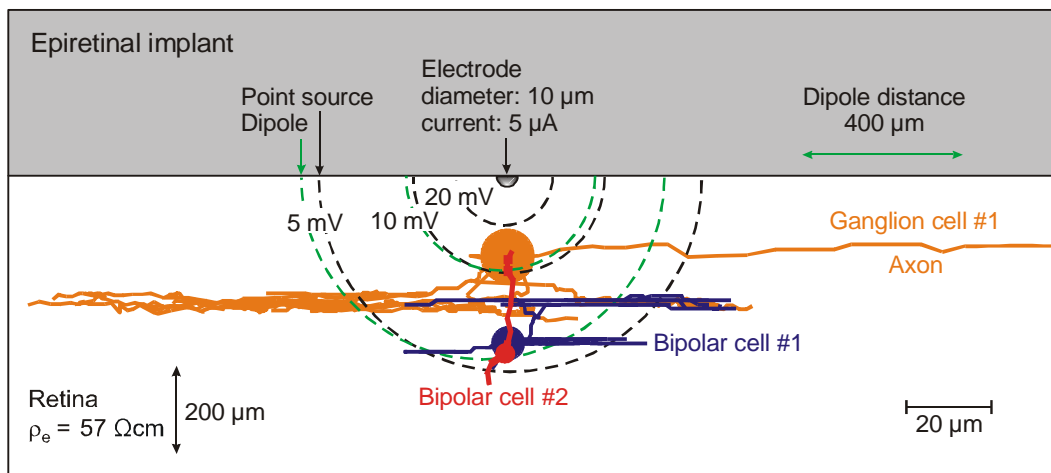


Fig. 6.1 Standard position of the three investigated retinal cells relative to the stimulating electrode. Electric field is calculated for a point source in a semi-infinite homogeneous retinal medium (black dashed lines) and for a dipole (second electrode 400 μm to the right) with a less conducting medium (sclera) below the retina (green dashed lines).

Fig. 6.2 shows the top view of cell body and axon of the ganglion cell #2 and the direct influence of the electric field for four electrodes (same anode, three cathode positions always above the center of an axon compartment). Axonal compartments have variations in diameters and distances to the retina surface which result in small deviations of the monopolar activating functions. For small dipole distances an intersection of the main peak regions of the monopolar activating functions occurs and causes substantially higher thresholds.

The lowest threshold current is required for a dipole distance of about 150 μm for both electrode shapes: disk and hemispheric, if the electrode tissue distance amounts 30 μm (Fig. 6.3). The difference in thresholds between the optimal dipole space and distances of 500 μm and more is about 13 % for the model with the disk electrode, and 15 % for the hemispheres. The thickness and specific resistance of the sclera is of minor influence on the extracellular potential

along the investigated cells, and consequently it does not crucially affect the required threshold currents for effective stimulation (Fig. 6.3 B).

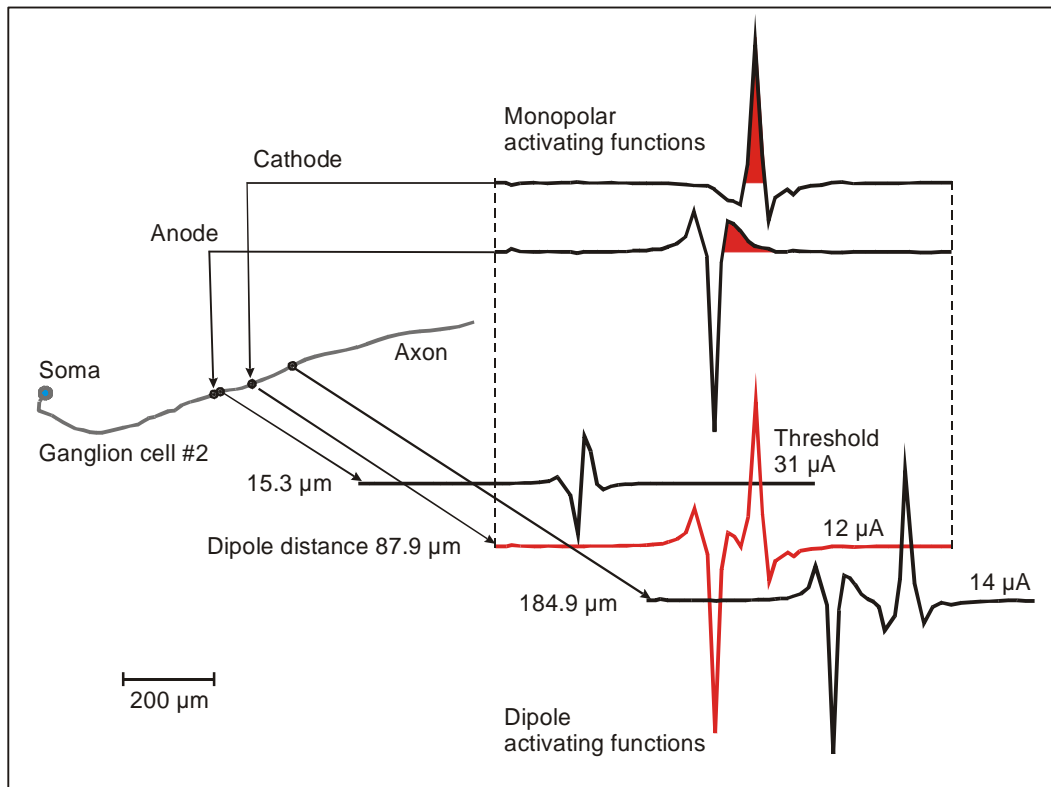


Fig. 6.2 Activating functions for hemispheric electrodes moved at the retina surface along the axon of the ganglion cell #2. The activating function for a dipole configuration is the sum of the monopolar components as demonstrated by the 87.9 center-center distance case (red curve). Simulated for semi-infinite retina, threshold calculation with the FCM model.

Minimum threshold is supported by a dipole distance where both the cathodic and anodic monopolar activating functions contribute with positive values as marked by the red regions in Fig. 6.2. However, the strong negative peak of the anodic pole causes inner-axonal current flow from the excited region and therefore the minimum dipole current is reached after a small shift of the cathode to the right side. The dipole separation for minimum threshold current depends on the electrode distance as predicted from the positive peaks of the activating function and on the fiber's length constant, but it is rather independent from the electrode type and the boundary conditions used in this models (Fig. 6.3).

As the dipole length, which causes the minimum threshold, depends on the distance between electrode and target structure, choosing the appropriate electrode spacing could be of help to achieve the goal of focused stimulation. Soma, axonal thin segment, and axons from distant parts of the retina are usually located in different z-distances to the stimulating electrodes. Therefore, support of a

selective stimulation of the thin segment or even soma is thinkable. Although one must consider that the activating function for an electrode above the soma differs (cf. Section 4.1 and Section 4.2), the principle concept of superposition of the driving positive parts of the monopolar activating functions is also applicable in this case. But all influences considered with conventional electrode design the determining factor will still be the z-distance and not the dipole length, so that a more sophisticated electrode concept is demanded. For additional investigations concerning the dipole distance see Resatz and Rattay 2002.

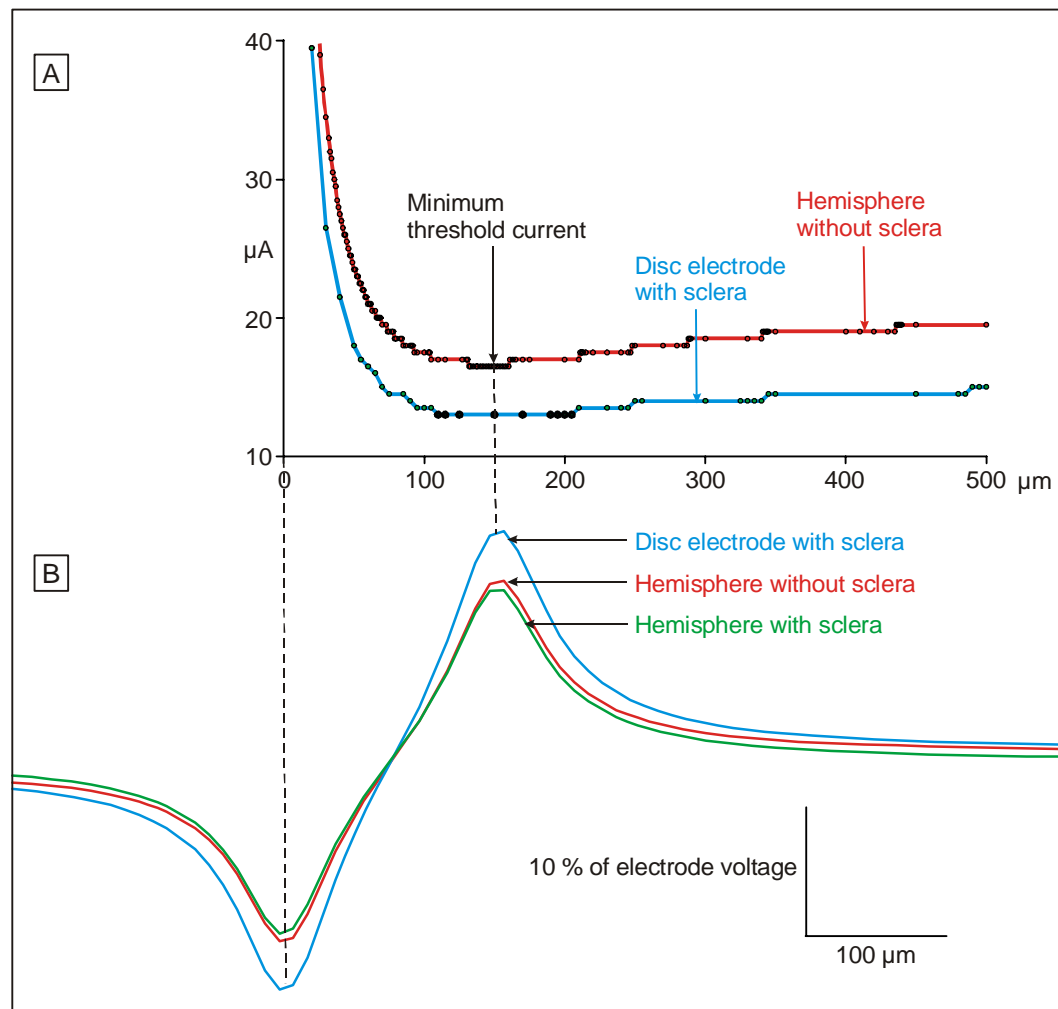


Fig. 6.3 A: Threshold current as function of dipole distance for a straight axon (1 μm diameter, 30 μm below electrode centers). B: Extracellular voltage along the axon for 150 μm electrode center-center distance, a value within the flat minimum threshold current region. Disk electrodes are more effective concerning current consumption in comparison with hemispheres in spite of half surface area. The thickness and specific resistance of the sclera is of minor influence on the extracellular potential along the investigated cells.

6.2 Different electrode shapes

A serious problem especially with epiretinal electrodes is the stimulation of superficial passing axons originating in distant retinal regions which hinder fine visual resolution with microelectrode arrays. In order to overcome this problem the dipole stimulation is simulated with long rectangular electrodes parallel to the orientation of passing groups of axons which cause rather high thresholds for their excitation in comparison with the perpendicular direction.

The volume conductor is modeled as rectangular solid with a $2000\text{ }\mu\text{m} \times 2000\text{ }\mu\text{m}$ base, consisting of several layers: on the top a $100\text{ }\mu\text{m}$ thick isolating plate where the rectangular or disc dipole electrodes are mounted, adjacent the $200\text{ }\mu\text{m}$ thick retinal layer (resistivity $\rho = 57\text{ }\Omega\text{cm}$), and the sclera on the bottom with the same extension but tenfold specific resistance. The target cells of this section are the retinal ganglion cell #1, bipolar cell #1, and #2 for the investigations concerning Table 3.3 and Fig. 6.4, and ganglion cell #2 for Table 6.2 and Fig. 6.5. For all ganglion cells of this and the following section the diameter of the somata was assumed to be $10\text{ }\mu\text{m}$, differing to the traced $24\text{ }\mu\text{m}$ soma, as this is a better approach for the human case. This modification is of minor relevance for the following case studies as the simulations of Section 4.2 showed only minimal threshold dependence on soma size. The stimulus duration for all investigations is $100\text{ }\mu\text{s}$.

Dipole stimulation with long rectangular electrodes parallel to the orientation of passing groups of axons will cause a nearly constant potential along an axonal segment that is close and parallel to the electrode. Within this segment the activating function is almost zero and therefore the neural membrane is hardly excitable. Retinal cells with somas proximal to the electrode are assumed to have lower thresholds caused by excitable structures transverse (i.e. not parallel) to the electrode.

This hypothesis is evaluated by three axons oriented parallel or perpendicular to the electrode: the axon of the traced ganglion cell #1 in connection with the soma and dendrites, a straight perpendicular and a straight parallel axon (Fig. 6.4 A, B). All the axons pass the same region close to the center of the cathode and therefore they get similar maximum extracellular potential values (Fig. 6.4 C). However, the perpendicular axon becomes about four times more excited as shown both by the activating function (Fig. 6.4 D) and the evaluation of the passive membrane model (Fig. 6.4 E and Table 3.3, which for comparison contains also the results for small electrodes and the responses of both bipolar cells).

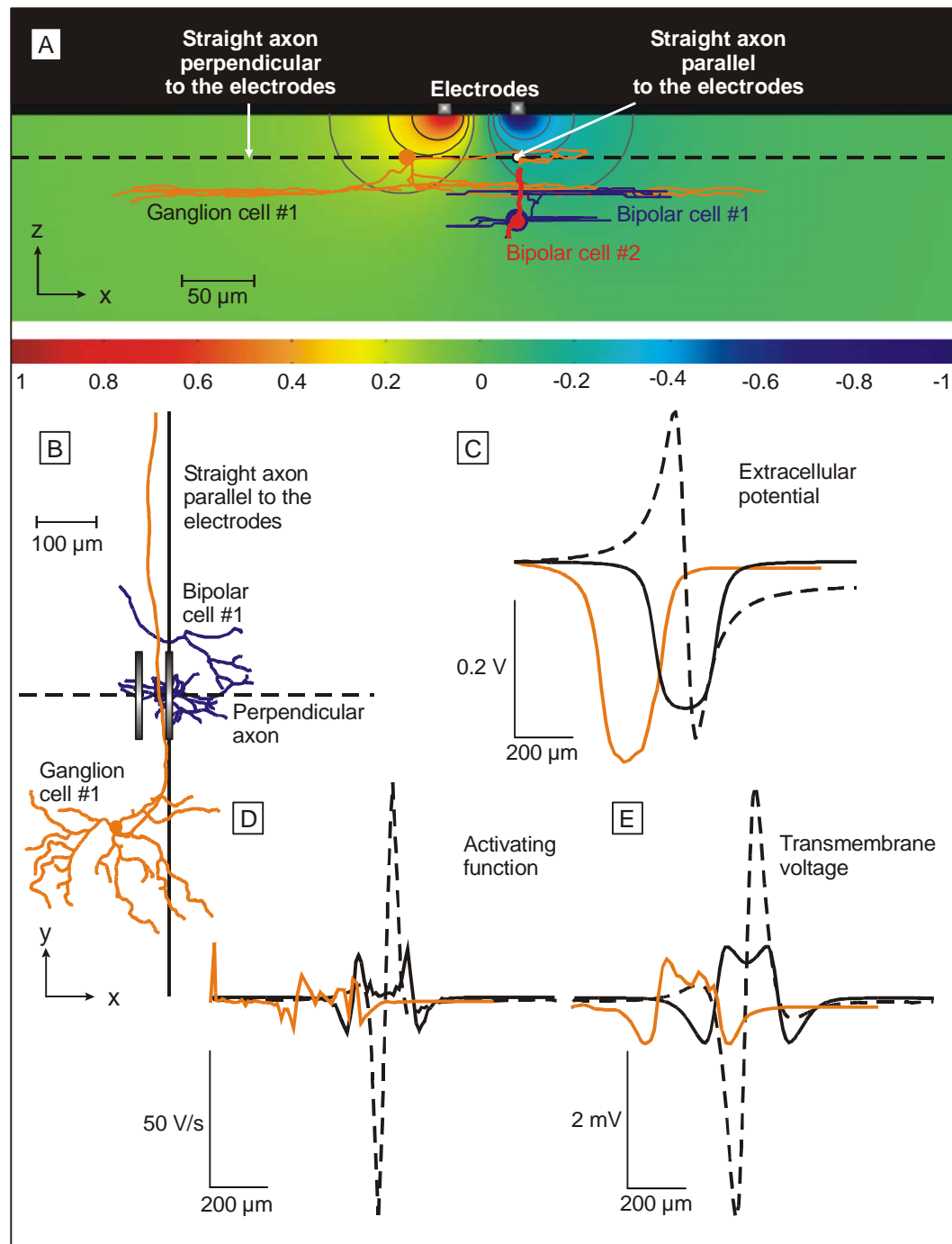


Fig. 6.4 Dipole stimulation with rectangular electrodes ($10\ \mu\text{m} \times 200\ \mu\text{m}$, center distance $50\ \mu\text{m}$) parallel to the axon of ganglion cell #1. Front (A) and top view (B) with cell positions. Parallel axons and both bipolar cell bodies (bipolar cell #1 and #2) are below the cathode ($-1\ \text{V}$). The excitation of two straight axons, parallel to the electrode (full line) and perpendicular to the electrode (dashed line), are compared with the traced ganglion cell. Extracellular voltages along the three axons are of similar magnitude (C), but the axons parallel to the electrodes are barely excited (D, E). Orange lines mark the ganglion cell related curves.

Threshold current generates a spike resulting from the positive parts of the activating function below the cathode endings (Fig. 6.4 D), which quickly merge to a single excited region of transmembrane voltage (Fig. 6.4 E). This effect is rather strong because the 200 μm cathode length is small compared to the fiber's length constant (λ is about 800 μm).

Table 6.1 Minimum and maximum transmembrane voltage in mV at the end of a 0.1 ms, 5 μA stimulus for the situation shown in Fig. 6.4.						
Electrodes		Perpen. axon	Parallel axon	GC #1 axon	BC #1	BC #2
Disk $d = 10 \mu\text{m}$	min	-5.23	-5.62	-7.00	-1.52	-7.98
	max	5.23	1.36	1.93	3.05	2.08
Rectangular $10 \times 200 \mu\text{m}$	min	-3.17	-0.65	-0.53	-2.01	-0.94
	max	3.17	0.75	0.70	0.76	2.59

Abbreviations: *Perpen.*: Perpendicular, *GC*: Ganglion cell, *BC*: Bipolar cell, *d*: diameter

In order to obtain more significant threshold differences between structures parallel and transverse to the electrode the amplifying effect can be reduced by longer electrodes. Additionally, the electrode surface should be separated from the retinal surface, e.g. 20 micrometers, to get a better distance relation between the close bypassing axons (which should not be stimulated) and the deeper retinal elements (cf. Fig. 2.2 and Fig. 2.5). Furthermore, the dipole distance was enlarged to 1000 μm in order to reduce threshold current, which actually approximates a monopolar stimulation mode.

Table 6.2 Threshold currents in μA for $10 \mu\text{m} \times 400 \mu\text{m}$ rectangular electrodes (Positions shown in Fig. 6.5)						
Stimulus current	Dipole distance	Electrode positions (cf. Fig. 6.5)			Threshold ratio	
		A	B	C	C/A	C/B
Positiv	400 μm	267	295	434	1.63	1.47
	1000 μm	235	268	308	1.31	1.15
Negativ	400 μm	-196	-178	-280	1.43	1.57
	1000 μm	-123	-110	-145	1.18	1.32

In Table 6.2 threshold for positive and negative single 100 μs pulses are listed for 400 μm and 1000 μm dipole distance. The three electrode positions and the target cell are shown in Fig. 6.5. Previous simulations [Resatz 2002] detect the lowest cathodic threshold for this cell for an electrode above the proximal end of the thin segment (position B in Fig. 6.5), which is consistent with electrophysiological recordings in salamander retinal ganglion cells [Carras et al. 1992, Fohlmeister and Miller 1997a, b].

Usually symmetric biphasic pulses are applied in neural prostheses, e.g. Laube, Schanze and collaborators report that a cathodic-anodic pulse sequence is more effective for epiretinal stimulation than anodic first stimulation [Schanze et al. 2002, Laube et al. 2003]. Table 6.2 demonstrates that the cathodic stimulus has essentially lower thresholds for positions **A**, **B**, **C** than anodic. Furthermore, position **A** has a 1.43 lower threshold than **C**, but the threshold ratio for **B** is even better: 1.57, which is a difference of 36 %. Increasing the dipole distance from 400 μm to 1000 μm causes generally lower thresholds, but the threshold ratio **C/A** and **C/B** is not as good.

From the data of Table 3.3 it can be concluded that even with the investigated disk electrodes the response of bipolar cells can be influenced with stimulus amplitudes being subthreshold to all passing axons. Notice that (cf. Section 2.1) bipolar retinal cells do not generate action potentials but operate by changing the amount of neurotransmitter release within a rather small range of membrane voltage (5 mV) [Teeters et al. 1997].

By in-vitro experiments with subretinal electrodes ganglion cell spiking can be initiated by synaptic activities from the electrically stimulated retinal network without direct stimulation of the ganglion cells or their axons [Saunders 1973, Stett et al. 2000]. However, it seems that this observation does not hold for all cases of epiretinal implants because in contrast to the subretinal devices, here, the ganglion cell axons are the elements closest to the electrodes. In order to avoid axonal spike initiation, the principle of the activating function concept is of help to design a useful electrode configuration. The proposed 10 $\mu\text{m} \times 400 \mu\text{m}$ long rectangular electrode generates an asymmetric electrical field with essentially different excitation properties concerning the direction of the axon.

The electrodes presented in this section operate well within the safe charge density limit both for anodic and for cathodic stimulation. For the electrodes

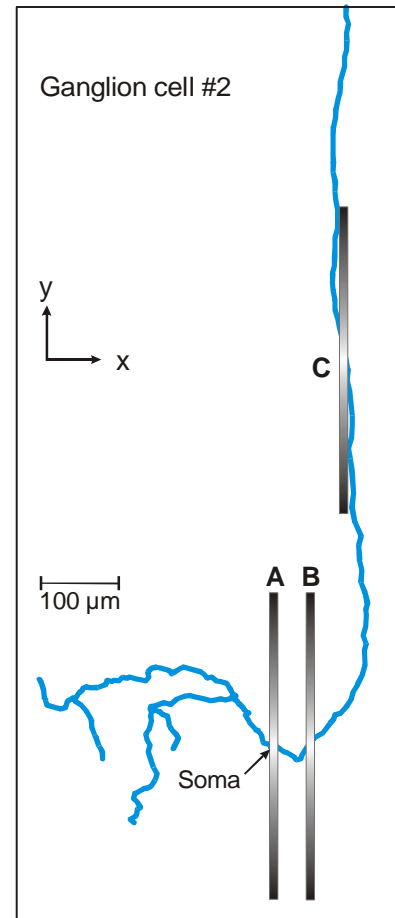


Fig. 6.5 Retinal ganglion cell #2 with 10 $\mu\text{m} \times 400 \mu\text{m}$ electrodes centered above the soma (**A**), the thin segment (**B**), and the straight axon part representing a bypassing fiber (**C**). The z-distance between soma and thin segment to the electrode is 50 μm , whereas the **C** position is only 30 μm above the axon because the bypassing axons are closer to the surface of the retina (cf. Fig. 2.2 and Fig. 2.5), i.e. 20 μm z-distance between retina and implant surface is simulated. The second electrode of the dipole has the same size and is shifted 400 μm or 1000 μm to the left.

shown in Fig. 6.5 and a dipole distance of 400 μm the charge densities are 545 $\mu\text{C}/\text{cm}^2$ and 830 $\mu\text{C}/\text{cm}^2$ for cathodic and anodic stimulation, respectively. Increasing the electrode spacing to 1000 μm decreases the values to 315 $\mu\text{C}/\text{cm}^2$ and 676 $\mu\text{C}/\text{cm}^2$, which is below from the assumed safe charge density limit of about 2000 $\mu\text{C}/\text{cm}^2$ for activated iridium electrodes [Humayun et al. 1996, 1999a., Harpster et al. 2000].

6.3 A special epiretinal implant

The method described in the previous section avoids the co-stimulation of bypassing axons under the electrode but it has the disadvantage to loose selectivity in the direction of the electrode. Moreover spikes can be generated at the edges of the electrodes, where the curvature of the potential distribution as well as the activating function will increase. Hence, for preventing co-stimulation of passing axons, it is important that excitation of these neurons will not occur at the edges. The epiretinal implant proposed in this section will minimize this ‘edge effect’ and improve the possibility of focal stimulation.

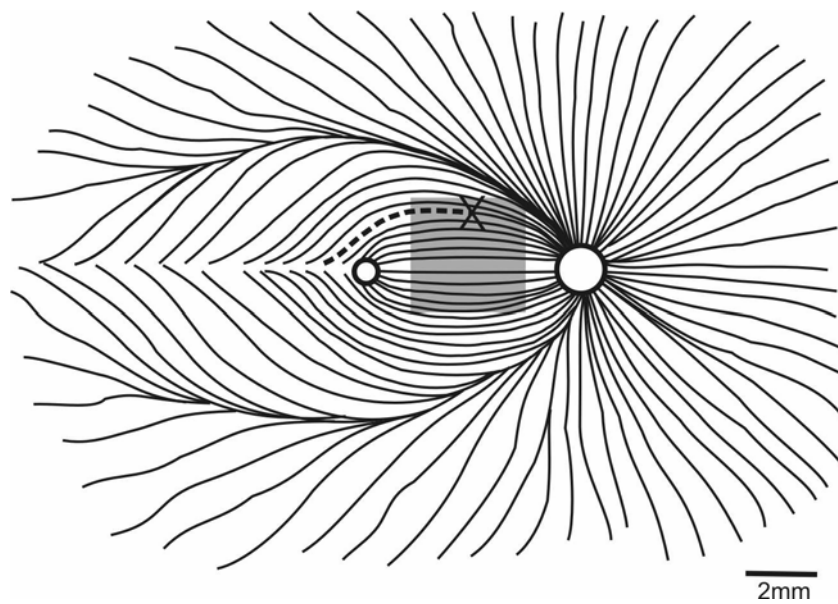


Fig. 6.6 Selected pathways of ganglion cell axons in a rectified human retina with a 3 mm \times 3 mm electrode array placed at the inner surface of the retina (gray square). Many fibers have their origin close to the fovea (small circle), but all axons leave the retina at the optic disk forming the optic nerve (right circle). An active small disk electrode marked as X can excite all axons from ganglion cell bodies placed along the dashed line instead of a focused region below the electrode (Retina redrawn after ‘Histology of the human eye: an atlas and textbook’ [Hogan et al. 1971]).

Potential distribution of an epiretinal implant with an active dipole is computed with the finite element software FEMLAB for a simplified prismatic

geometry, consisting of several $2000\ \mu\text{m} \times 2000\ \mu\text{m}$ layers (the x-y extension is smaller compared to Fig. 6.6 in order to spare elements): electrode carrier ($100\ \mu\text{m}$ thick), aqueous body layer (i.e. distance between implant and retina surface): $0\ \mu\text{m}$ or $20\ \mu\text{m}$, retina ($200\ \mu\text{m}$), sclera ($200\ \mu\text{m}$). The first layer is an insulating plate (electrode carrier) where the $10\ \mu\text{m} \times 10\ \mu\text{m}$ metallic contacts of an electrode array are embedded. Each line of electrodes which is designed to be placed parallel to the axonal main paths (Fig. 6.6) is in contact with a conducting material filling a $10\ \mu\text{m}$ wide and $50\ \mu\text{m}$ deep slot in the lower region of the implant (Fig. 6.7). Two electrodes in different slots are assumed to be active at the same time resulting in a dipole distance of, e.g. $400\ \mu\text{m}$ or $1000\ \mu\text{m}$, respectively.

The specific resistances of all tissue and technical materials are defined relative to the retina with $\rho_{\text{retina}} = 57\ \Omega\text{cm}$ [Gedden and Baker 1967, Doslak et al. 1980] by the following factors: electrode carrier (1000), conducting slot medium (0.001, 0.003, 0.01), aqueous body layer (1), and sclera (10). The thickness and specific resistance of the sclera was found to have minor influence on the extracellular potential along the investigated cells (see Section 6.2). The investigated cell of this section is ganglion cell #2.

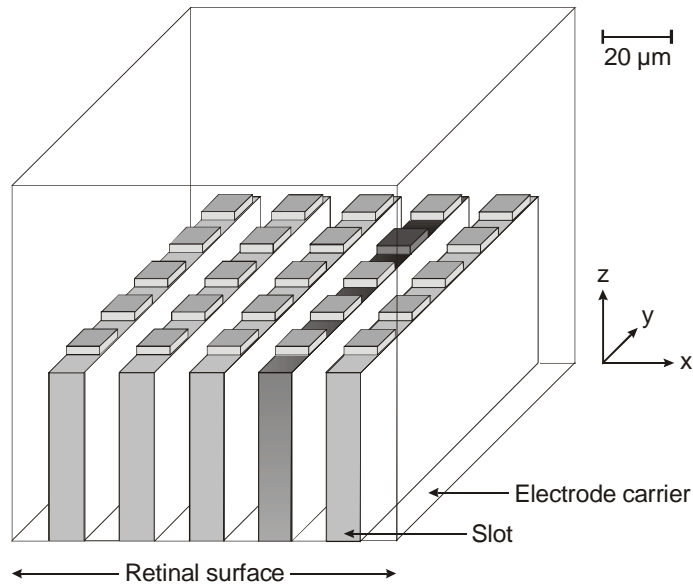


Fig. 6.7 Section of the proposed epiretinal implant. The slots are filled with conducting material (gray). The electrode carrier is transparent; the dark square symbolizes the active electrode. The second electrode (not shown) has a x-distance of $400\ \mu\text{m}$ and $1000\ \mu\text{m}$, respectively. The lower part of the implant is either assumed to be in direct contact with the inner retinal surface or it has a distance of $20\ \mu\text{m}$.

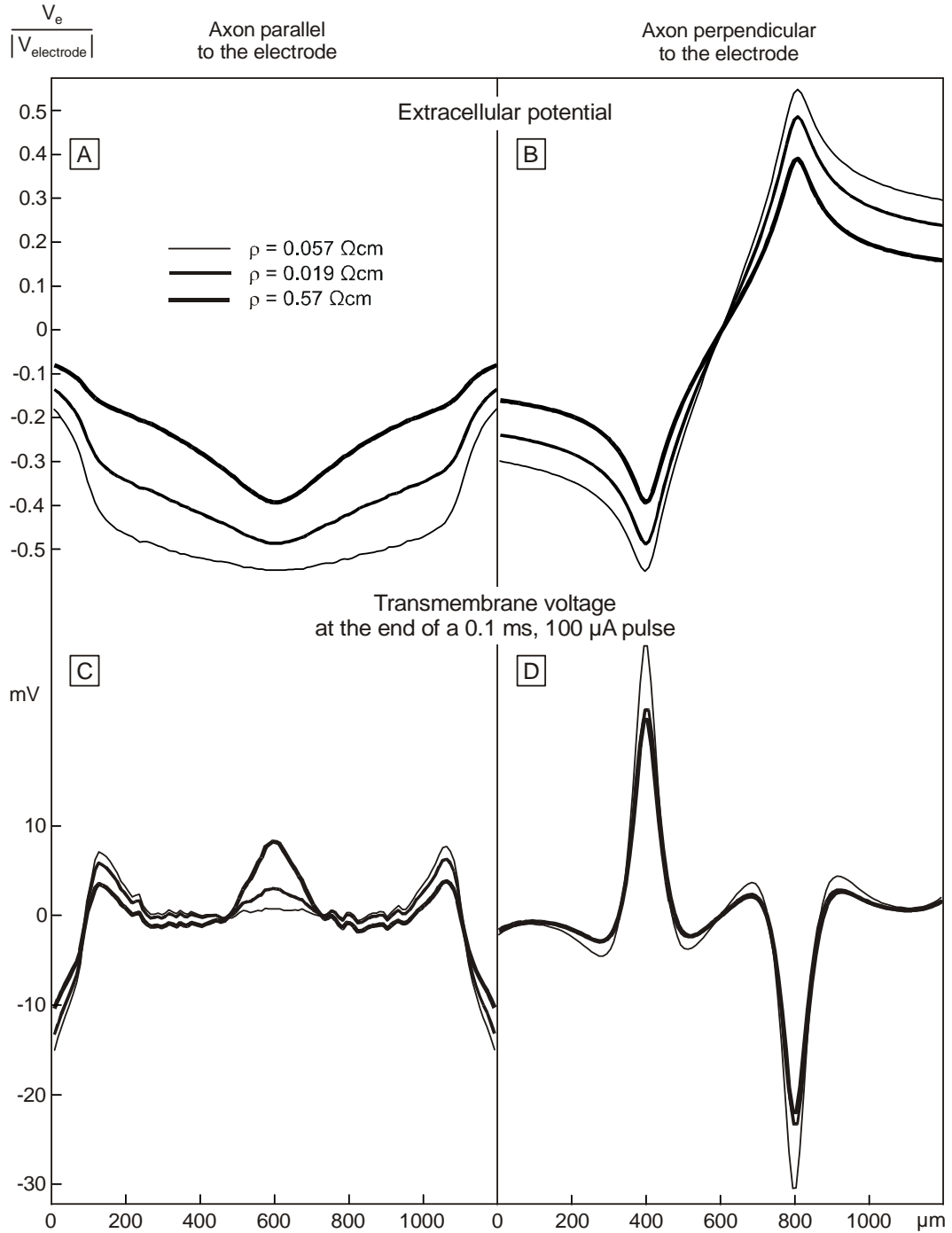


Fig. 6.8 Dipole stimulation of straight axons with electrode array as in Fig. 6.7. Extracellular potential and transmembrane voltages at the end of a 100 μA , 100 μs pulse are shown as functions of the axonal length coordinate for three specific resistances of the slot medium of the implant. Dipole distance: 400 μm , slot length 1000 μm .

The epiretinal electrode design according to Fig. 6.7 causes a flat gradient of extracellular potentials for the bypassing axons parallel to the slots (Fig. 6.8 A). Comparing the results of Fig. 6.8, the case $\rho = 0.57 \Omega\text{cm}$ corresponding to 100

fold retina conductance is recommended because it results in a good combination of two conditions: (i) a pronounced extremum of the extracellular potential along the slot (Fig. 6.8 A) in order to obtain a focal effect for transverse neural elements both in x- and y-direction and (ii) similar small sizes of the transmembrane voltage extrema along the parallel axon (Fig. 6.8 C) in order to avoid spiking in the parallel axon. For this case the threshold currents for monophasic 100 μ s pulses are listed in Table 6.3 and for comparison the extracellular potential and transmembrane voltage for an axon perpendicular to the electrode is shown in Fig. 6.8 B and D, respectively.

Table 6.3 Threshold currents in μ A for the electrodes of Fig. 6.7 (Positions shown in Fig. 6.5)						
Stimulus current	Dipole distance	Electrode positions (cf. Fig. 6.5)			Threshold ratio	
		A	B	C	C/A	C/B
Positiv	400 μ m	837	874	874	1.04	1.00
	1000 μ m	1033	994	776	0.75	0.78
Negativ	400 μ m	-454	-323	-763	1.68	2.36
	1000 μ m	-446	-333	-747	1.67	2.24

Excitation threshold for an active $10 \mu\text{m} \times 10 \mu\text{m}$ electrode in a $10 \mu\text{m} \times 1000 \mu\text{m}$ slot positioned above ganglion cell #2. The second electrode is shifted 400 μm to the right and 1000 μm to the right, respectively. Specific resistance of the slot medium: $\rho = 0.57 \Omega\text{cm}$ corresponding to 100 fold retina conductance.

To sum up the aim of the sophisticated stimulation method for epiretinal implants proposed here is to excite local areas below the electrodes without axons originating in other regions. This problem is investigated with three target cells. Instead of one cell with 3 electrode positions, the results of Table 6.2 and Table 6.3 can be interpreted as one electrode that stimulates three different ganglion cells of the same shape shifted to three positions (**A**, **B**, **C**): cell **C** represents the bypassing axon, cell **B** has the thin axonal segment below the center of the electrode and cell **A**'s soma is below the electrode.

To avoid charge accumulation we assume application of a train of 100 μ s pulses with equal positive and negative amplitudes and interpulse intervals of some milliseconds. According to Table 6.3, e.g. a 460 μ A stimulus is subthreshold for cell **C** but initiate spikes both in cell **A** and **B**. For a dipole distance of 400 μ m cell **C** has a 2.36 (2.24 for 1000 μ m dipole distance) times higher threshold than **B** but this relation is reduced to a 'safety' factor of 1.57 (1.32) for the 'simple' rectangular electrodes as listed in Table 6.2. This means an increasing from 36 % to 58 % in threshold difference between bypassing axon and near the cell body for the proposed electrode design. Note that the soma is not the most excitable cell region but the smallest thresholds are observed for cathodic stimulation above the thin axonal segment (Table 6.2 and Table 6.3), cf. Section 4.4, and Section 5.2.

The activating function concept was helpful for designing the ‘sophisticated’ electrode: a higher slot medium resistance causes a stronger curvature in the central part of the extracellular potential profile (Fig. 6.8 A) resulting in (i) increase of the activating function implying smaller thresholds for the bypassing axons and (ii) sharper focal effect in slot direction. The y-resolution with the proposed parameters is still rather poor and the question arises: How much can we support the sharpening effect on cost of the ‘safety’ factor reduction?

The ‘safety’ factor for avoiding bypassing axon stimulation has a second component contributing to ganglion cell soma excitation in form of synaptic activities from other stimulated retinal cells. The proposed electrode design will support neurotransmitter release of the bipolar cells which is an essential help for focused stimulation.

The technical realization of the electrode array (Fig. 6.7) is not planed in detail. One possibility is to use doped semiconductors as conducting medium in the slot material; another one is to generate the calculated potential distribution with a line of active electrodes instead of the approach with the slots. And last but not least it should be mentioned that threshold current densities are within safe limits of available electrodes, e.g. a current of 460 μA (super-threshold to positions **A** and **B** according to Table 6.3) causes a mean value of 460 $\mu\text{C}/\text{cm}^2$ for the $10\text{ }\mu\text{m} \times 1000\text{ }\mu\text{m}$ slot, which is in the range of experimental data reviewed by Loewenstein et al. [Loewenstein et al. 2004].

7. Concluding discussion

The response of retinal cells, diverse in type and shape, to an applied electric field was simulated and the excitation process was carefully analyzed, to clarify the neuronal targets of electrical stimulation. The obtained insights were used to develop an implant design for selective activation of the retinal cells underlying the electrode that avoids co-stimulation of bypassing fibers from distant regions of the retina. This was done with awareness to the safety charge density limit which is a critical factor in retina implant technology.

The excitation process of the electrically stimulated retinal cells is simulated in a two step procedure. In the first step the extracellular potential along the neural structure is calculated either with a finite element method considering the volume conductor inhomogeneities of the eye or analytically in a simpler approach assuming an infinite homogenous medium. In a second step the target cells are represented by compartment models, here the membrane kinetics of the diverse retinal cell types are evaluated with three different models (the HH and the FCM model for the retinal ganglion cells and a linear passive model for the simulations of the bipolar cells; cf. Section 3.2).

It turns out that assuming an infinite homogeneous medium as a volume conductor is an appropriate approach for most of the investigated tasks. Including additional structures in the model besides the retina, like the sclera, is of minor influence (Section 5.2), because the distance between stimulating electrode and target cell is rather small in contrast to the dimensions of the eye. Nevertheless, the finite element model is necessary for the electrode design, as analytically only formulae for the extracellular potentials of spherical and disk electrodes are available.

The FCM model is based on voltage clamp studies in salamander retinas. It is of great advantage to simulate the externally stimulated retinal ganglion cells, although it also has its limitations. It is derived from an amphibian retina which is on one hand good because it goes with the traced cells, but on the other hand there are great differences between an amphibian and a human retina so as for example the salamander retina has no fovea.

A special feature of the FCM membrane model is the inclusion of active dendrites, which means that they are able to develop rudimental action potentials. The membrane model of the dendritic tree is closely matched with its size, number of ramifications, and geometry, a modification of these features (like in ganglion cell #2) leads to unrealistic threshold values for electrodes above a dendrite. Fortunately the reduction of the dendritic tree has little influence on

models with electrodes above soma or axon, which were the important cases for the simulations of this thesis. As the FCM model is derived from patch clamp experiments of the soma, which were extrapolated for the properties of the axon, comparing simulations with the HH model are useful since this model is derived directly from an unmyelinated axon.

For the retinal bipolar cell a better model than the linear passive used here would be desirable. Unfortunately the necessary physiological recordings are not available. If the rheobase and chronaxie values were known it would be easier to decide whether bipolar or ganglion cells are preferably excited by the stimulating electrode current.

Another remark concerns the compartment model described in Section 3.1. For the simulations of this thesis the software ACSL is used to solve the system of differential equations with both Runge-Kutta and Adams-Moulton integration algorithms. These are explicit integration methods which are not suited for extreme small compartment sizes which are needed e.g. for very small electrode tissue distances. In such cases the equations can be evaluated efficiently with the Crank-Nicholson algorithm.

There is only one type of rod bipolar cell, but many types of cone bipolar cells have been recognized in several mammalian species, e.g. in a monkey retina 10 types have been described from Golgi staining [Kolb et al. 1992]. The shapes of the bipolar cells differ concerning the size of the branching terminals and extension of the dendritic trees. ON and OFF bipolar cells make synaptic contacts in different levels of the interplexiform layer, and thereby they have different functional distances to the electrode. In addition, there are approximately 12-15 specific types of ganglion cell populations [Roska and Werblin 2001, Rockhill et al. 2002]. Each type generates unique spiking patterns that are carried to distinct downstream visual sites, to both cortical and noncortical areas [Roska and Werblin 2001] (cf. Section 2).

Two rather extreme bipolar cell shapes were investigated. The first cell has a rather straight vertical extension through the retina. The two dendritic branches have no bifurcations. The second investigated bipolar cell on the contrary has a large dendritic tree with many ramifications and dendritic endings (cf. Section 2.3). It shows that ON cells (which make synaptic contact in the upper part of the interplexiform layer with respect to the retinal surface) with few terminal branches are most excitable for the assumed electric field. The endings vertical to the retinal surface react as the hot spots of excitation, whereas cell endings parallel to the retinal surface are not sensitive to the applied electric field (Section 4.5).

Retinal ganglion cells are most excitable at the distal end of the thin segment (Section 4.4 and Section 5.2). But although bipolar cells have no compartment as close to the electrode as the ganglion cells, it is possible that they respond with stronger transmembrane voltage. The reason for this is the geometric orientation of both cells, at least in the region with high extracellular potential values, i.e. close to the electrode. The processes of the ganglion cell are tangential

to the isopotentials, which means that a target compartment in that area has extracellular potential values similar to that of its neighbors. Therefore, the numerators of both activating functions are small in such cases. Besides, the local cell geometry defines also the amount of threshold changes for different stimulus durations (Section 5.2). All things considered, the geometry of the cells and their orientation in the applied electric field are the determining factors.

Size and structure of the neural elements depend on the distance to the fovea, because the different types of ganglion or bipolar cells are not uniformly distributed throughout the retina. Usually the cells of the peripheral part are larger, with widespread dendritic trees. Therefore the visual percepts created by a retinal implant will depend on the location on the retina. Clinical trials performed by Rizzo and coworkers support this conclusion [Rizzo et al. 2003b].

To obtain focal perceptions it would be preferable to elicit neurotransmitter release in bipolar cells or excite the soma, the initial segment of the axon respectively, before a spike is initiated in axons from distant sites of the retina which overlie the individual ganglion cell bodies. It seems that this target can be reached even in the case of epiretinal stimulation where blind patients already reported focal phosphenes [Humayun et al. 2003, Rizzo et al. 2003b]. Although this can not be taken for granted since the threshold for activation increases linearly with the electrode distance in the case of near field stimulation (electrode close to the target structure), and changes gradually to a third power relation in the distance in the case of far field stimulation (Section 4.3).

Therefore the short distance of the bypassing axons below the electrode is a strong argument for their co-stimulation, but this relation also implies the fact that only axons passing close can be reached. In Section 4.3 a rough estimation for the number of axons is given, about 80 for a small electrode close to the retinal surface for a 10 % above threshold current. This number seems to be too small to cause large wedge shape perceptions as proposed by Greenberg and coworkers [Greenberg et al. 1999]. However it can be an argument for the observations of Rizzo et al. that single percepts induced by single-electrode stimulation were relatively small, but the form of percepts, especially after multielectrode stimulation, often did not match the stimulation pattern [Rizzo et al. 2003b]. Evidence of axon stimulation is also given by experiment 6 of Rizzo and colleagues (Fig. 7.1).

Beside the simulation results there are also experimental indications that electrical stimulation targets bipolar cells. Jensen et al. reported that the spiking response to electrical stimulation consists of short- and long-latency components and that the latency of the late component, ranged from 8-60 ms, arose from activation of bipolar cells [Jensen et al. 2005]. Note that the operating range of the graded potentials of the bipolar cells is essentially lower than the threshold voltage for a propagating spike in the ganglion cell [Werblin and Dowling 1969, Boycott and Wässle 1999, Rieke 2001]. Therefore, the bipolar cells are expected to answer with neurotransmitter release before a spike is initiated directly in the

ganglion cell. Short stimulation pulses are expected to cause a small amount of neurotransmitter release in spite of remarkable membrane voltage, but how much transmitter release must occur till a ganglion cell fires solely driven by bipolar cells is unknown.

Greenberg and coworkers expect more support from the bipolar network and in the following rounder percepts for stimuli longer than 0.5 ms [Greenberg 1998, Weiland et al. 1999]. This hypothesis was tested with nearly 100 trials by Rizzo and his colleges in volunteers with epiretinal electrodes, but unfortunately it could not be proved [Rizzo et al. 2003b]. But with respect to the generally limited results different reasons are thinkable.

Admittedly, long pulse durations increase the threshold charge, which is a critical safety factor in effective retinal stimulation (Section 5.3). Decreasing the required threshold charge is possible by increasing the electrode size, which goes with a loss of selectivity and is therefore not desirable. The minimum which was found at 0.6 ms in the strength-curves could lower the threshold charge density by 12 %. (This minimum was found only for simulations with a HH membrane, but it seems likely that the simulations with the FCM model reveal such a minimum for a longer pulse

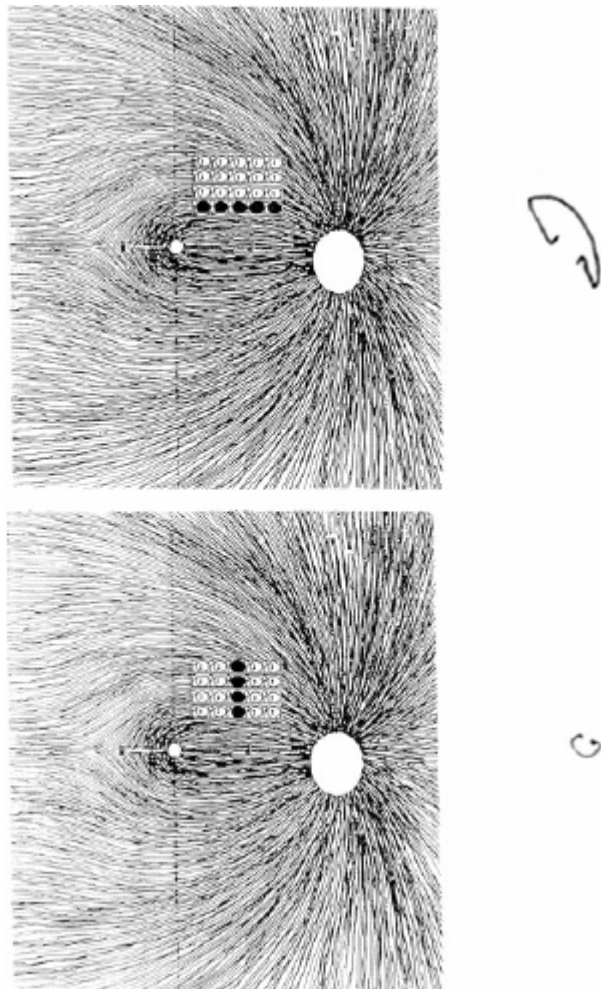


Fig. 7.1 Left: Location of the electrode array with respect to the orientation of retinal ganglion cell axons of the right eye. Right: Subject's drawing of the induced perceptions. The first trial (top) drove electrodes that were oriented in parallel to the axons, which yielded a banana-shaped percept. The orientation of the banana, with the lower end tilted to the right, matched an expectation based on activation of axons under the array that were extensions of ganglion cell bodies that were distributed along a curved line between the array and the horizontal raphe. The second trial (bottom), which drove electrodes that were oriented perpendicular to the axons, yielded a percept of a circular object. All stimuli were performed with 250 μA per electrode, 4 ms pulses delivered in monopolar configuration through the darkened electrodes. The large, open circular regions represent the optic nerve head; the small, open circular regions represent the fovea [Rizzo et al. 2003b].

duration if the resolution of the strength-duration curve is calculated with more points than in Section 5.1.)

All things considered, a sophisticated implant design for selective excitation of neuronal structures underlying the electrode in a greater distance is desirable. Besides the challenge of focused stimulation, special attention has to be paid on the safe charge density limits of the device. Based on a hypothesis of Grumet, that long stimulating elements parallel to the main directions of bypassing axons avoid their excitation [Grumet 1994], a special retinal implant design was developed (Section 6.3).

The main idea is that each line of electrodes of an array is in contact with a long slot filled with conducting material, which is placed parallel to the axonal pathways (Fig. 5.7). The stimulating slots cause a flat gradient of extracellular potentials for the bypassing axons to avoid their excitation, but in dependence of the conductance of the slot material also a focus effect is achievable, to stimulate the soma, axonal thin segment or even bipolar cells. A higher slot medium resistance causes a stronger curvature in the central part of the extracellular potential profile, which leads on one hand to smaller thresholds for the bypassing axons and on the other hand in a sharper focusing effect in slot direction. Thus choosing the slot material with the appropriate conductance is the posed challenge for the proposed implant.

Threshold currents in patients and animal experiments are often smaller than in computer simulations of the presented type. As an example, the calculated threshold for the small ganglion cell stimulated with a 10 μm disk electrode 25 μm above the thin segment is -30 μA for a 100 μs pulse, -11 μA for a 400 μs pulse and -3.4 μA for 5 μm electrode distance (400 μs pulse). For situations similar to the last case Grumet reports sub-microampere threshold currents based on his own experiments and reviewed data [Grumet 1999].

Several phenomena, not included in the simulation, can reduce the threshold currents, but they will not change the presented qualitative results: the amount of neurotransmitter release e.g. from bipolar cells, which helps to activate the ganglion cells increases with pulse duration and electrode size [Jensen et al. 2003]; the spontaneous activity of ganglion cells [Sakmann and Kreutzfeld 1969] is expected to be influenced by a weak electrical field; ion current fluctuations across the cell membrane [Verveen and Derksen 1968], which can be modeled proportional to the square root of the number of the sodium channels involved [Rattay 2000].

Electrical stimulation of the retina activates multiple classes of retinal neurons complicating the generation of precise temporal patterns of spiking. In response to light, bipolar cells deliver excitatory input to both ganglion cells and amacrine cells. Activated amacrine cells deliver inhibitory input in a feed-forward manner to ganglion cells and via feedback to bipolar cells (cf. Section 2). The precise interplay between these excitatory and inhibitory signals shapes the retinal response. Since electrical stimulation targets bipolar cells, it is likely that

amacrine cells are targeted as well. Activation of amacrine cells is likely to lead to long-lasting inhibitory signals feeding both forward and backward and therefore may lead to many undesirable effects, such as increased threshold levels. Under normal conditions light stimuli do not simultaneously activate ON and OFF ganglion cells while large diameter electrodes likely do.

Future investigations should pay attention to this physiological interactions and should include amacrine cells in the investigations (traced amacrine cells are available, but the proper membrane model has to be developed). New methods that lead to more physiological patterns of activation are likely to lead to more meaningful visual percepts in blind patients. But currently there are no methods to identify or separately activate different cell types (e.g., ON versus OFF, sustained versus transient, etc.). A future prosthetic device should be capable of targeting the appropriate spiking pattern to the correct cell type and surely simulations will help to develop and understand them.

References

- Agnew W.F., Yuen T.G., McCreery D.B., and Bullara L.A. Histopathologic evaluation of prolonged intracortical electrical stimulation. *Exp. Neurol.* 92, 62-85, 1986.
- Basser P.J., Wijesinghe R.S., and Roth. B.J. The activating function for magnetic stimulation derived from a 3-dimensional volume conductor model. *IEEE Trans. Biomed. Eng.* 39, 1207-1210, 1992.
- Bogacki P. and Shampine L.F. A 3(2) pair of Runge-Kutta formulas. *Appl. Math. Letters* 2, 1-9, 1989.
- Boycott B.B. and Wässle H. The morphological types of ganglion cells of the domestic cat's retina. *J. Physiol.* 240, 397-419, 1974.
- Boycott B.B. and Wässle H. Morphological classification of bipolar cells of the primate retina. *Eur. J. Neurosci.* 3, 1069-1088, 1991.
- Boycott B.B. and Wässle H. Parallel processing in the mammalian retina: the proctor lecture. *Invest. Ophthalmol. Vis. Sci.* 40, 1313-1327, 1999.
- Breitenecker F., Ecker H., and Bausch-Gall I. *Simulation mit ACSL*. Verlag Vieweg, Braunschweig-Wiesbaden, 1993.
- Bron A.J., Tripathi R.C., and Tripathi B.J. *Wolff's Anatomy of the Eye and Orbit*. Chapman and Hall Medical, 1997.
- Brown W.J., Babb T.L., Soper H.V., Lieb J.P., Ottino C.A., and Crandall P.H. Tissue reactions to long-term electrical stimulation of the cerebellum in monkeys. *J. Neurosurg.* 47, 366-379, 1977.
- Carras P.L., Coleman P.A., and Miller R.F. Site of action potential initiation in amphibian retinal ganglion cells. *J. Neurophysiol.* 67, 292-304, 1992.
- Cha K., Horch K.W., and Normann R.A. Mobility performance with a pixelized vision system. *Vision Res.* 32, 1367-1372, 1992.
- Chow A.Y., Pardue M.T., Chow V.Y., Peyman G.A., Liang C., Perlman J.I., and Peachey N.S. Implantation of silicon chip microphotodiode arrays into the cat subretinal space. *IEEE Trans. Neural. Syst. Rehabil. Eng.* 9, 86-95, 2001.

- Chow A.Y., Chow V.Y., Packo K.H., Pollack J.S., Peyman G.A., and Schuchard R. The artificial silicon retina microchip for the treatment of vision loss from retinitis pigmentosa. *Arch. Ophthalmol.* 122, 460-469, 2004.
- Clark J. and Plonsey R. The extracellular potential field of the single active nerve fiber in a volume conductor. *J. Biophys.* 8, 842-864, 1968.
- Coburn B. Neural modeling in electrical stimulation. *Crit. Rev. Biomed. Eng.* 17, 133-178, 1989.
- Coleman P.A. and Miller R.F. Measurement of passive membrane parameters with whole-cell recording from neurons in the intact amphibian retina. *J. Neurophysiol.* 61, 218-230, 1989.
- Doslak M.J., Plonsey R., and Thomas C.W. The Effects of Variations of the Conducting Media Inhomogeneities on the Electroretinogram. *IEEE Trans. Biomed. Eng.* 27, 88-89, 1980.
- Eckmiller R. Learning retina implants with epiretinal contacts. *Ophthalmic Res.* 29(5), 281-289, 1997.
- Fohlmeister J.F., Coleman P.A., and Miller R.F. Modeling the repetitive firing of retinal ganglion cells. *Brain Res.* 510, 343-345, 1990.
- Fohlmeister J.F. and Miller R.F. Impulse Encoding Mechanisms of Ganglion Cells in the Tiger Salamander Retina. *J. Neurophysiol.* 78, 1935-1947, 1997a.
- Fohlmeister J.F. and Miller R.F. Mechanisms by Which Cell Geometry Controls Repetitive Impulse Firing in Retinal Ganglion Cells. *J. Neurophysiol.* 78, 1948-1964, 1997b.
- Garnham C.W., Barker A.T., and Freeston. I.L. Measurement of the activating function of magnetic stimulation using combined electrical and magnetic stimuli. *J. med. Eng. and Techn.* 19, 57-61, 1995.
- Geddes L.A. and Baker L.E. The specific resistance of biological material-a compendium of data for the biomedical engineer and physiologist. *Med Biol Eng.* 5, 271-293, 1967.
- Greenberg R.J. Analysis of electrical stimulation of the vertebrate retina - Work toward a retinal prosthesis. *Ph.D. Thesis, The Johns Hopkins University, Baltimore*, 1998.
- Greenberg R.J., Velte T.J., Humayun M.S., Scarlatis G.N., and Juan E.A. computational model of electrical stimulation of the retinal ganglion cell. *IEEE Trans. Biomed. Eng.* 46(5), 505-514, 1999.
- Grill W.M., Simmons A.M., Cooper S.E., Miocinovic S., Montgomery E.B., Baker K.B., and Rezai A.R. Temporal excitation properties of paresthesias

- evoked by thalamic microstimulation. *Clin. Neurophysiol.* 116, 1227-1234, 2005.
- Grumet A.E. *Extracellular Electrical Stimulation of Retinal Ganglion Cells*. M.S. thesis, Massachusetts Institute of Technology, 1994.
- Grumet A.E. *Electric Stimulation Parameters for an epi-retinal prosthesis*. PhD. thesis, Massachusetts Institute of Technology, 1999.
- Harpster T., Hauvespre S., Dokmeci M., Stark B., Vosoughi A., and Najafi K. A passive humidity monitoring system for in situ remote wireless testing of micropackages. *Proc. of the MEMS 2000 Conference*, 335-340, 2000.
- Hodgkin A.L. and Huxley A.F. A quantitative description of membrane current and its applications to conduction and excitation in nerve. *J. Physiol. (Lond.)* 117, 500-544, 1952.
- Hogan M.J., Alvarado J.A., and Weddell J.E. *Histology of the human eye: an atlas and textbook*. Philadelphia: WB Saunders, 1971.
- Humayun M.S., Propst R., de Juan E.Jr., McCormick K., and Hickingbotham D. Bipolar surface electrical stimulation of the vertebrate retina. *Arch. Ophthalmol.* 112, 110-116, 1994.
- Humayun M.S., de Juan E.Jr., Dagnelie G., Greenberg R.J., Propst R.H., and Phillips D.H. Visual perception elicited by electrical stimulation of retina in blind humans. *Arch. Ophthalmol.* 114, 40-46, 1996.
- Humayun M.S., de Juan E.Jr., Weiland J.D., Dagnelie G., Katona S., Greenberg R.J., and Suzuki S. Pattern electrical stimulation of the human retina. *Vision Res.* 39, 2569-2576, 1999a.
- Humayun M.S., Prince M., de Juan E.Jr, Barron Y., Moskowitz M., Klock I.B., and Milam A.H. Morphometric analysis of the extramacular retina from postmortem eyes with retinitis pigmentosa. *Invest. Ophthalmol. Vis. Sci.* 40, 143-148, 1999b.
- Humayun M.S., Weiland J.D., Fujii G.Y., Greenberg R.J., Williamson R., Little J., Mech B., Cimmarusti V., Van Boemel G., Dagnelie G., and de Juan E. Visual perception in a blind subject with a chronic microelectronic retinal prosthesis. *Vision Res.* 43, 2573-2581, 2003.
- Humayun M.S, Yanai D., Greenberg R.J., Little J., Mech B.V., Mahadevappa M., Weiland J.D., Fujii G.Y., and de Juan E.Jr. Chronically implanted intraocular retinal prosthesis in three blind subjects. *Invest. Ophthalmol. Vis. Sci.* 45, E-Abstract 3397, 2004.
- Jensen R.J., Ziv O.R., and Rizzo J.F.3rd. Thresholds for direct and indirect activation of ganglion cells with an epiretinal electrode: effect of stimulus duration and electrode size. *ARVO Conference*, Abstract 5048, 2003.

- Jensen R.J., Ziv O.R., and Rizzo J.F.3rd. Thresholds for activation of rabbit retinal ganglion cells with relatively large, extracellular microelectrodes. *Invest. Ophthalmol. Vis. Sci.* 46, 1486-1496, 2005.
- Kolb H., Nelson R., and Mariani A. Amacrine cells, bipolar cells and ganglion cells of the cat retina: A Golgi study. *Vision Res.* 21, 1081-1114, 1981.
- Kolb H. The neural organization of the human retina. In: *Principles and Practices of Clinical Electrophysiology of Vision*. Eds. J.R. Heckenlively and G.B. Arden, Mosby Year Book Inc., St. Louis, 25-52, 1991.
- Kolb H., Linberg K.A., and Fisher S.K. Neurons of the human retina: A Golgi study. *Journal of Comparative Neurology* 31, 147-187, 1992.
- Kuhn A.A., Brandt S.A., Kupsch A., Trottenberg T., Brocke J., Irlbacher K., Schneider G.H., and Meyer B.U. Comparison of motor effects following subcortical electrical stimulation through electrodes in the globus pallidus internus and cortical transcranial magnetic stimulation. *Exp. Brain Res.* 155, 48-55, 2004.
- Lapicque L. Definition experimentale de l'excitation. *Comptes Rendus Acad. Sci.* 67, 280-283, 1909.
- Lapicque L. *L'Excitabilite en Function du Temps*. Presses Universitaires de France, 1926.
- Laube T., Schanze T., Brockmann C., Bolle I., Stieglitz T., and Bornfeld N. Chronically implanted epidural electrodes in Gottinger minipigs allow function tests of epiretinal implants. *Graefes Arch. Clin. Exp. Ophthalmol.* 241, 1013-1019, 2003.
- Lipton S.A. and Tauck D.L. Voltage-dependent conductances of solitary ganglion cells dissociated from rat retina. *J. Physiol.* 385, 361-391, 1987.
- Loewenstein J.I., Montezuma S.R., and Rizzo J.F.3rd. Outer retinal degeneration: an electronic retinal prosthesis as a treatmentstrategy. *Arch. Ophthalmol.* 122, 587-596, 2004.
- Lukasiewicz P. and Werblin F. A slowly inactivating potassium current truncates spike activity in ganglion cells of the tiger salamander retina. *J. Neurosci.* 8, 4470-4481, 1988.
- Margalit E., Maia M., Weiland J.D., Greenberg R.J., Fujii G.Y., Torres G., Piyathaisere D.V., O'Hearn T.M., Liu W., Lazzi G., Dagnelie G., Scribner D.A., de Juan E.Jr., and Humayun M.S. Retinal prosthesis for the blind. *Surv. Ophthalmol.* 47, 335-356, 2002.
- Masland R.H. The fundamental plan of the retina. *Nature Neurosci.* 4, 877-886, 2001.

- McCreery D.B., Agnew W.F., Yuen T.G., and Bullara L.A. Comparison of neural damage induced by electrical stimulation with faradaic and capacitor electrodes. *Ann. Biomed. Eng.* 16, 463-481, 1988.
- McCreery D.B., Agnew W.F., Yuen T.G., and Bullara L. Charge density and charge per phase as cofactors in neural injury induced by electrical stimulation. *IEEE Trans. Biomed. Eng.* 37, 996-1001, 1990.
- McCreery D.B., Yuen T.G., Agnew W.F., and Bullara L.A. A characterization of the effects on neuronal excitability due to prolonged microstimulation with chronically implanted microelectrodes. *IEEE Trans. Biomed. Eng.* 44, 931-939, 1997.
- Merabet L.B., Rizzo J.F.3rd., Amedi A., Somers D.C., and Pascual-Leone A. What blindness can tell us about seeing again: merging neuroplasticity and neuroprostheses. *Nature Reviews Neurosci.* 6, 71-77, 2005.
- Nadig M.N. Development of a silicon retinal implant: cortical evoked potentials following focal stimulation of the rabbit retina with light and electricity. *Clin. Neurophysiol.* 110, 1545-1553, 1999.
- Plonsey R. The active fiber in a volume conductor. *IEEE Trans. Biomed. Eng.* 21, 371-381, 1974.
- Polyak S.L. *The Retina*. University of Chicago Press, Chicago, 1941.
- Ranck J.B. Which elements are excited in electrical stimulation of mammalian central nervous system: A review. *Brain Res.* 98, 417-440, 1975.
- Rattay F. Analysis of models for external stimulation of axons. *IEEE Trans. Biomed. Eng.* 33, 974-977, 1986.
- Rattay F. Analysis of models for extracellular fiber stimulation. *IEEE Trans. Biomed. Eng.* 36, 676-682, 1989.
- Rattay F. *Electrical Nerve Stimulation: Theory, Experiments and Applications*. Springer Wien - New York, 1990.
- Rattay F. The basic mechanism for the electrical stimulation of the nervous system. *Neuroscience* 89, 335-346, 1999.
- Rattay F. Basics of hearing theory and noise in cochlea implants. *Chaos, Solitons and Fractals* 11, 1875-1884, 2000.
- Rattay F., Greenberg R.J., and Resatz S. Neuron Modeling. In: *Handbook of Neuroprosthetic Methods*. Eds. W.E. Finn and P.G. LoPresti, CRC Press, 39-71, 2002.
- Rattay F., Resatz S., Lutter P., Minassian K., Jilge B., and Dimitrijevic M.R. Mechanisms of electrical stimulation with neural prostheses. *Neuromodulation* 6, 42-46, 2003.

- Rattay F. and Resatz S. Effective electrode configuration for selective stimulation with inner eye prostheses. *IEEE Trans. Biomed. Eng.* 51, 1659-1664, 2004.
- Resatz S. Electrical stimulation of the retinal ganglion cell: a computer simulation. *Master thesis, Vienna Univ. Techn.*, 2002.
- Resatz S. and Rattay F. Stimulating neural networks with microelectrodes: a modeling study for the retina implant. *Proc. IFESS Ljubljana*, 170-172, 2002.
- Resatz S. and Rattay F. The electrically stimulated retina: a simulation study. *Proc. 4th MATHMOD Vienna*, 1636-1645, 2003a.
- Resatz S. and Rattay F. Excitability of bipolar and ganglion cells with retinal prosthesis: a modeling study. *Proc. Engineering in Medicine and Biology Society, 25th Annual International Conference Cancun, Mexico*, 2039-2042, 2003b.
- Resatz S. and Rattay F. A model for the electrically stimulated retina. *Mathematical and Computer Modelling of Dynamical Systems*, 10, 93-106, 2004.
- Resatz S., Rattay F., Edthofer F., Schöbel M., and Valla A. A compartment model of the electrically stimulated retinal ganglion cell. *Proc. World Congress on Neuroinformatics*, Argesim/Asim Verlag Vienna, Part II, 217-218, 2001.
- Rieke F. Temporal contrast adaptation in salamander bipolar cells. *J. Neurosci.* 21, 9445-9454, 2001.
- Rizzo J.F.3rd., Wyatt J., and Loewenstein J.I. Acute intraocular retinal stimulation in normal and blind humans. *Invest. Ophthalmol. Vis. Sci.* 41, 102, 2000.
- Rizzo J.F.3rd., Wyatt J., Loewenstein J.I., Kelly S., and Shire D. Methods and perceptual thresholds for short-term electrical stimulation of human retina with microelectrode arrays. *Invest. Ophthalmol. Vis. Sci.* 44, 5355-5361, 2003a.
- Rizzo J.F.3rd., Wyatt J., Loewenstein J.I., Kelly S., and Shire D. Perceptual efficacy of electrical stimulation of human retina with a microelectrode array during short-term surgical trials. *Invest. Ophthalmol. Vis. Sci.* 44, 5362-5369, 2003b.
- Rockhill R.L., Daly F.J., MacNeil M.A., Brown S.P., and Masland R.H. The diversity of ganglion cells in a mammalian retina. *J. Neurosci.* 22, 3831-3843, 2002.
- Rose T.L. and Robblee L.S. Electrical stimulation with Pt electrodes. VIII. Electrochemically safe charge injection limits with 0.2 ms pulses. *IEEE Trans. Biomed. Eng.* 37, 1118-1120, 1990.

- Roska B. and Werblin F. Vertical interactions across ten parallel, stacked representations in the mammalian retina. *Nature* 410, 583-587, 2001.
- Roska B. and Werblin F. Rapid global shifts in natural scenes block spiking in specific ganglion cell types. *Nat. Neurosci.* 6, 600-608, 2003.
- Sakmann B. and Kreutzfeldt O.D. Scotopic and mesopic light adaptation in the cat's retina. *Pflügers Arch.* 313, 168-185, 1969.
- Santos A., Humayun M.S., de Juan E.Jr., Greenburg R.J., Marsh M.J., Klock I.B., and Milam A.H. Preservation of the inner retina in retinitis pigmentosa: a morphometric analysis. *Arch. Ophthalmol.* 115, 511-515, 1997.
- Saunders F.A. Electrotactile sensory aids for the handicapped. *4th Annu. Meeting Biomedical Engineering Society*, Los Angeles, CA, 1973.
- Schanze T., Wilms M., Eger M., Hesse L., and Eckhorn R. Activation zones in cat visual cortex evoked by electrical retina stimulation. *Graefes Arch. Clin. Exp. Ophthalmol.*, 240, 947-954, 2002.
- Sterling P. and Demb J.B. Retina. In: *Synaptic organization of the brain*. Ed. G.M. Sheperd. Oxford University Press, 217-269, 2004.
- Stett A., Barth W., Weiss S., Haemmerle H., and Zrenner E. Electrical multisite stimulation of the isolated chicken retina. *Vision Res.* 40, 1785-1795, 2000.
- Stone J.L., Barlow W.E., Humayun M.S., de Juan E.Jr., and Milam A.H. Morphometric analysis of macular photoreceptors and ganglion cells in retinas with retinitis pigmentosa. *Arch. Ophthalmol.* 110, 1634-1639, 1992.
- Teeters J., Jacobs A., and Werblin F. How neural interactions form neural responses in the salamander retina. *J. Comput. Neurosci.* 4, 5-27, 1997.
- Tehovnik E.J. Electrical stimulation of neural tissue to evoke behavioral responses. *J. Neurosci. Methods* 65, 1-17, 1996.
- Toris C.B., Eiesland J.L., and Miller R.F. Morphology of Ganglion Cells in the Neonotous Tiger Salamander Retina. *J. Comp. Neurol.* 352, 535-559, 1995.
- Van Buren J.M. *The retinal ganglion cell layer*. Ed. Charles C. Thomas, Springfield, Illinois, 1963.
- Velte T.J and Masland R.H. Action potentials in the dendrites of retinal ganglion cells. *J. Neurophysiol.* 81, 1412-1417, 1999.
- Verveen A.A. and Derksen H.E. Fluctuation phenomena in nerve membrane. *Proc. IEEE* 56, 906-916, 1968.

- Vetter P., Roth A., and Hausser M. Propagation of action potentials in dendrites depends on dendritic morphology. *J. Neurophysiol.* 85, 926-937, 2001.
- Weiland J.D., Humayun M.S., Dagnelie G., de Juan E.Jr., Greenberg R.J., and Iliff N.T. Understanding the origin of visual percepts elicited by electrical stimulation of the human retina. *Graefes Arch. Clin. Exp. Ophthalmol.* 237, 1007-1013, 1999.
- Weiss G. Sur la possibilité de rendre comparable entre eux les appareils servant a l'excitation électrique. *Arch. Ital. Biol.* 35, 413–446, 1901.
- Werblin F.S. and Dowling J.E. Organization of the retina of the mudpuppy, *Necturus maculosus*. II. Intracellular recording. *J. Neurophysiol.* 32, 339-355, 1969.
- Wiley J.D. and Webster J.G. Analysis and control of the current distribution under circular dispersive electrodes. *IEEE Trans. Biomed. Eng.* 29, 381-385, 1982.
- Young B. and Heath J.W. *Wheater's Functional Histology. A Text and Colour Atlas*. Edingburgh, London: Churchill Livingstone, 382-393, 2000.
- Zrenner E., Stett A., Weiss S., Aramant R.B., Guenther E., Kohler K., Miliczek K.D., Seiler M.J., and Haemmerle H. Can subretinal microphotodiodes successfully replace degenerated photoreceptors? *Vision Res.* 39, 2555-2567, 1999.
- Zrenner E. Will retinal implants restore vision? *Science* 295, 1022-1025, 2002.

Curriculum vitae

Personal Information

- Name: Susanne Resatz
- Nationality: Austria
- Date and place of birth: 08.12.1964, Mödling, Austria
- Children: Lisa (born on 25.05.1984 in Vienna)
- Private address: Novaragasse 24/15, 1020 Vienna
- Email: susanne.resatz@tuwien.ac.at

Education

- | | |
|--------------|--|
| 1970 - 1974 | Primary school in Vienna |
| 1974 - 1978 | Secondary school in Wr. Neustadt with emphasis on sports |
| 1978 - 1982 | Rudolf-Steiner school in Vienna |
| June 1991 | Graduation exam (Matura) |
| October 2002 | Graduate with honor from Vienna University of Technology
Degree in Technical Mathematics with emphasis on Natural Science (DI)
Diploma thesis:
'Electrical stimulation of the retinal ganglion cell: a computer simulation'
Advisor: Ao. Univ. Prof. DDr. Frank Rattay |

Professional Experiences

- | | |
|-------------|--|
| 1983 - 1988 | Commercial clerk at the Kindergarten 'Alt-Wien' |
| 1989 - 2001 | Commercial clerk at the tax consultancy office 'REP' |
| 2001 - 2002 | Scholarship of the European Union |
| since 2002 | Teaching assistant at the Institute of Analysis and Scientific Computing Vienna University of Technology |
| since 2003 | Research assistant in the project 'Modeling LLPG activity in incomplete SCI subjects' granted by the Austrian Science Foundation |

Publications

- Resatz S., Rattay F., Edthofer F., Schöbel M., and Valla A. A compartment model of the electrically stimulated retinal ganglion cell. *Proc. World Congress on Neuroinformatics*, Argesim/Asim Verlag Vienna, Part II, 217-218, 2001.
- Resatz S. and Rattay F. Stimulating neural networks with microelectrodes: a modeling study for the retina implant. *Proc. IFESS Ljubljana*, 170-172, 2002.
- Rattay F., Greenberg R. J., and Resatz S. Neuron Modeling. In: *Handbook of Neuroprosthetic Methods*. Eds. W.E. Finn and P.G. LoPresti. CRC Press, 39-71, 2002.
- Rattay F., Resatz S., Lutter P., Minassian K., Jilge B., and Dimitrijevic M.R.. Mechanisms of electrical stimulation with neural prostheses. *Neuromodulation* 6, 42-46, 2003.
- Resatz S. and Rattay F. The electrically stimulated retina: a simulation study. *Proc. 4th MATHMOD Vienna*, 1636-1645, 2003.
- Resatz S. and Rattay F. Excitability of bipolar and ganglion cells with retinal prosthesis: a modeling study. *Proc. Engineering in Medicine and Biology Society, 25th Annual International Conference Cancun*, Mexico, 2039-2042, 2003.
- Rattay F., Reichel M., Martinek J., Persy I., Resatz S., and Mayr W. Functional electrical stimulation of denervated skeletal muscles: a modeling study. *Proc. Engineering in Medicine and Biology Society, 25th Annual International Conference Cancun*, Mexico, 1553-1556, 2003.
- Resatz S. and Rattay F. A model for the electrically stimulated retina. *Mathematical and Computer Modelling of Dynamical Systems* 10, 93-106, 2004.
- Rattay F. and Resatz S. Effective electrode configuration for selective stimulation with inner eye prostheses. *IEEE-Trans. BME* 51 1659-1664, 2004.
- Leao R.N., Resatz S., Rattay F., and Walmsley B. Altered synaptic and membrane properties of the auditory pathway in congenital deafness: implications for sound localization. (abstract) *4-th Forum of European Neuroscience*, Lisbon, 2004.